A STUDY IN AIRCRAFT EFFICIENCY ENHANCEMENTS VIA PRANDTL-TAILORED DYNAMICALLY AEROCOMPLIANT WINGTIP EXTENSIONS

By

Submitted to the graduate degree program in Aerospace Engineering and the Graduate Faculty of the University of Kansas in partial fulfillment of the requirements for the degree of Master's of Science.

_____

Dr. Ronald Barrett
Associate Professor of Aerospace Engineering
(Chairperson)

_____

Dr. Ray Taghavi
Professor of Aerospace Engineering
(Committee Member)

_____

Dr. Haiyang Chao
Assistant Professor of Aerospace Engineering
(Committee Member)

Date Defended: 27 June 2014

The Thesis Committee for Samantha Schueler
certifies that this is the approved version of the following thesis:

A STUDY IN AIRCRAFT EFFICIENCY ENHANCEMENTS VIA PRANDTL-TAILORED DYNAMICALLY AEROCOMPLIANT WINGTIP EXTENSIONS

_____
Dr. Ronald Barrett
Associate Professor of Aerospace Engineering
(Chairperson)

_____
Dr. Ray Taghavi
Professor of Aerospace Engineering
(Committee Member)

_____
Dr. Haiyang Chao
Assistant Professor of Aerospace Engineering
(Committee Member)

Date approved: _____

Abstract

In 2008, the commercial aerospace industry saw substantial reductions in aircraft operating hours because of the struggling economy and high operating costs. Recurring fuel costs range from 10-40% of total operating cost revealing an inherent need for increased fuel efficiency for in-service aircraft. Current methods, such as control system improvements and winglet installments, yield little improvement. Wingtip extensions using a new design philosophy, however, indicate significant progress in the area through large scale reductions in the span loading of the aircraft thereby dramatically reducing induced drag. The adaptability of the wingtip extension allows for the span limitations set by the aircraft group classification to be met through the inclusion of a folding mechanism. Unlike currently used folding mechanisms, the Prandtl-tailored dynamically aerocompliant wingtip extension, explored herein, maintains the aerodynamic surface on both the upper and lower surface, thereby reducing drag further over the state of the art in active hinge mechanisms.

The philosophy behind the Prandtl-tailored dynamically aerocompliant wingtip extensions follows technology commonly used in the helicopter and missile communities along with an approach by Ludwig Prandtl for reductions in induced drag. Strong pitch-flap coupling in the folding region results in reduced flapping tendencies and reduced fatigue while the shaping of the wingtip extension reduces the force increase due to the retrofit. By combining these techniques and adaptive materials, the benefits predicted through the retrofit of in-service aircraft with the wingtip extensions include: fatigue reduction, gust load alleviation, improved fuel burn efficiency,

improved marketability through an increase in the design range, and improved safety during adverse flying conditions.

This study uses the Boeing 727-200 as an analytical proof of concept aircraft to retrofit with the Prandtl-tailored dynamically aerocompliant wingtip extensions. This aircraft was used due to the abundance of publicly available technical data while the aircraft is still in-service but out of production, therefore the study is applicable while being “non-controversial”. The aerodynamic results of this study indicate substantial improvement in the fuel efficiency of the aircraft during the cruise segment of the flight profile. The smallest span wingtip extension which was analyzed resulted in a 2% cruise fuel consumption reduction while the largest span wingtip extension analyzed resulted in a 48% cruise fuel consumption reduction.

Although the Boeing 727-200 was used as the basis for this analysis, this wingtip extension design philosophy can be applied to most commercial aircraft with slight modifications to the layout and design. By proving the concept with wingtip extensions, the market can become accustomed to adaptive wing technology in commercial applications which, eventually, could lead to fundamentally new wing designs.

Acknowledgements

I would like to thank my father, Daryl Schueler; stepfather, Stewart Platz; and mother, Sindey Schueler-Platz for their influence not only on myself but also my research. Their unwavering support and encouragement have allowed me to enjoy many opportunities which would not be possible without them. I also thank my sisters, Sabrea Platz and Sindra Schueler, and fiancé, Adam Emerson, for their untiring support.

I offer my sincerest gratitude to my advisor and committee chair, Dr. Ronald Barrett, for his continued support and patience in the completion of this thesis. His encouragement and knowledge made this study possible.

I would also like to thank Dr. Ray Taghavi, and Dr. Haiyang Chao for their service on my committee.

The author would like to acknowledge the support of the United States Department of Transportation under Assistance Number: DTD 559-06-G-0047 to the University of Kansas Transportation Research Institute, TRI.

Table of Contents

Table of Contents (continued) Page #

List of Figures

Page #

List of Figures (continued) Page #

List of Figures (continued) Page #

List of Figures (continued) Page #

List of Figures (continued) Page #

List of Figures (continued) Page #

List of Tables

Page #

List of Symbols

Symbol	Definition	Units
A	Aspect Ratio	~
b	Span	ft
C_D	Coefficient of Drag	~
C_{Di}	Induced Drag	~
C_{Do}	Parasitic Drag	~
c_j	Specific Fuel Consumption (jet)	lbf/lbf/hr
C_L	Coefficient of Lift	~
D	Drag	lbf
e	Oswald's Efficiency Factor	~
f	Parasite Area	ft^2
F	Shear Force	lbf
h	Altitude	ft
L	Lift	lbf
M	Moment	ft-lbf
n	Load Factor	g
N	Force	lbf
R	Range	nmi
S	Area	ft^2
t	Thickness	ft
V	Velocity	ft/s
W	Weight	lbf
y	Spanstation	ft

Greek Symbol	Definition	Units
α	Angle of Attack	deg
γ	Shear Strain	in/in
Γ	Dihedral Angle	deg
δ	Delta Angle	deg
ε	Twist Angle, Strain	deg, in/in
κ	Curvature	ft^{-1}
λ	Taper Ratio	~
Λ	Sweep Angle	deg
ρ	Density	lbf/ft^3
σ	Stress	lbf/ft^2
τ	Shear Stress	lbf/ft^2

Subscript	Definition
∞	Freestream
baseline	Baseline wing
extension	Wingtip extension
gust	Gust condition
i	Inboard, Flight profile stage
max	Maximum
o	Outboard
r, root	Wing root
w	Wing
winglet	Winglet
x	X-direction location
y	Y-direction location
z	Z-direction location

Acronym	Definition
AXD	Alexandroupolis International Airport
BERP	British Experimental Rotor Program
CDP	Cell Differential Pressure
DARPA	Defense Advanced Research Projects Agency
DOF	Degree of Freedom
FAR	Federal Aviation Regulations
IXZ	Veer Savarkar International Airport
JFK	John F. Kennedy International Airport
JID	Job Identification
KIX	Kansai International Airport
MZF	Maximum Zero Fuel
NACA	National Advisory Committee for Aeronautics
NASA	National Aeronautics and Space Administration
P(VDF-TrFE)	Poly[vinylidenefluoride-co-trifluoroethylene]
PVDF	Polyvinylidene Fluoride
PZT	Lead Zirconium Titanate
RITA	Research and Innovative Technology Administration
SMA	Shape Memory Alloy
SRI	Stanford Research Institute
TRI	Transportation Research Institute
USAF	United States Air Force

1 Introduction and Literature Review

While there are many aspects to creating a more efficient aircraft, one which is continually changing in commercial industry is Wing Design. Currently, a trend can be seen in which companies are designing wings which push the limits in terms of manufacturability and airport compatibility. With new winglet and wingtip extension designs every company is looking for a balance between manufacturability, cost, compatibility with airport operations, and fuel efficiency.

Recently certified aircraft reveal that many companies are turning to ever higher aspect ratios of their FAR 25 new wing designs in an attempt to increase fuel efficiency. By increasing the aspect ratio of the wing, there is an inherent tendency to push against the gate spacing limitations to which each aircraft of a given group type adheres. To try and accommodate both aspects of a design, high aspect ratio and gate spacing requirements, many new wingtip designs are taking shape. With recent commercial aircraft designs, industry is showing the importance of increased efficiency by sacrificing weight and mechanical complexity in the form of movable wingtips, more complex flap systems, and more advanced materials some of which being adaptive.

1.1 History of Adaptive Aircraft

Aircraft have been designed to be adaptive for many years with one of the first examples coming from John Joseph Montgomery in the 1890's [1]. Montgomery used wing-warping to increase control in roll; a concept which was later utilized by the

Wright brothers independently [2]. In 1931, Ivan Makhonine turned to variable geometry in the design of the Makhonine Mak-10 [3].

Figure 1.1: Makhonine Mak-10 [3]

The reasoning behind the variable geometry for this aircraft was improved performance during high speed flight. This was accomplished through the use of a telescopic wing; during takeoff the wing was approximately 60% of the high speed configuration span. In 1951, the Bell X-5 was flown [4].

Figure 1.2: Bell X-5 [4]

This aircraft was inspired by the Messerschmitt P.1101 prototype recovered in 1945 by United States troops in Germany. The P.1101 had a wing design which

allowed the sweep angle to be changed during ground operations. Bell took this concept and designed a system which allowed the sweep to be adjusted during flight. Aircraft following the X-5 which employed a variable sweep wing design include: the Sukhoi Su-17, the Mikoyan-Gurevich MiG-23, the Grumman F-14 Tomcat, the Rockwell B-1 Lancer, and the Tupolev Tu-160 [5]. In 1964, the North American XB-70 Valkyrie had its first flight [6].

Figure 1.3: North American XB-70 [6]

This design used variable dihedral outboard wing sections to increase the directional stability of the aircraft at supersonic speeds, strengthen the compression lift effect, and shift the center of lift at high speeds to a more favorable position.

From the past uses of adaptive wing designs, it is seen that significant benefits can be attained through proper design. Table 1.1 outlines the major benefits and weaknesses of the various changes that can occur in the wing through adaptive design.

Table 1.1: Summary of Adaptive Characteristics

Adaptive Element	Benefits	Challenges
Twist 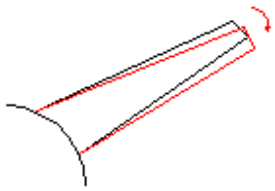	Increase: higher lift capability and possible improvement to aerodynamic loading Decrease: Reduced tendency for tip stall	Increase: higher drag
Span 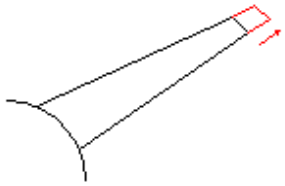	Increase: improved performance Decrease: increased maneuverability	Increase: higher root bending moments
Sweep 	Increase: improved high speed performance Decrease: improved low speed performance	Increase: lower lift capability
Dihedral 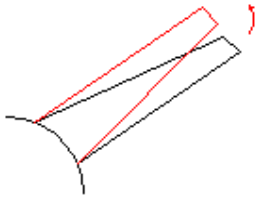	Increase: higher lateral stability Decrease: increased maneuverability	Increase: lower maneuverability Decrease: lower stability
Chord 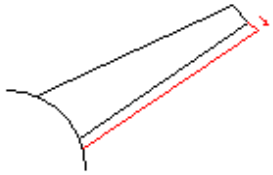	Increase: higher lift capability Decrease: improved high speed performance	Increase: higher drag
Camber Morphing 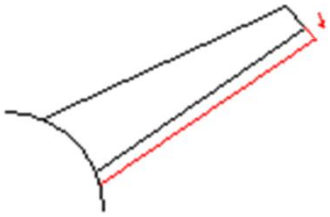	Increase: higher lift capability Decrease: improved high speed performance	Increase: higher drag

The previously stated examples show a trend to use one form of adaptation in a wing design restricting it to 1-degree of freedom (DOF). Some research being conducted currently looks at expanding the capability of a 1-DOF adaptive wing design by combining multiple adaptive elements. This research will be discussed further in Section 1.3.

1.2 Overview of Wingtip Devices

The aerospace industry is continually searching for ways to improve aircraft performance while balancing the weight and cost for attaining these improvements. Wingtip devices have proven to be advantageous for various reasons in commercial applications. These will be discussed in the following sections along with the aerodynamic reasoning behind these improvements.

1.2.1 History of Wingtip Devices

In 1897, Frederick Lanchester patented wing end-plates [7]. He found that installing vertical plates at the tip of wings could reduce the wing drag during flight at high lift conditions by disrupting the lift induced flow above and below the wing at the tip. Unfortunately, these benefits were offset by increased wetted area resulting in increased viscous drag and interference drag at the connection corner. Through Dr. Sighard Hoerner's research, further advantages of wingtips were found. Hoerner found that through the use of drooped wingtips with pointed tips the wingtip vortices

which resulted could be directed away from the upper wing surface thereby increasing the wing lift-to-drag ratio [8].

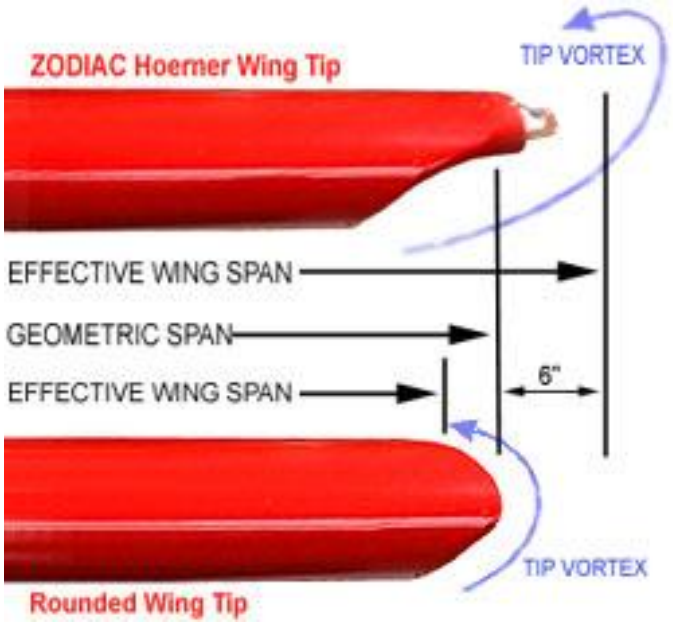

Figure 1.4: Hoerner Wingtip [9]

Richard Whitcomb continued to research the use of wingtips in the 1970s at NASA [10]. Unlike Lanchester and Hoerner, Whitcomb viewed the wingtip as an extension of the actual wing and as such, designed it to have an efficient aerodynamic cross-section and sized it consistently with the cross-section load carrying capacity.

Figure 1.5: Whitcomb Winglet [11]

Instead of wingtip, he referred to his design as a winglet due to the design similarities it bore to the actual wing. The benefits seen through the use of this design philosophy are on the order of a 6-7% reduction in drag [12]. This sparked interest in the use of winglets in commercial applications including the Rutan VariEze and the Learjet Model 28 in 1979 [13].

a)  b) 

Figure 1.6: a) Rutan Varieze [14], b) Learjet Model 28 [15]

The Learjet Model 28 showed improved directional stability with the addition of the winglets as well as a 6.5% increase in range.

Companies are continuing to explore the benefits of winglet designs for current and future designs, adapting the shape and size to fit the various aircraft needs. Several types that are now being used include: raked wingtip (Figure 1.7), blended winglet (Figure 1.8), tip feathers (Figure 1.9), and wingtip fences (Figure 1.10). Although each of these types varies in their design, they all have similar goals for improving the aircraft including: fuel burn reduction, range increase, takeoff and landing field length reduction, increased cruise speed, noise reduction, and increased stability.

Figure 1.7: Raked Wingtip [16]

Figure 1.8: Blended Winglet [17]

Figure 1.9: Tip Feathers [18]

Figure 1.10: Wingtip Fence [19]

1.2.2 Aerodynamic Basis for Wingtip Devices

The ultimate goals of wingtips are to reduce the drag of the wing and therefore increase the lift-to-drag ratio of the wing. Drag can be considered in two parts: parasitic drag and pressure drag. Parasitic drag takes the size and shape of the body into account in the form of skin friction drag, form drag, and interference drag. One component of pressure drag is induced drag. In the case of wingtips, a reduction of induced drag is the goal. Induced drag is the aft component of the lift vector following the lift vector being skewed backwards due to the air that is deflected by the wing lift.

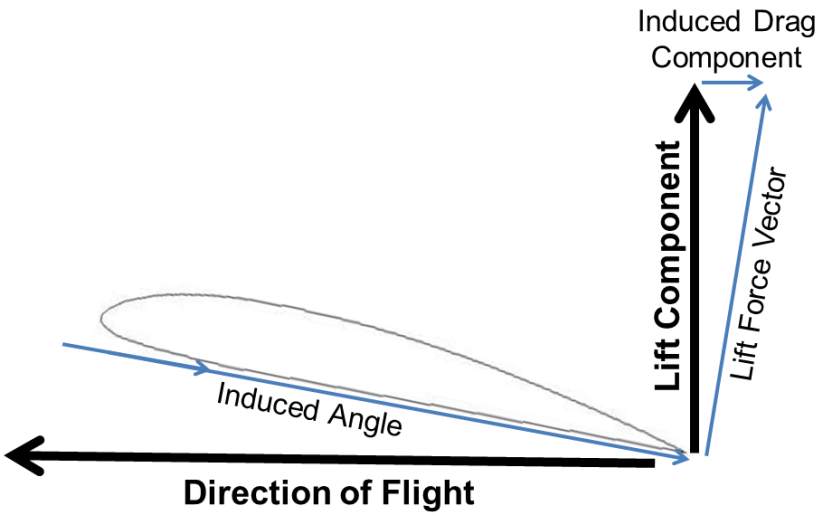

Figure 1.11: Lifting Force Directions

The span wise distribution of vortices which are shed downstream from the trailing edge of the wing determine the magnitude of the induced drag. This is difficult, however, due to the flow mechanisms overlapping and interacting causing the components to not add in a linear manner.

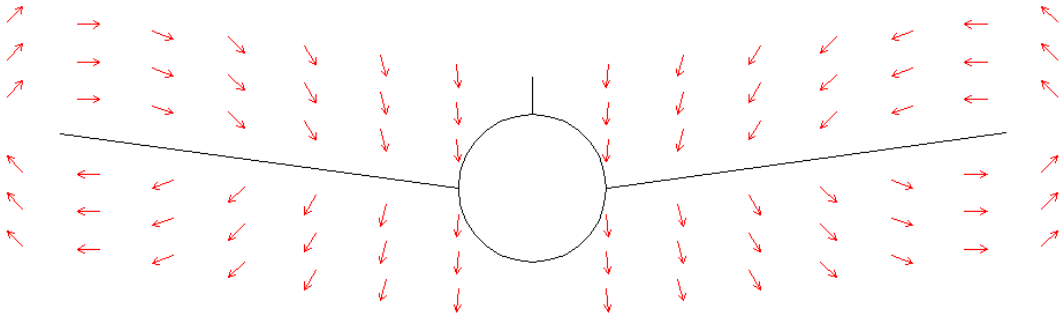

Figure 1.12: Velocity Flow Field

Using vortex lattice theory, it is possible to make an estimation of the induced drag. Vortex lattice theory uses the distribution of vortex panels over the lifting body from an idealized flow field to generate the estimation. As the aircraft flies forward, the flow field is shed from the wing trailing edge creating a vortex wake. The wake continues downstream from the aircraft and can cause issues with stability, efficiency, and can affect surrounding aircraft.

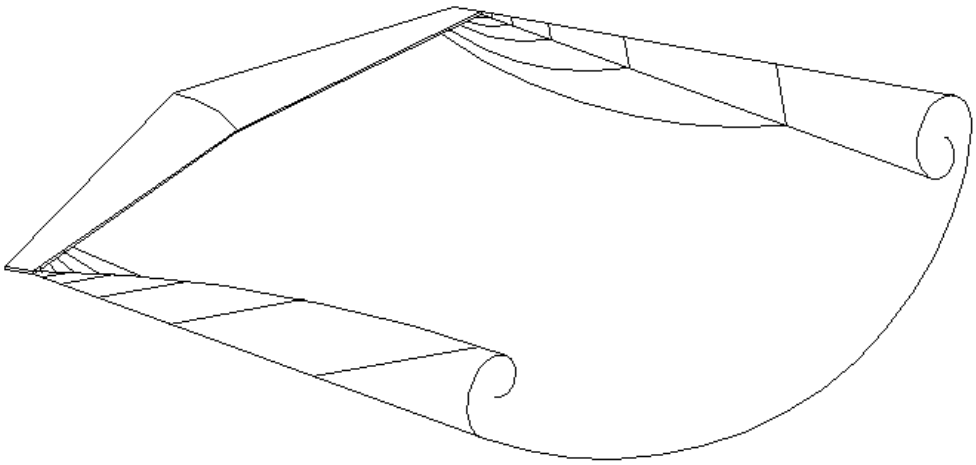

Figure 1.13: Vortex Wake

Another way to decrease the induced drag of the aircraft is to reduce the strength of the vortex wake. This can be done by increasing the effective span of the

aircraft wing while maintaining the same effective lift and wing area. This will be explained further in Section 3.1.2.

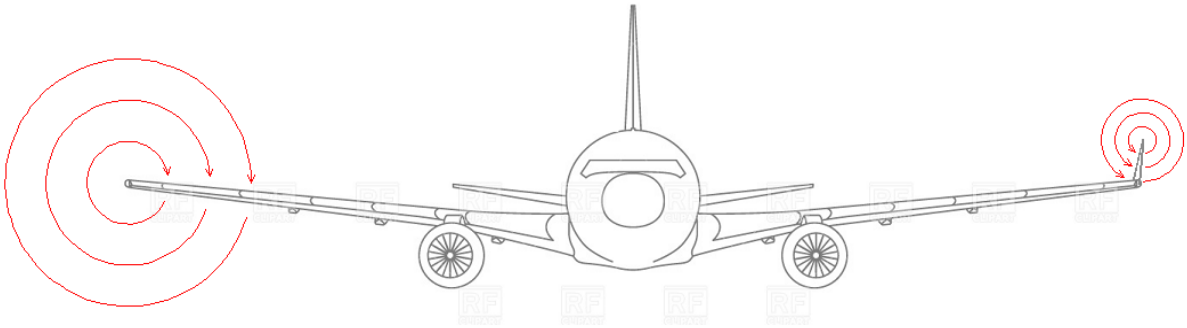

Figure 1.14: Velocity Field, Left: Base Wing, Right: Base Wing and Winglet [20]

1.3 Adaptive Wingtip Research

Much research has been completed looking into shape optimization of wingtips and winglets as well as adaptive structures. One study explored the possibilities of a four-segment morphing winglet (MORPHLET) for use on an in-service narrow body aircraft. Figure 1.15 shows the basic scheme of the winglet [21].

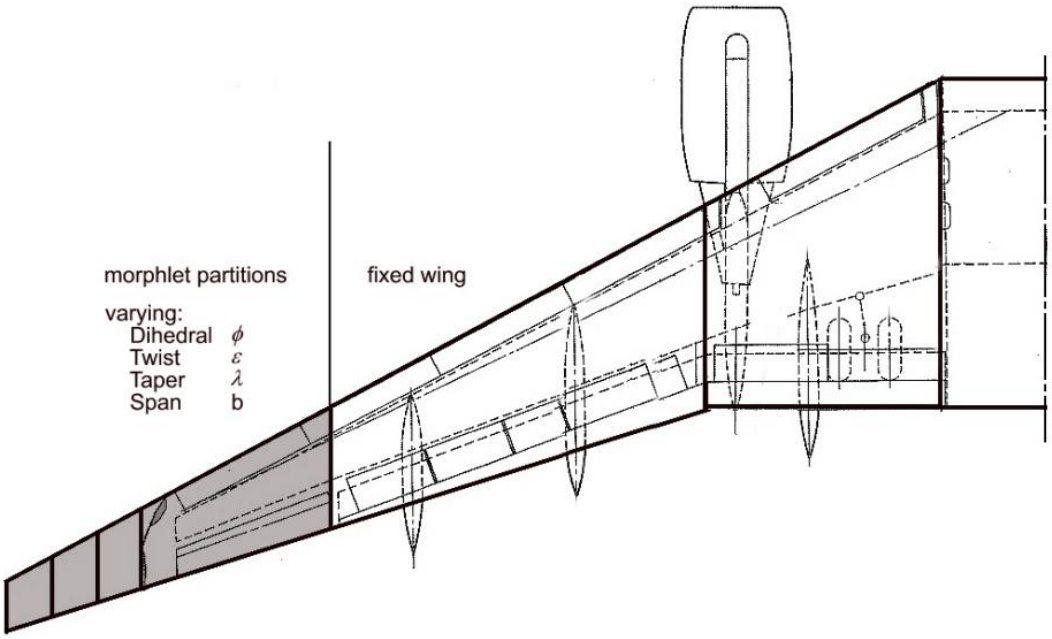

Figure 1.15: Wing Planform with MORPHLET [21]

The aileron panel is augmented with the addition of MORPHLET to further optimize the scheme. The four MORPHLET partitions are able to change during flight to optimize the aircraft performance depending on the flight segment and flight conditions. The figures below show three pictorial representations of the configuration changes which take place during a single flight profile.

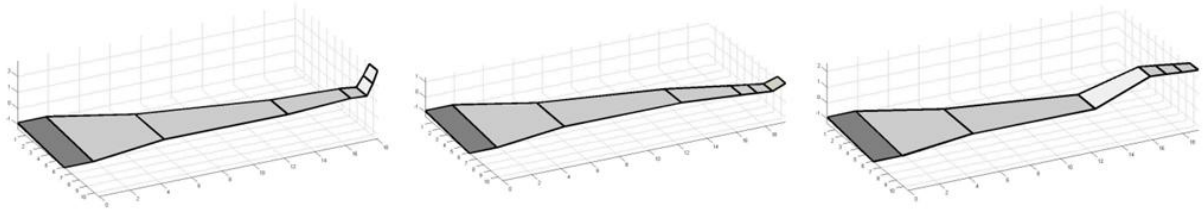

Figure 1.16: MORPHLET Configurations: start cruise, end cruise, end descent [21]

Results from this study for a long range mission showed a 4.5% increase in the lift-to-drag ratio during the climb segment of the flight profile and a 6% increase in the

range during the cruise segment [21]. Similar to this concept the Prandtl-tailored dynamically aerocompliant wingtip extensions will morph during flight, adapting to the various flight segments. But whereas the adaptability of the MORPHLET is limited to streamwise bending, the Prandtl-tailored dynamically aerocompliant wingtip extensions will be capable of streamwise bending as well as off-axis coupling to further adapt to the given flight conditions.

Another study investigated the use of bistable winglet which snapped between two stable states allowing for enhanced lift characteristics of a wing which is transitioning between low and high subsonic flight speeds [22].

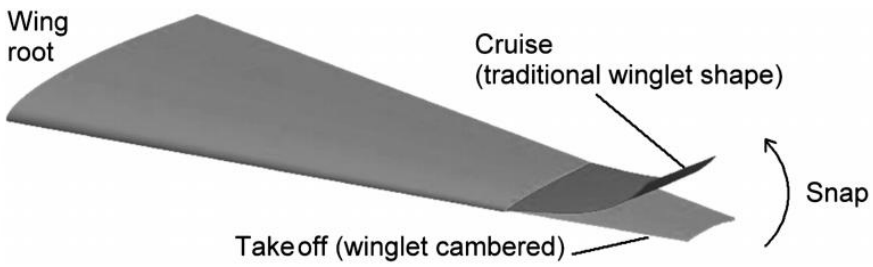

Figure 1.17: Bistable Winglet Concept [22]

While the analysis supported the concept of the bistable winglet for enhancing the lift capability of the wing prior to the snap through but during the snap through stage the dynamic loading that is transmitted through the wing is significant. The lack of any method for controlling the snap through process and randomness induced by a real atmosphere are inhibitory factors for the concept.

A study also using a multi-stable composite was conducted which looked at variations in the cant angle and toe angle of the wingtip during flight [23].

Figure 1.18: Multistable Winglet Concept [23]

Though the concept proposed a multistable composite structure be used, the difficulties in implementing this were realized and a hinged model was created which controlled the cant angle and toe angle independently through the use of servo actuators. The model created for testing is shown in Figure 1.19.

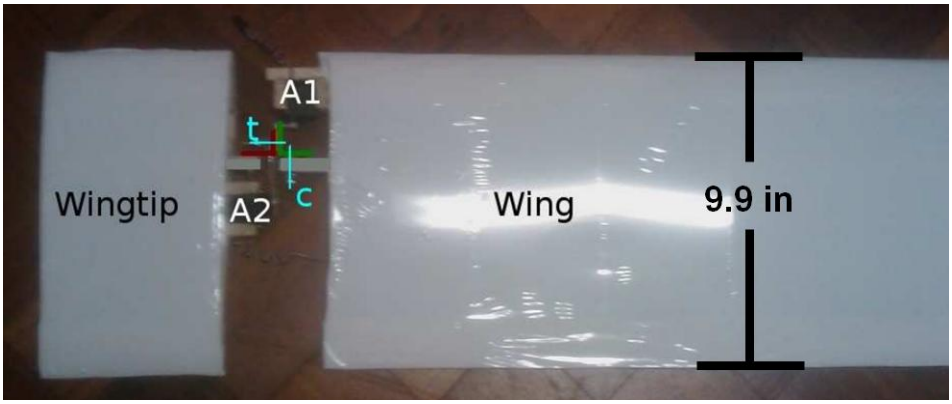

Figure 1.19: Variable Angle Wingtip Model [23]

The performance improvements found with this concept were an 11% improvement in stall speed, a 20% reduction in takeoff ground roll, and a 0.5% improvement in maximum endurance, all at the expense of weight, complexity, and cost [23].

1.4 Thesis Motivation and Overview

The Prandtl-tailored adaptive aerocompliant wingtip extension offers large increases in the maximum lift-to-drag ratio for in-service aircraft, along with dramatic reductions in fuel burn, improved aeromechanical properties, all with negligible moment transfer into the base wing. These improvements have been proposed to NASA and planned to be accomplished through the use of helicopter rotor hub and missile fin design philosophies combined with adaptive materials and Ludwig Prandtl's 82 year old theory for reducing induced drag [24].

The overall progression of the program was proposed to be:

Phase I: Class I Design and Economics Analysis

Phase II: Fleet Downselection and Class II Analysis

Phase III: Class III System Design, Wind Tunnel and Ground Testing

Phase IV: Aircraft Installation and Flight Testing

Phase V: Fleet Installation

The focus of this thesis is limited to Phase I. Future studies will be completed in accordance with the phases following Phase I. Within Phase I, the aerodynamics, marketability and economics, flight operations, and safety considerations of the wingtip extension design was explored.

While there are various studies which have been conducted focusing on adaptive winglet geometry in the form of dihedral, camber, sweep, toe angle, and cant angle, there is a lack of research into the theory behind the basic outer mold line geometry and the span increase. The advantages which can be gained through increased span are well known, but the limiting factor is ground operations and gate

spacing. As many of the previous studies state nature, in particular bird wings, as the basis for the research, bird wings also provide methods for getting around span limitations.

The figures below show an albatross in two states, relaxed and flying. While there are not necessarily span constraints like with an aircraft, an albatross' ability to completely fold its wings in can provide the basis from which to design an aircraft which significantly surpasses the span limitations during flight but then adapts for ground operations to satisfy them.

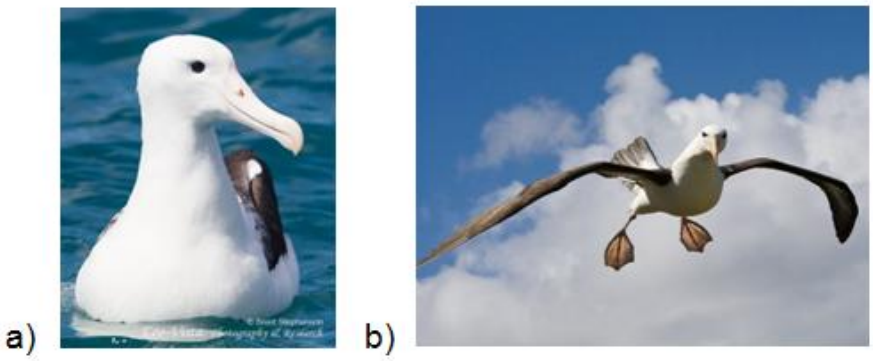

Figure 1.20: Albatross in a) Relaxes State [25], b) Flying State [26]

This ability to fold their wings is made possible through their joint structure.

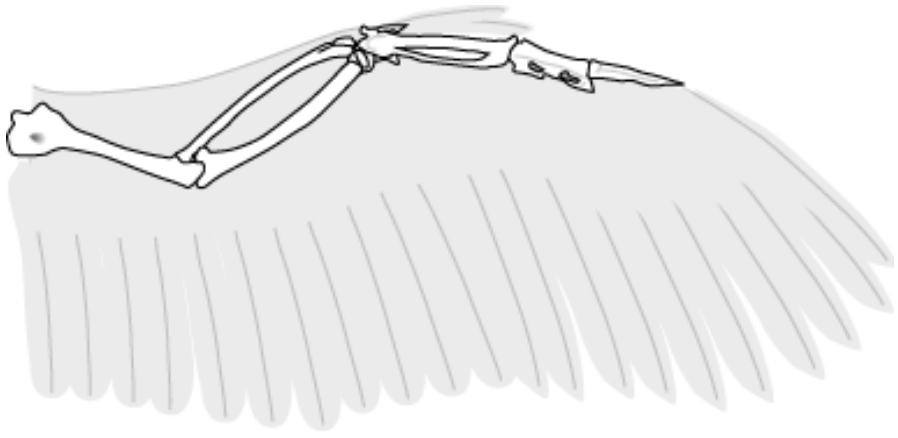

Figure 1.21: Bird Wing Structure [27]

Using this joint structure as the basis for a wing design allows for a significantly higher span wing to be operational out of current airports. But a wing fold is not a new concept. What makes the Prandtl-tailored adaptive aerocompliant wingtip extension wingtip fold unique is its ability to fold without having a joint which reduces aerodynamic performance. Similar to the feathers on a bird's wing, the wingtip skin will expand and retract with the deformation of the internal structure maintaining a smooth aerodynamic surface whether the wing is folded or unfolded.

Another aspect of wing design which can be ascertained through the study of bird wings is the outer mold line shape variation for different flight performance. Different birds have different wing shapes which help them to fly in the particular manner they typically employ. Several of these shapes are shown in Figure 1.22.

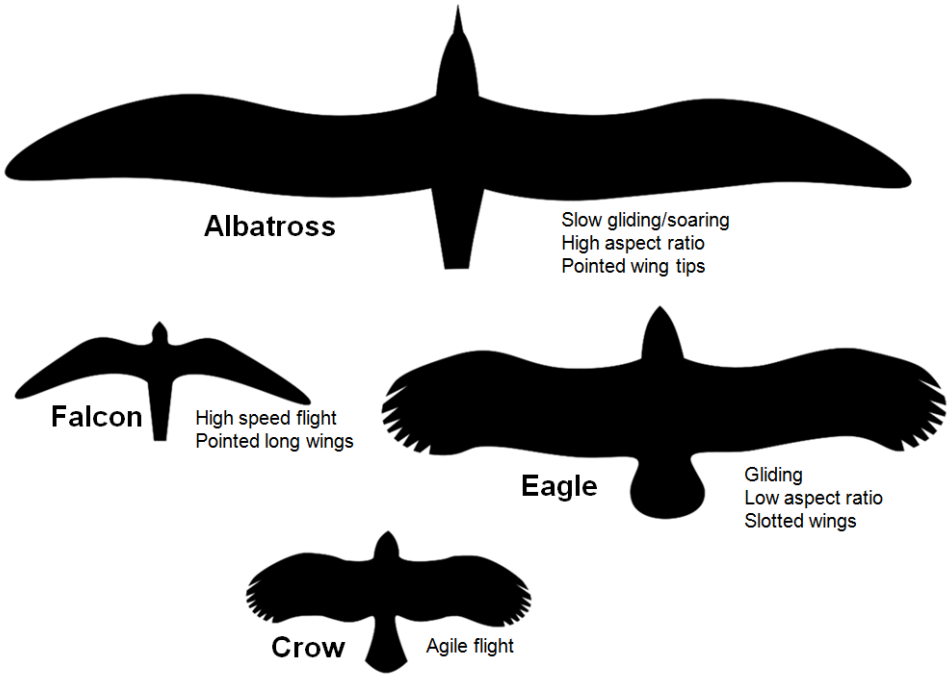

Figure 1.22: Wing Shapes for Various Birds [28]

For commercial transport aircraft, the bird which has the most similar flight path is the albatross with slow gliding and soaring flight. From Figure 1.22 it is seen that the albatross has a high aspect ratio, pointed wing shape. This supports Ludwig Prandtl's theory on minimizing the induced drag of a wing [29].

There is a need for reduced fuel burn in the commercial transport industry. With rising fuel prices, airlines are looking towards improving efficiency even if some amount of complexity is added to the aircraft. In the late 1970s, the United States Air Force and NASA conducted experiments in adding winglets to a KC-135.

Figure 1.23: KC-135 [30]

With these experiments it was discovered that the moments imparted by the winglets on the base wing were large enough to split fuel tanks, spar caps, and spar cap doublers. Following are memos from the Acting Director of the NASA Dryden Test Liaison Office, R. Barber, to the NASA Dryden Tech Director concerning the flight test of the KC-135 with the winglet retrofit [31].

11 September 1979

"A myriad of problems has slowed the flight activity below the scheduled level. KC-135 fuel leaks, lack of USAS flutter facility support, and KC-135 instrumentation problems have been the primary causes of the reduced flight activity."

8 November 1979

"Fuel leaks have prevented obtaining the scheduled number of flights in October."

14 January 1980

"Airplane fuel leaks and instrumentation problems severely curtailed flying in December."

1 February 1980

"Three flights were flown in January. The first flight was aborted due to excessive turbulence for speed power test points and a failure of a fuel flow meter. The second flight was aborted due to a fuel leak that became apparent to the flight crew approximately two hours after takeoff. This leak was large enough that fuel "streamed" over the wing and off the trailing edge. The fuel leak was not present after the airplane had landed. Pressure and vacuum checks of all the associated plumbing and tanks failed to show the leak on the ground. The airplane was flown again with dye in the fuel tanks. This flight confirmed that the leaking fuel came directly from No. 4 fuel tank. Again, the leak would not repeat itself on the ground."

14 March 1980

“The fuel leak reported last month has been tracked to a crack in the lower wing spar cap. This crack is located immediately behind the number 3 engine outboard pylon attach fitting."

17 April 1980

“A trade study review was held at Boeing in Wichita, Kansas on March 6 and 7, 1980. The Trade Study was a USAF/Boeing contractor meeting wherein Boeing was to identify the Winglet configuration that they would elect to pursue for fleet retrofit. The trade study review resulted in Boeing selecting the Whitcomb Winglet at the 15 deg. cant angle and 4 deg incidence angle configuration. Boeing quoted a 7.1 percent decrease in drag for this winglet at the optimum flight condition. This increment was based on the flight test data with an analytical factor of 0.4 percent applied to correct for the winglet skin wrinkles. Using this winglet and its measured drag decrease, Boeing predicted a fleet retrofit would return fuel savings ten times greater than the cost of the retrofit over the expected lift of the fleet.”

8 July 1980

“The fuel leaks mentioned in last month's report continue to delay flying. The airplane was brought out of the fuel cell on June 13, 1980. Subsequent fueling resulted in a leak in the aft body tank. This leak has eluded repair attempts to date.”

8 December 1980

“Presently it appears that two or three more flights will be required to fill out the data for this configuration. Fuel leaks have prevented attaining these flights to date.”

One option following the realization that the increased loads from the winglet retrofit caused a crack in the lower wing spar cap would be to add doublers to accommodate those loads. In the event of a failure within the added doubler, the load is redistributed and a failure is likely just inboard of the failed doubler. These findings show the importance in consideration of the increased load from wing modifications in the form of winglets or wingtip extensions. This is where the application of Ludwig Prandtl's theory maintains the practicality of a large wingtip extension without a base wing redesign. By minimizing the moments transferred into the base wing, the problems seen by the KC-135 winglet can be avoided.

2 Wingtip Extension Considerations

An addition like a wingtip extension requires careful consideration of the aspects of the flight profile which it will affect. A commercial transport aircraft, typically, has a very simple flight profile. An example profile can be seen in Figure 2.1. With each phase of the flight profile there are different requirements and limitations placed on the aircraft.

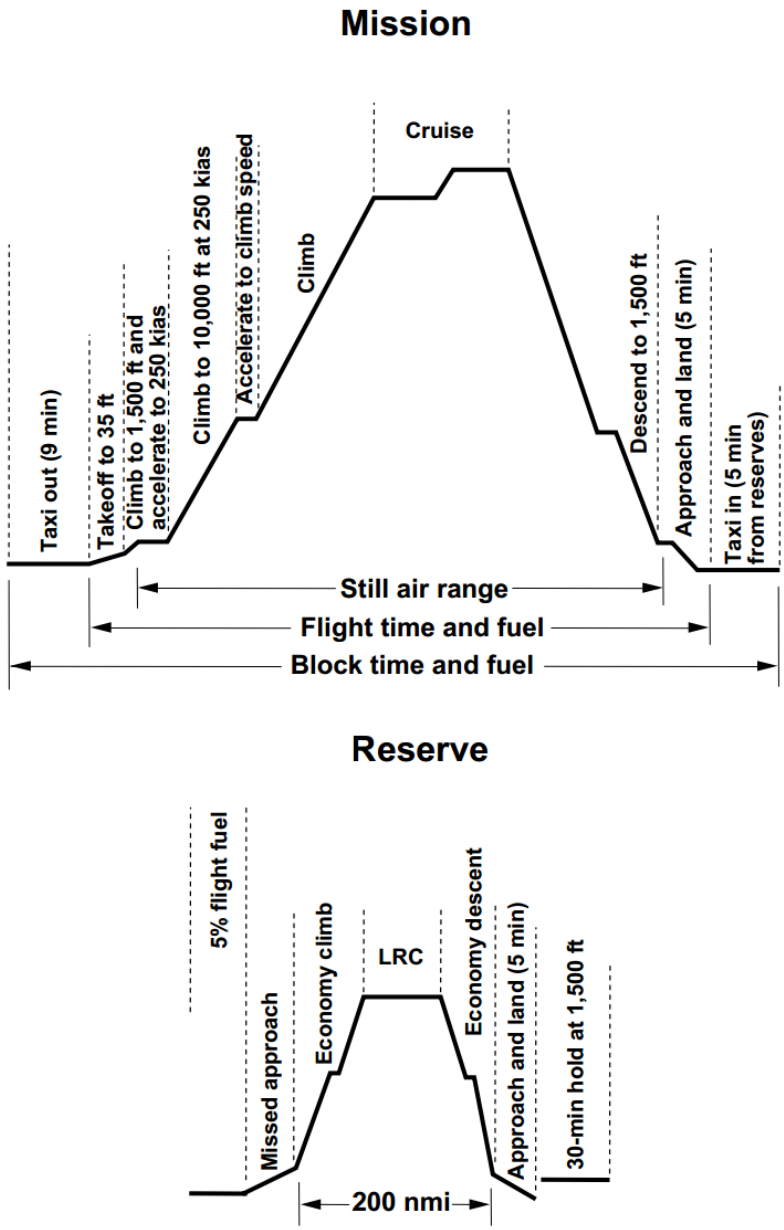

Figure 2.1: Typical 737 Mission Profile, Standard Day, Nominal Performance [32]

During the loading and taxi out stages, the aircraft must abide by the gate spacing span requirements. These are shown in Table 2.1.

Table 2.1: Span Limitations [33]

Group	Wing Span (ft)	
	Minimum	Maximum
I	0	<49
II	49	<79
III	79	<118
IV	118	<171
V	171	<214
VI	214	<262

These limitations are important for knowing which airport terminals are capable of handling aircraft of a certain size. Figure 2.2 shows an aerial view of an airport with aircraft in the loading position.

Figure 2.2: Charlotte Douglas Airport [34]

This shows the close proximity which the aircraft are to each other and the importance of abiding by these gate spacing requirements. It also shows that the space above the aircraft wing is clear of obstructions, once fueling is complete.

During this stage, the wingtip is completely folded and locked in place to avoid a gust deforming the wingtip and causing damage to itself, another aircraft, or ground crew personnel. A representation of this configuration is shown in Figure 2.3.

Figure 2.3: Wingtip Extension in Folded Position [24]

In the takeoff and climb state the wingtip is unfolded in the horizontal position. This is shown in Figure 2.4.

Figure 2.4: Wingtip Extension in Unfolded Position [24]

When a force acts on the wing that is outside the steady-state cruise forces, like a gust, the wingtip deforms with that force. This is shown in Figure 2.5.

Figure 2.5: Wingtip Extension in Partially Unfolded Position [24]

Upon descending and landing, the wingtip will return to its previous configuration, first in the horizontal unfolded position and then the folded position during taxi and gate approach.

3 Wingtip Extension Configuration

The fundamental theory behind the Prandtl-tailored adaptive aerocompliant wingtip extension was to offer airlines and other operators an optional wingtip extension which could be installed on an already in-service aircraft. By leaving it as an optional installment, the acquisition cost of the aircraft is not increased and the production line is not affected. To not vary the in-service aircraft production, the changes made to the aircraft to accommodate the wingtip must be minimized. This is done by minimizing the bending moment applied to the tip of the base wing, while allowing shear force transfer into the original wing at the connection point as well as the bending moment imparted along the span of the wing. The shaping of the wingtip is used to control these forces and moments and will be discussed further in Section 3.1.

Discussed in Section 3.2 is the structure within the wingtip, an ongoing concern with span extensions and a limiting factor with much of the current research. The different sections of the wingtip will be discussed and how they interface with the base wing.

3.1 Shaping

The shaping of the wingtip was completed following a theory which differs from much of the current research. Instead of simply treating the wingtip as an extension of the wing, designed much in the same way, the Prandtl-tailored adaptive aerocompliant wingtip extension was designed to also minimize the moment transferred into the base wing while still producing a positive effective lift.

The wingtip is shaped to also have a section near the tip which protrudes forward past the leading edge of the wing inboard of this section. This concept was inspired by the British Experimental Rotor Program (BERP) blade, shown in Figure 3.1.

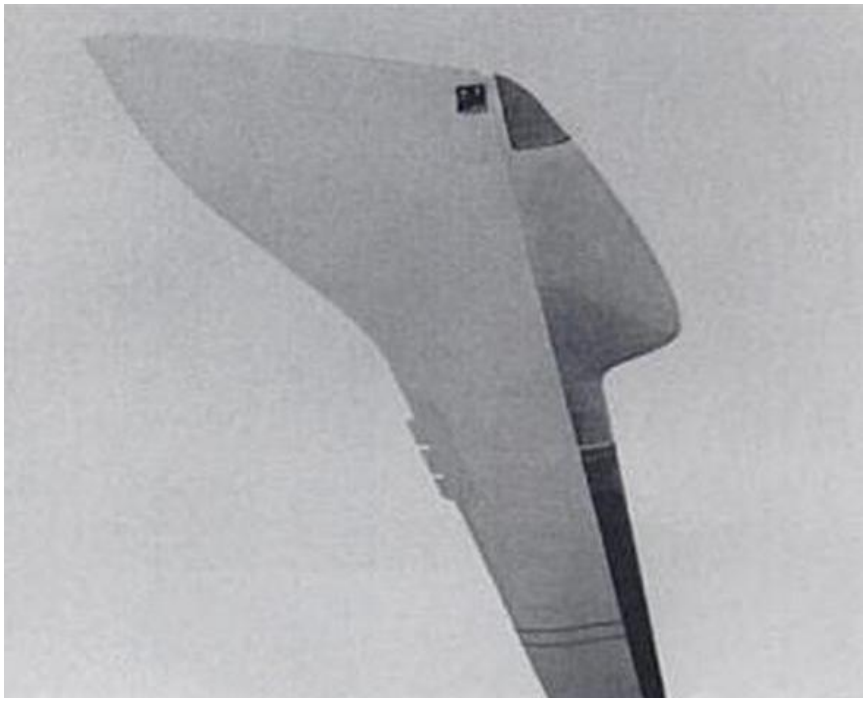

Figure 3.1: BERP Blade [35]

The BERP blade was designed as a helicopter rotor blade to satisfy conflicting aerodynamic requirements of the advancing and retreating rotor blade conditions, both of which can limit the lift-to-drag ratio of the blade and its performance in high-speed forward flight [35]. The design of the BERP blade allows for operation at very high angles of attack without stalling, in part, due to the generation of stable vortex flows which delay the onset of flow separation in the tip region while enhancing the lift generation (Figure 3.2).

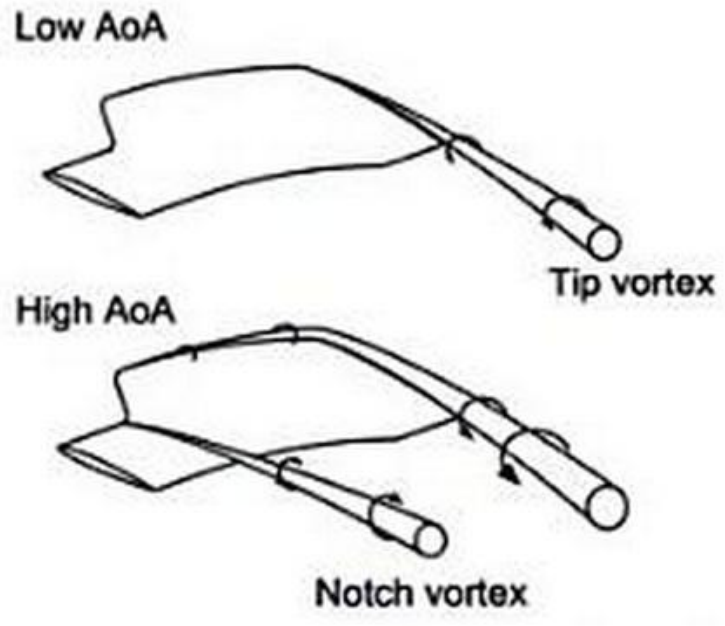

Figure 3.2: Vortex Flow over BERP Blade Tip [35]

The performance of the BERP blade design was confirmed following flight tests using the Lynx helicopter. The BERP blade concept has since been used in retrofitting the fleet of military Lynx helicopters and the EH-101 helicopter.

a)  b) 

Figure 3.3: a) Lynx Helicopter [36], b) EH-101 [37]

The purpose of this section which protrudes forward is for dynamic aeroelastic benefits, namely reducing flutter tendencies and fatigue by enabling not only structural pitch-flap coupling, but inertial pitch-flap coupling.

3.1.1 δ_3 Coupling

Pitch-flap coupling is a motion where the flapping displacement induces a pitching motion. This coupling effect is often taken advantage of in the helicopter industry for rotor blade design. For positive pitch-flap coupling, the blade flaps upward decreasing the blade pitch, or angle of attack. With the reduction in the blade angle of attack, the lift produced is also reduced which opposes the original flap motion. This causes the pitch-flap coupling to act as an aerodynamic spring to the flap motion. A simple method for inducing this positive pitch-flap coupling is skewing the hinge angle. When the hinge line is skewed in the direction shown in Figure 3.4, the inherent pitch-flap coupling is positive.

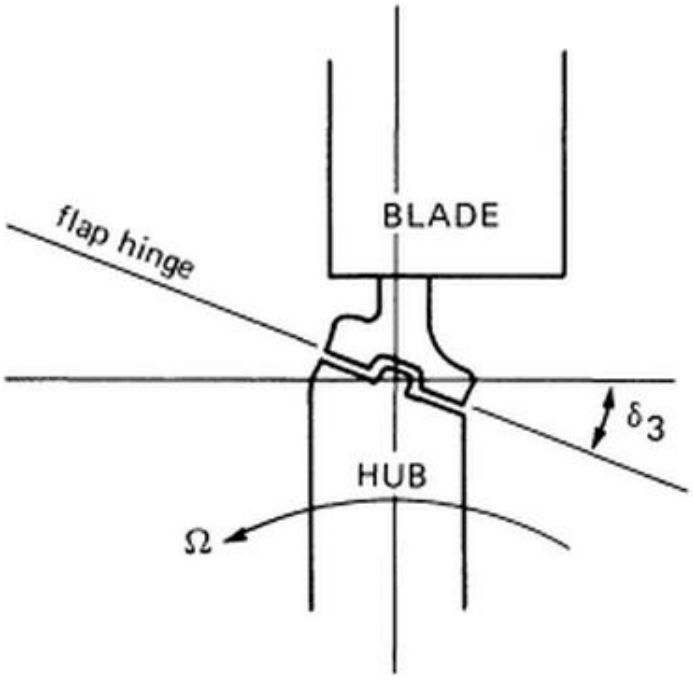

Figure 3.4: Pitch-Flap Coupling Hinge Geometry of a Rotor Blade [38]

One example of using pitch-flap coupling for stabilization is in the AIM-9 missiles. Each of the fins contain a rolleron along the trailing edge which provides passive stabilization against rotation during flight. This is shown in Figure 3.5.

Figure 3.5: AIM-9M [39]

Each rolleron has a metal wheel with notches. During flight these notches are pushed by the airflow causing the wheel to spin causing the wheel to perform as a gyroscope and deflect the rollerons to counteract any rotation. The rolleron assembly is shown in its locked, non-deflected state in Figure 3.6 and its deflected state in Figure 3.7.

Figure 3.6: AIM-9 Rolleron Assembly in Locked Position [40]

Figure 3.7: AIM-9 Rolleron Assembly in Unlocked, Deflected Position [40]

The hinge line of the rolleron is at a 45 degree angle, as can be seen in Figure 3.7. This provides the necessary inherent stabilization for the AIM-9.

A concept similar to pitch-flap coupling, bend-twist coupling, was used in the wing design of the Grumman X-29. In the case of forward swept wings, the aerodynamic lift generated by the wings generates a twisting force which forces the wing leading edge upward resulting in an increased angle of attack. This increase in angle of attack increases the lift which causes an even greater twisting force which can lead to structural failure. This increasing twisting force is known as aeroelastic divergence.

Figure 3.8: X-29 [41]

One method for combating aeroelastic divergence is a torsionally stiff structural design which can resist the twisting force applied to the wing. In the case of the X-29, an anisotropic composite design was used which coupled the bending and torsion loads. During flight, when the lift increases the bending loads force the wingtips upward. Meanwhile, the torsion loads which attempt to twist the wing towards higher angles of attack is resisted due to the coupling effects and the angle of attack is reduced thereby further decreasing the lift produced. This results in the avoidance of aeroelastic divergence.

The Prandtl-tailored adaptive aerocompliant wingtip extension uses not only the δ_3 hinge line angle as is used in helicopter rotor blade designs and the AIM-9 missile, but also an anisotropic composite layup as in the X-29 wing. The combination of these provides the wingtip extension with the ability to inherently stabilize itself while prolonging controlled flight through the delay of tip stall and aeroelastic divergence.

3.1.2 Prandtl Theory

It was found that the lift distribution over a three-dimensional wing is more complicated than simply combining the two-dimensional analyses for each wing segment because the lift at one section is strongly affected by the sections surrounding it. Prandtl lifting-line theory provides a method for predicting the lift for a three-dimensional wing through use of an estimated lift distribution along the span wise direction. This lift distribution is generated based on the wing span wise chord, airfoil, and twist, as well as the flow conditions around the wing. To account for the effect of each wing segment on its surrounding geometry, the circulation over the wing

span is found through the use of the Kutta-Joukowski theorem and is dependent on the local lift. This dependence results in an equivalent span wise change in circulation for every span wise change in lift. Using Helmholtz theorems, span wise changes in lift are modeled as a vortex which is shed behind the wing. This shed vortex in turn affects the surrounding wing sections as upwash on the outboard section and downwash on the inboard section. When this is extrapolated over the entire wing, the following equation is used to generate the total lift estimation.

$$L_{total} = \rho V_{\infty} \int_{tip}^{tip} \Gamma(y)\, dy$$

Equation 3.1 [29]

It is widely accepted that an elliptical lift distribution minimizes the induced drag of a wing.

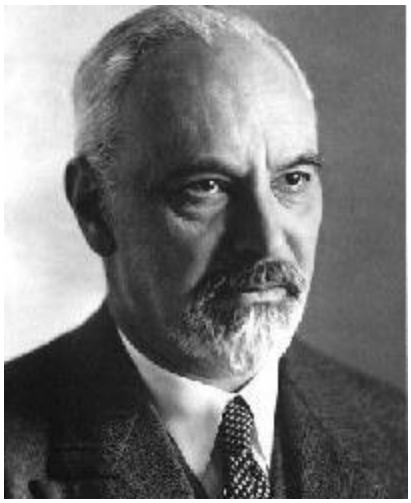

Figure 3.9: Ludwig Prandtl [42]

Ludwig Prandtl proved, in 1933, that this is not necessarily the case. Prandtl used the assumption that the effective lift generated by the wing stayed constant. Operating under this philosophy means that the lift from the wing is reduced by the

amount of lift that is produced by the wingtip. This will be an important factor, later, in the structural design of the wing modifications. The point at which Prandtl's theory diverges from currently explored designs is in the lift direction. Logically it is assumed that the wingtip should generate positive lift over its span to reduce the wing required lift. Prandtl assumes that the entirety of the wingtip is not necessarily generating a positive lift vector. This can be seen in Figure 3.10.

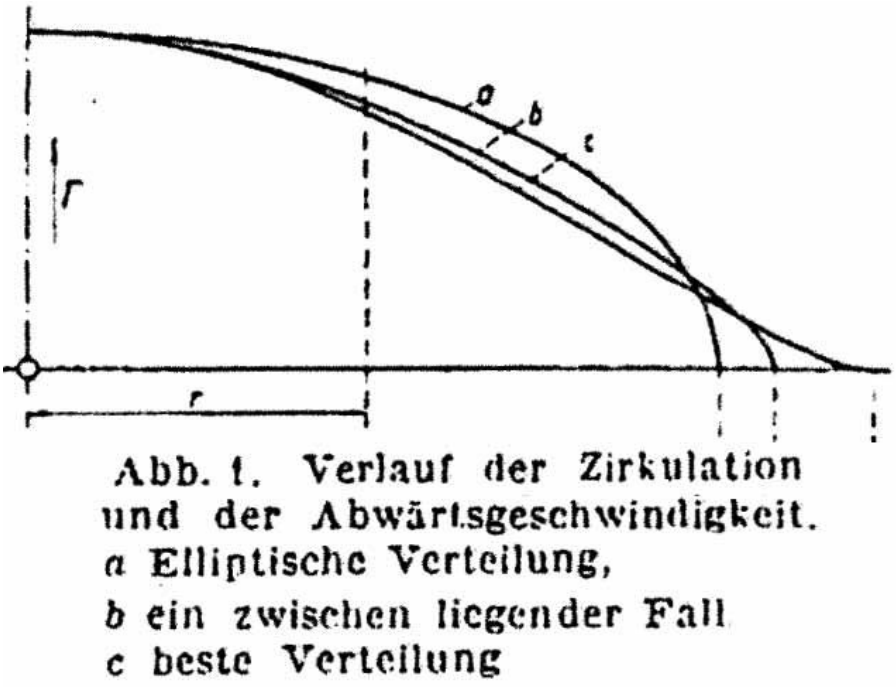

Abb. 1. Verlauf der Zirkulation und der Abwärtsgeschwindigkeit.
a Elliptische Verteilung,
b ein zwischen liegender Fall
c beste Verteilung

Figure 3.10: Prandtl Lifting Force Distribution [43]

By segmenting the wingtip into a positive lift generating section inboard and a negative lift generating section outboard, the resulting moment at the wingtip root can be effectively nulled through proper design. By nulling the wingtip root bending moment, the structurally modified connection point to the base wing is only required to transfer the shear force from the wingtip thereby reducing the necessary base wing structural modifications.

Figure 3.11 shows a comparison of the wing root bending moment of a conventional wing, a wing with a conventional winglet design added, and a Prandtl-tailored adaptive aerocompliant wingtip extension retrofit on the same base wing. It can be seen that the root bending moment is lowered with the wingtip extension as opposed to the conventional winglet design.

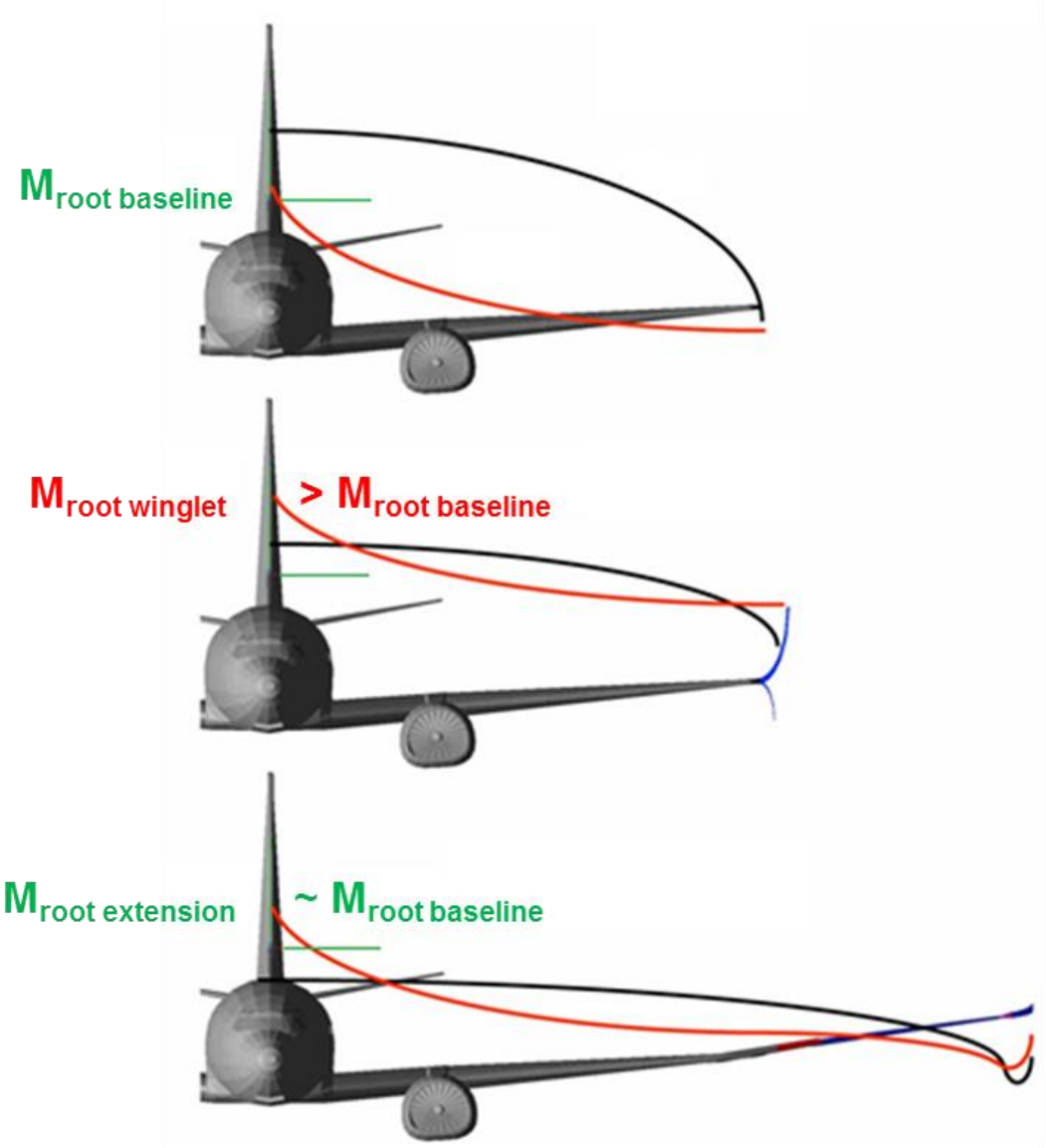

Figure 3.11: Span Loading Distribution Comparison for Conventional Wing (top), Conventional Winglet Retrofit (middle), Wingtip Extension Retrofit (bottom) [24]

3.1.3 Raptor Tip Design

The wingtip design was split into four parts each of which has a specific purpose. Section 1 is the first transition area which deforms when the wing tip needs to be folded for ground operations. It also serves as the connection area and transfers load into the base wing. The second section is the positive lift section and provides the majority of the upward lift generated by the wingtip. Section 3 is the second transition area and its main purpose is to adapt to the flight conditions and deflect the fourth section to which it is connected. The fourth section provides the downward lift which serves to counteract the moment generated by the positive lift of the second section. Each of these sections can be seen in Figure 3.12.

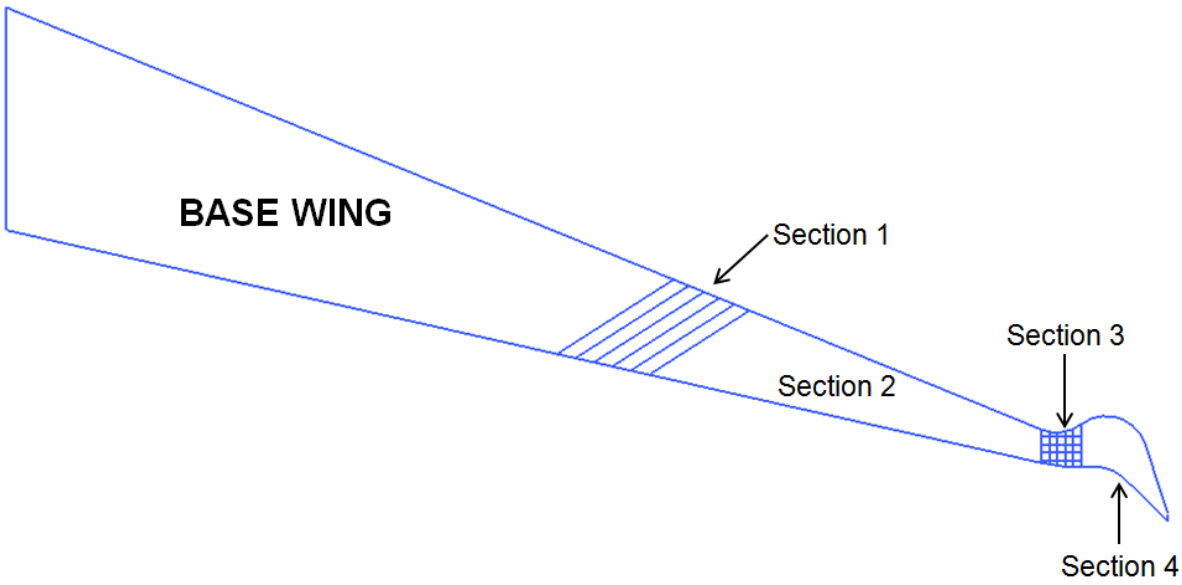

Figure 3.12: Wingtip Extension Sections

A retrofitted aircraft wing can be seen in Figure 3.13.

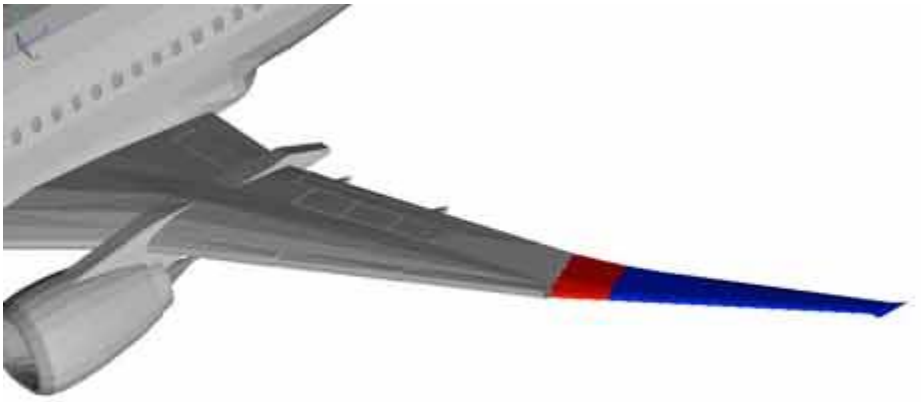

Figure 3.13: Aircraft with Wingtip Extension Retrofit [24]

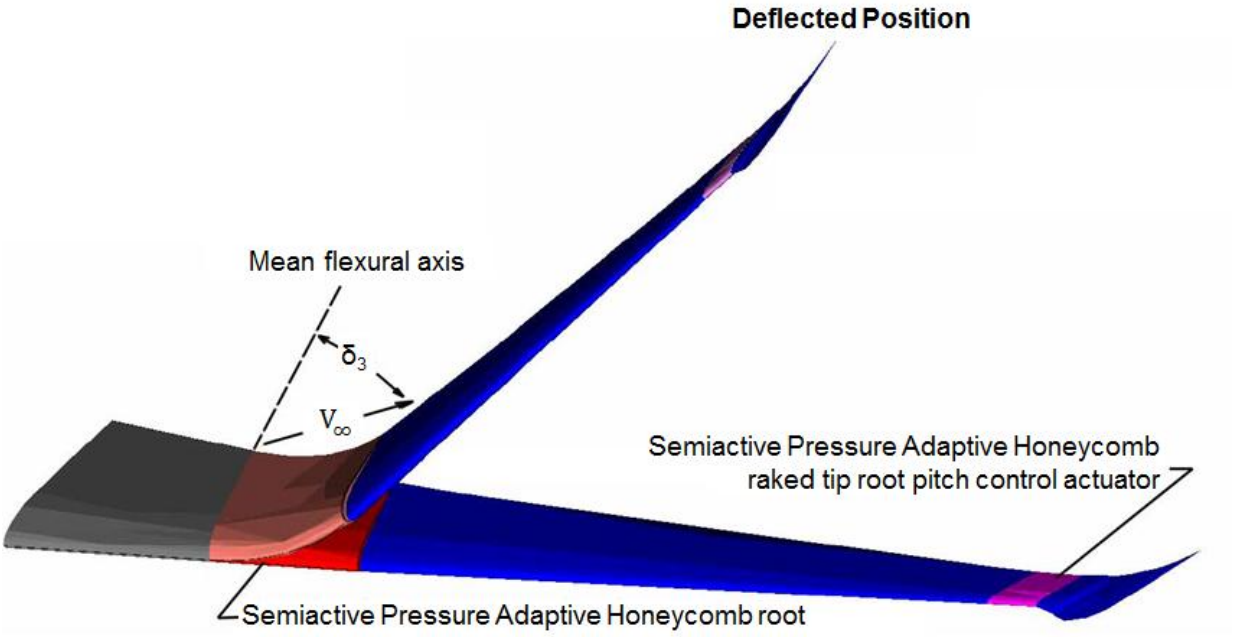

Figure 3.14: Wingtip Extension Fold Angle, Components, and Deflected Position [24]

Figure 3.14 shows the mean flexural axis which is the angle that the wingtip extension folds around. This aspect of the design was based on helicopter and missile designs. The two adaptive sections are shown in red and pink with the upward and downward lift sections shown in blue.

3.2 Wingtip Structure

The wingtip is composed of two main components: pressure adaptive honeycomb and a composite actuator. When no force is applied to the wingtip, it is folded in its ground operation state. When the pressure adaptive honeycomb is pressurized, the wingtip is unfolded to its cruise condition state. In this state, the pressure adaptive honeycomb provides the force on the actuator. Once the honeycomb cells are no longer pressurized, the actuator overcomes the stiffness of the honeycomb and the wingtip returns to its folded state.

3.2.1 Pressure Adaptive Honeycomb

Pressure adaptive honeycomb is a structural component which operates using plain honeycomb with cells that are capable of extending or contracting a significant length when activated. A bladder is located in each of the honeycomb cells. Each of these bladders can be pressurized thereby changing the shape and stiffness of the honeycomb cells.

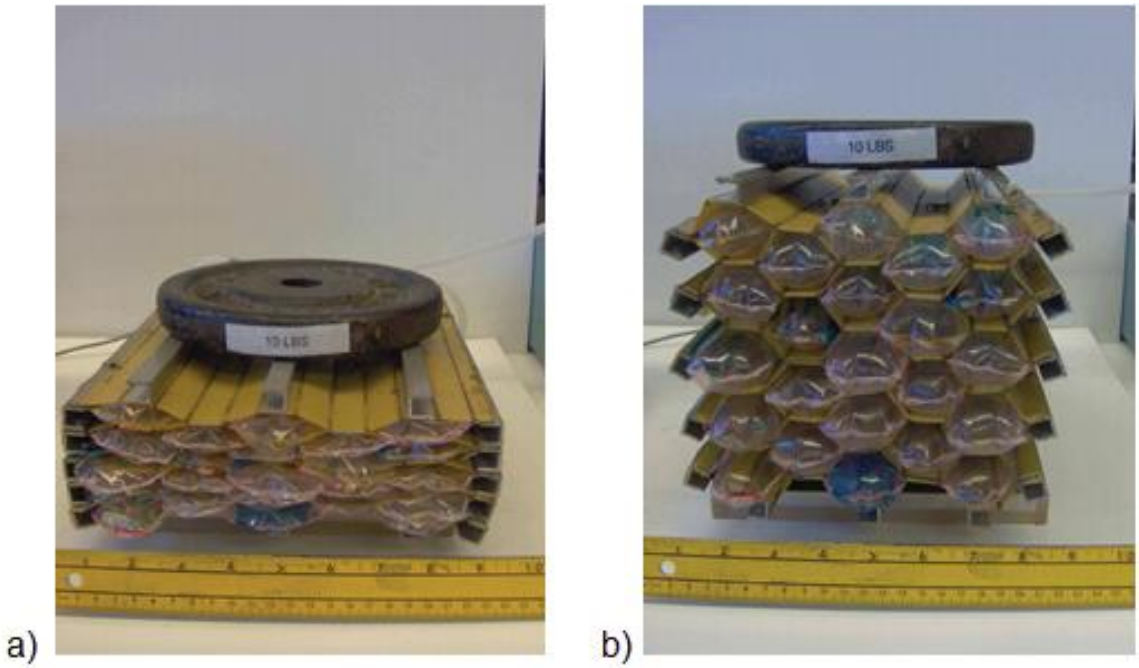

Figure 3.15: Pressure Adaptive Honeycomb Structure, a) Depressurized, b) Pressurized [44]

The honeycomb cell geometry allows control of the deformation of the honeycomb when a particular pressure or force is applied to the structure. Depending on the cell wall thickness and length, the ratio between the stiffness of the cell in the pressurized and unpressurized state can be varied. One benefit to using pressure adaptive honeycomb is its ability to be certified. This stems from its use of well characterized materials simply arranged in manners which lend a high level of adaptability.

A study was done using pressure adaptive honeycomb to show its usefulness in an adaptive trailing edge flap application. It employed a directionally biased pressure adaptive honeycomb system which employed an external force in the form of a spring [44]. Figure 3.16 shows the pressurized and depressurized state of the airfoil.

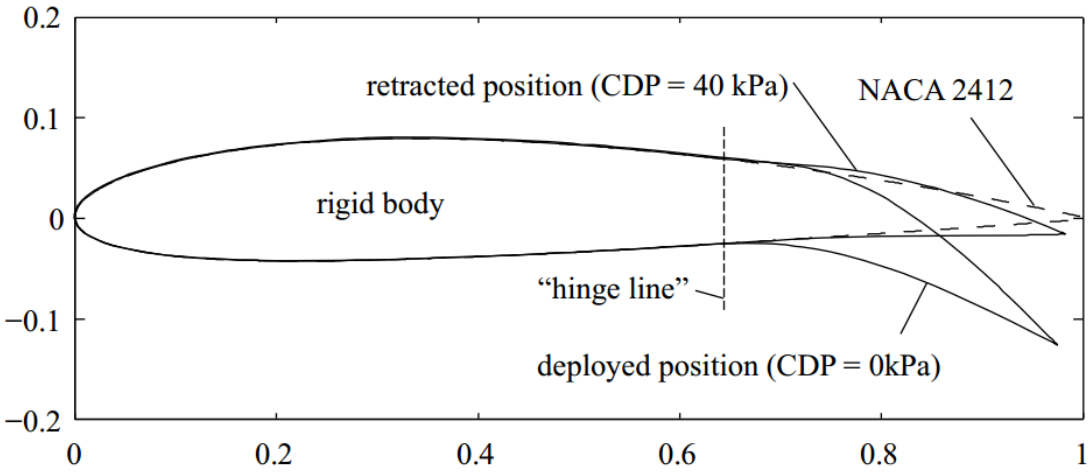

Figure 3.16: Airfoil Deflection using Pressure Adaptive Honeycomb [44]

A wing section was constructed as a proof of concept of the pressure adaptive trailing edge concept (Figure 3.17). This model was then tested in a low-speed wind tunnel test.

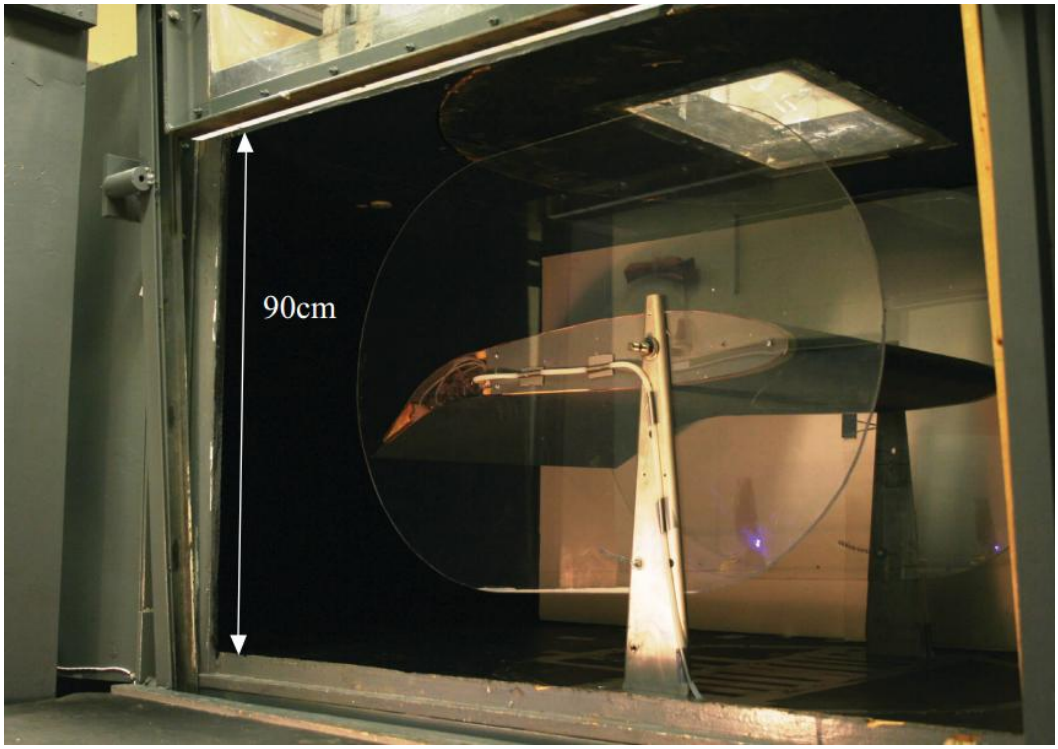

Figure 3.17: Experimental Setup for Pressure Adaptive Honeycomb Trailing Edge [44]

SRI and DARPA carried out a study in which active materials were investigated in a manner which allowed for the comparison of their overall characteristics [45]. Using this data for active materials and the data gathered from the pressure adaptive honeycomb wind tunnel tests, a comparison was made of the volumetric energy density of each material [44]. This is shown in Figure 3.18. It can be seen that pressure adaptive honeycomb is among a group which shows the highest strains.

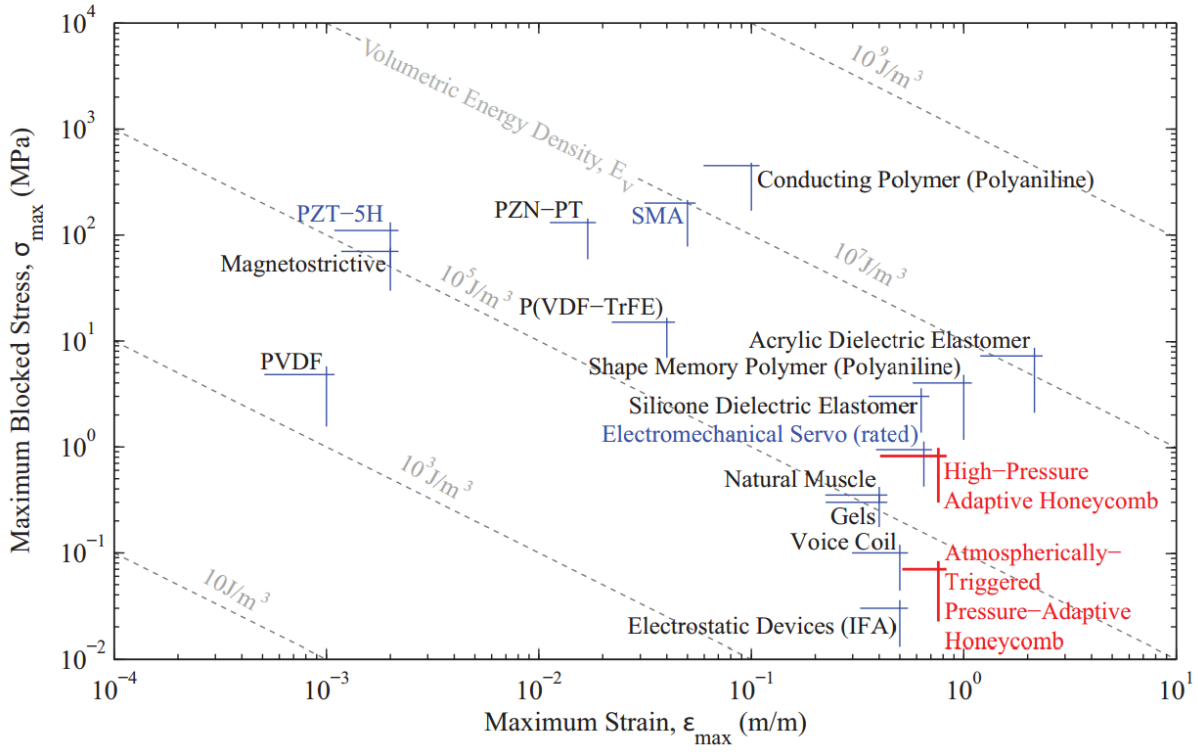

Figure 3.18: Stress and Strain Comparison of Pressure Adaptive Honeycomb to State-of-the-Art Active Materials [44]

The mass-specific energy density of each material can be found by dividing the volumetric energy density by the material density. This was done for the materials shown in Figure 3.18. This comparison can be seen in Figure 3.19.

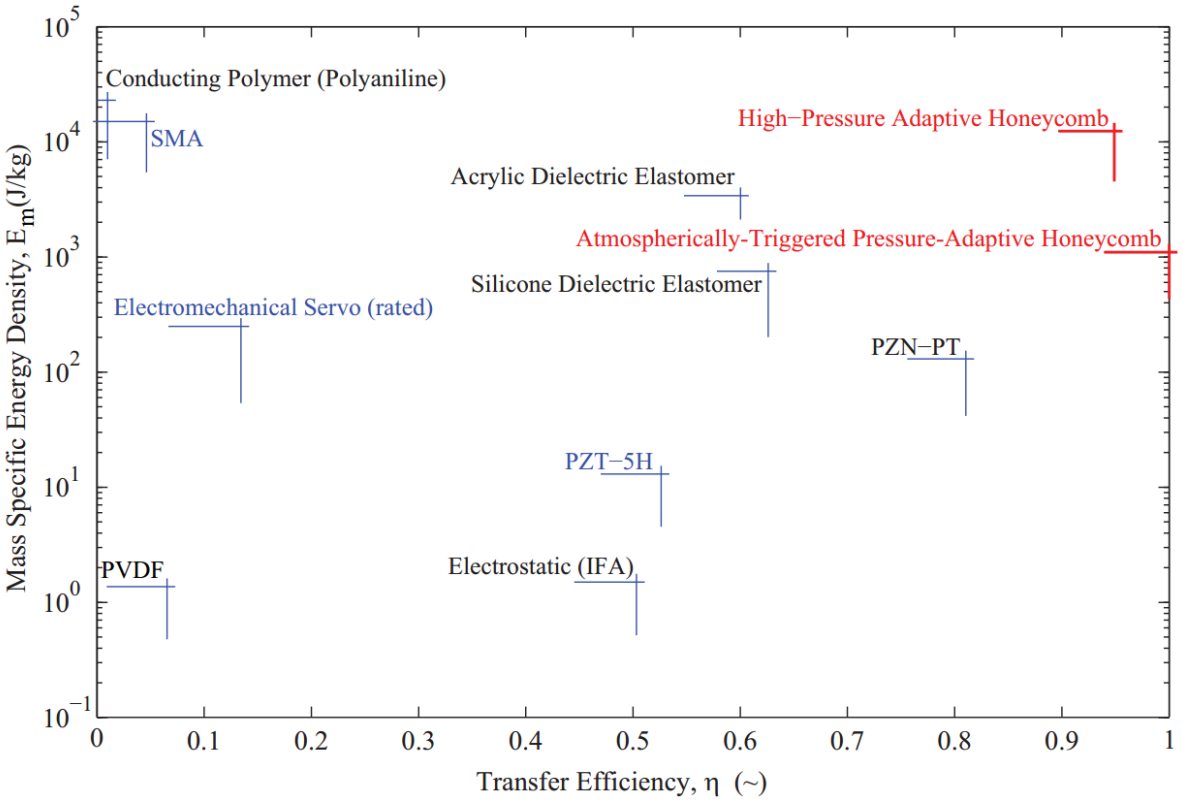

Figure 3.19: Mass-Specific Energy Density Comparison of Pressure Adaptive Honeycomb and State-of-the Art Active Materials [44]

From this comparison, it is seen that the mass specific energy density of the pressure adaptive honeycomb is of the same order of magnitude as shape memory alloys. The difference between these two can be seen in the form of transfer efficiency. While the shape memory alloy has a transfer efficiency of approximately 10%, the pressure adaptive honeycomb is between 90% and 100% depending on the type of pressure adaptive honeycomb. This leads to the conclusion that no onboard energy source is required to actuate the atmospherically-triggered pressure adaptive honeycomb.

The coefficient of lift results found from the wind tunnel tests using pressure adaptive honeycomb are shown in Figure 3.20 in the form of lift curves.

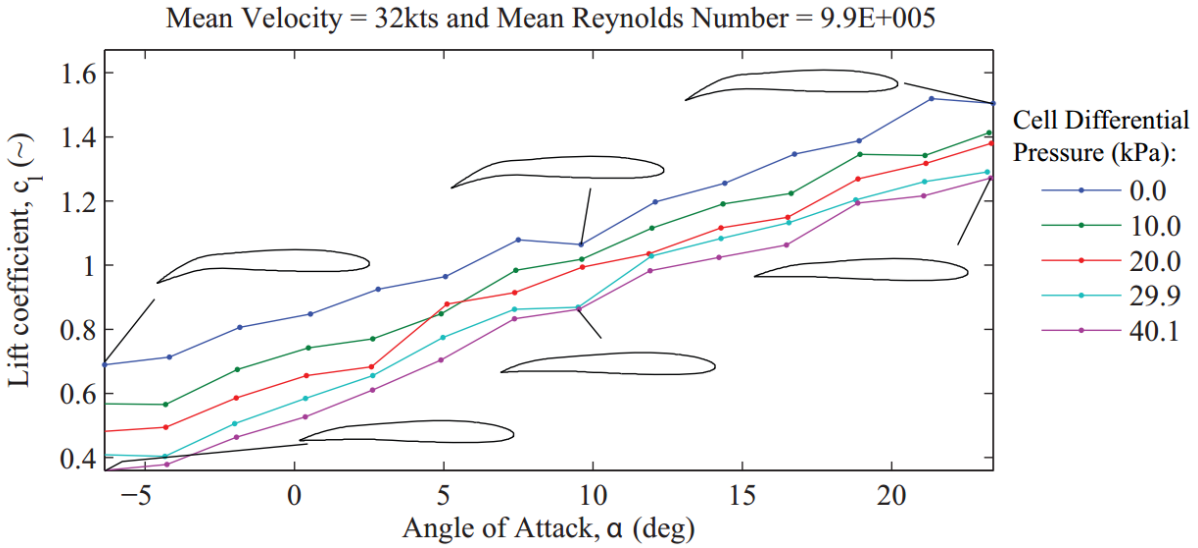

Figure 3.20: Experimental Lift Curve at Different Pressures [44]

3.2.2 Actuator

Typically, to cause movement of a surface or structure a mechanical actuator is used which applies a force and causes a deflection. The actuator used in the wingtip is a composite laminate which has a scheme catered to each of the specific sections' purposes. The analysis was completed using classical lamination theory in which the integration of the stresses within each layer of the laminate through the thickness yields the resultant forces and moments. Figure 3.21 shows the layup of the lamina.

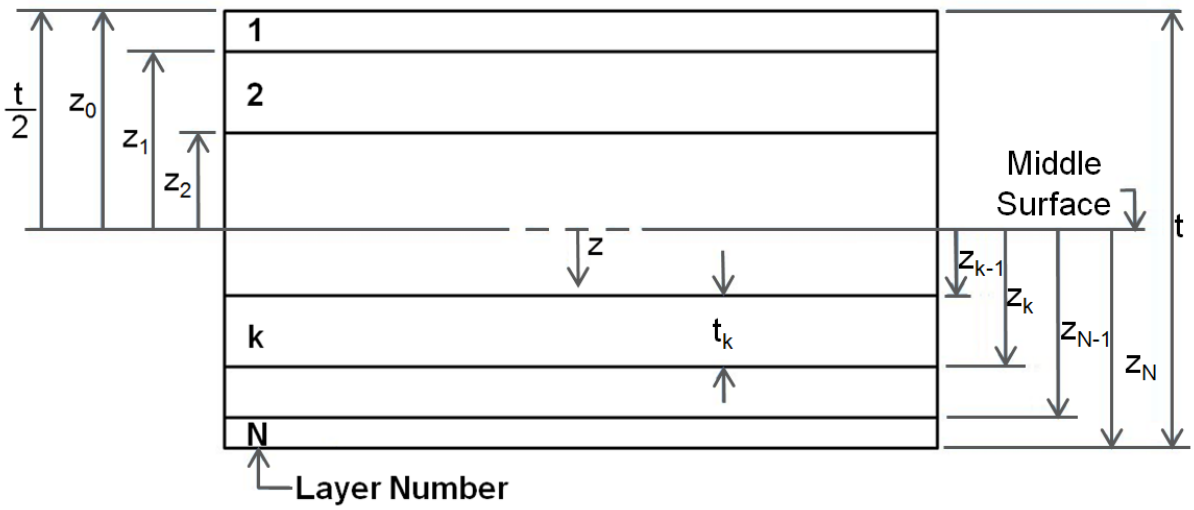

Figure 3.21: Composite Thickness Nomenclature [46]

The equations below show the relation between the lamina stresses and the resultant forces and moments followed by a diagram showing the resultant forces and moments for a laminate:

$$\begin{bmatrix} N_x \\ N_y \\ N_{xy} \end{bmatrix} = \int_{-\frac{t}{2}}^{\frac{t}{2}} \begin{bmatrix} \sigma_x \\ \sigma_y \\ \tau_{xy} \end{bmatrix} dz = \sum_{k=1}^{N} \int_{z_{k-1}}^{z_k} \begin{bmatrix} \sigma_x \\ \sigma_y \\ \tau_{xy} \end{bmatrix}_k dz$$

Equation 3.2 [46]

$$\begin{bmatrix} M_x \\ M_y \\ M_{xy} \end{bmatrix} = \int_{-\frac{t}{2}}^{\frac{t}{2}} \begin{bmatrix} \sigma_x \\ \sigma_y \\ \tau_{xy} \end{bmatrix} z\, dz = \sum_{k=1}^{N} \int_{z_{k-1}}^{z_k} \begin{bmatrix} \sigma_x \\ \sigma_y \\ \tau_{xy} \end{bmatrix}_k z\ dz$$

Equation 3.3 [46]

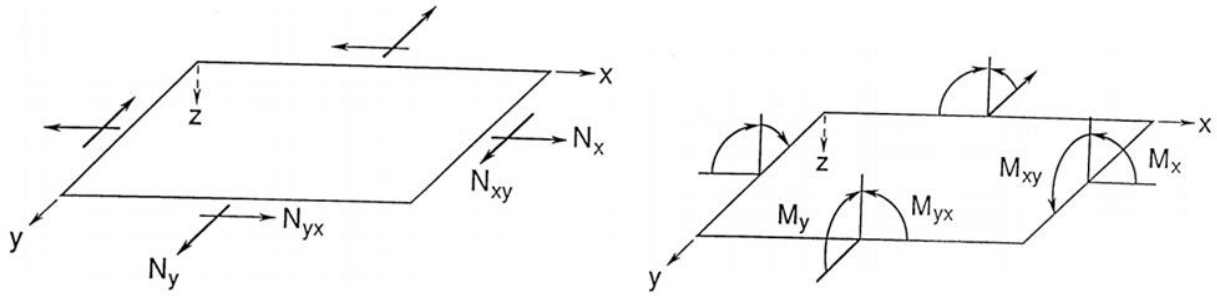

Figure 3.22: Orientation of Forces and Moments [46]

Through substitution of the strain variation through the thickness into the stress-strain relations, the stresses in each lamina can be found in terms of the middle-surface strains and curvatures of the laminate (Eq. 3.4).

$$\begin{bmatrix}\sigma_x\\ \sigma_y\\ \tau_{xy}\end{bmatrix}_k = \begin{bmatrix}\bar{Q}_{11} & \bar{Q}_{12} & \bar{Q}_{16}\\ \bar{Q}_{12} & \bar{Q}_{22} & \bar{Q}_{26}\\ \bar{Q}_{16} & \bar{Q}_{26} & \bar{Q}_{66}\end{bmatrix}\left[\begin{bmatrix}\varepsilon_x^0\\ \varepsilon_y^0\\ \gamma_{xy}^0\end{bmatrix} + z\begin{bmatrix}\kappa_x\\ \kappa_y\\ \kappa_{xy}\end{bmatrix}\right]$$

Equation 3.4 [46]

These relations can then be used to simplify the resultant forces and moments equations until they are in terms of the stiffness matrices. This is shown below:

$$\begin{bmatrix}N_x\\ N_y\\ N_{xy}\end{bmatrix} = \begin{bmatrix}A_{11} & A_{12} & A_{16}\\ A_{12} & A_{22} & A_{26}\\ A_{16} & A_{26} & A_{66}\end{bmatrix}\begin{bmatrix}\varepsilon_x^0\\ \varepsilon_y^0\\ \gamma_{xy}^0\end{bmatrix} + \begin{bmatrix}B_{11} & B_{12} & B_{16}\\ B_{12} & B_{22} & B_{26}\\ B_{16} & B_{26} & B_{66}\end{bmatrix}\begin{bmatrix}\kappa_x\\ \kappa_y\\ \kappa_{xy}\end{bmatrix}$$

Equation 3.5 [46]

$$\begin{bmatrix}M_x\\ M_y\\ M_{xy}\end{bmatrix} = \begin{bmatrix}B_{11} & B_{12} & B_{16}\\ B_{12} & B_{22} & B_{26}\\ B_{16} & B_{26} & B_{66}\end{bmatrix}\begin{bmatrix}\varepsilon_x^0\\ \varepsilon_y^0\\ \gamma_{xy}^0\end{bmatrix} + \begin{bmatrix}D_{11} & D_{12} & D_{16}\\ D_{12} & D_{22} & D_{26}\\ D_{16} & D_{26} & D_{66}\end{bmatrix}\begin{bmatrix}\kappa_x\\ \kappa_y\\ \kappa_{xy}\end{bmatrix}$$

Equation 3.6 [46]

Where:

$$A_{ij} = \sum_{k=1}^{N} \left(\bar{Q}_{ij}\right)_k (z_k - z_{k-1})$$

Equation 3.7 [46]

$$B_{ij} = \frac{1}{2} \sum_{k=1}^{N} \left(\bar{Q}_{ij}\right)_k ({z_k}^2 - {z_{k-1}}^2)$$

Equation 3.8 [46]

$$D_{ij} = \frac{1}{3} \sum_{k=1}^{N} \left(\bar{Q}_{ij}\right)_k ({z_k}^3 - {z_{k-1}}^3)$$

Equation 3.9 [46]

The A, B, and D matrices reveal important aspects of the laminate they characterize. The A-terms are extensional stiffnesses, the B-terms are bending-extension coupling stiffnesses, and the D-terms are bending stiffnesses. Within the design of each of these stiffness matrices, special consideration was taken into the purpose of the actuator in each of the wingtip sections. This will be discussed further in Sections 3.2.3 through 3.2.6.

3.2.3 Section 1: Transition Area

The first section of the wingtip serves as the connection area from the base wing to the wingtip as well as the folding mechanism for ground operations.

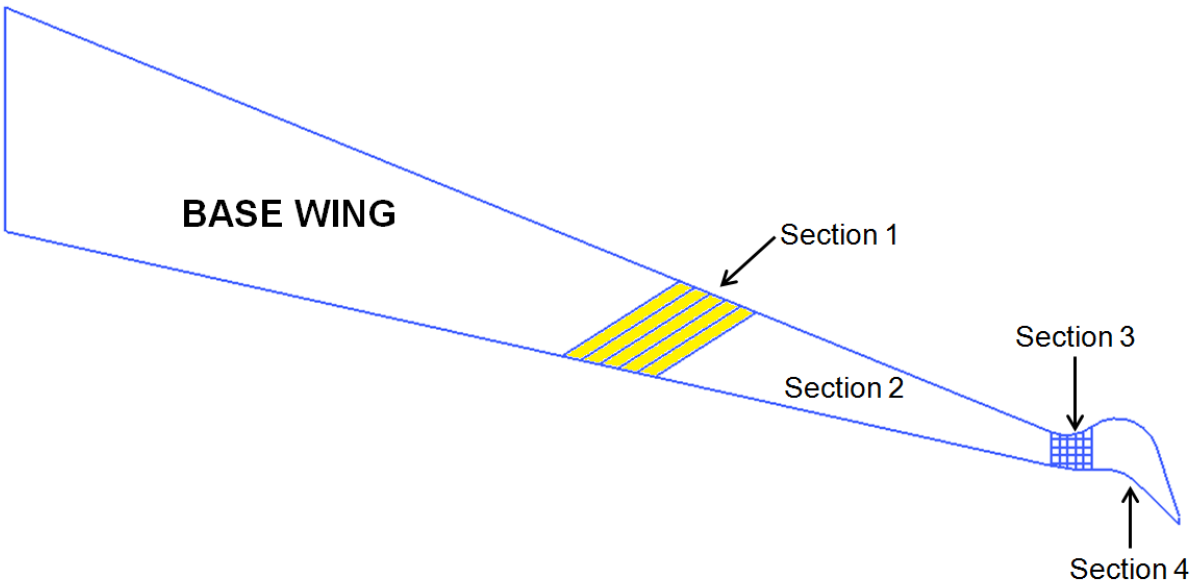

Figure 3.23: Wing Schematic with Section 1 in Yellow

As the connection between the wing and wingtip, section 1 must transfer the loads experienced on the wingtip into the original structure of the wing. Due to the design and shaping of the wingtip, only shear loads must be transferred.

The structure of the first section is made up of pressure adaptive honeycomb and a composite actuator. To ensure a smooth, aerodynamic upper surface, a Kevlar™ layer is installed on the upper surface of the pressure adaptive honeycomb.

When the transition area deforms to the folded state, the Kevlar™ will deform with the honeycomb to maintain the smooth surface. The composite actuator, which provides the force to deform the wingtip into the folded state, was assumed to be located at the mid-plane of the airfoil. It could be located elsewhere within the cross-section of the airfoil, but the mid-plane was chosen to decrease the required deformation of the honeycomb cells to maintain a constant actuator length, shown by red line in Figure 3.24. The actuator does not change length, therefore the

honeycomb must adapt around it. With a mid-plane actuator, the upper honeycomb and lower honeycomb deform around the actuator allowing the upper surface to retract while the lower surface expands. If the actuator is placed at the base of the airfoil, the upper surface must retract the entire length reduction. The blue lines in Figure 3.24 show the surface lengths from the un-deformed configuration. The green lines show the change in surface lengths which must be accommodated by the skin surface to maintain an aerodynamic surface.

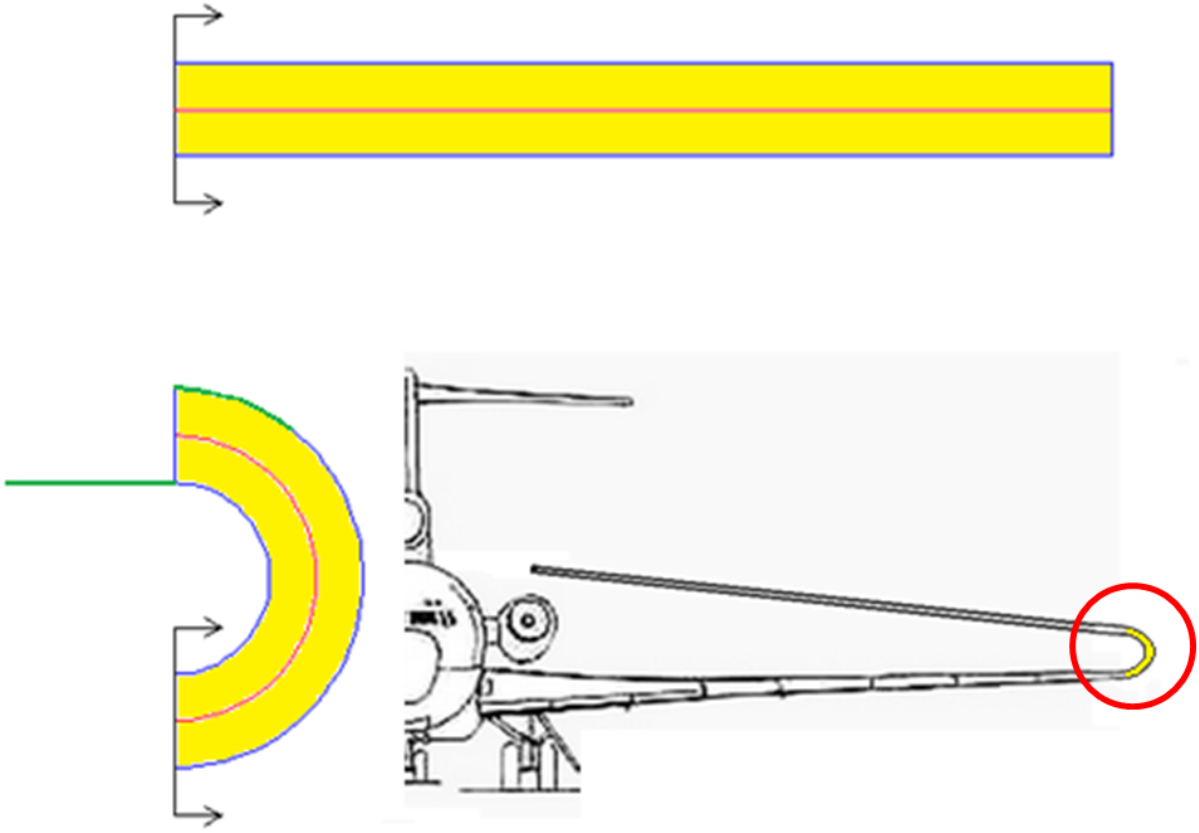

Figure 3.24: Front View of Section 1 Change in Surface Lengths [20]

The actuator design must account for the various load reactions that are desired. First, the unfolded, cruise state was considered. In this state, the pressure adaptive honeycomb is pressurized and provides the deflecting force to the actuator.

At this state, the actuator is responsible for carrying the shear loading on the wingtip extension. To do this, it must have adequate strength in the longitudinal direction. The shear loading also requires the actuator to have adequate strength in the lateral direction due to the folding angle being in the d_3 direction. The longitudinal and lateral directions of the composite actuator are out-of-plane with the wing orientation due to the d_3 direction.

The layup of the Section 1 actuator takes into account the need for twisting under certain loading conditions. With a conventionally constructed wing when the angle of attack is increased or a gust hits the wing from below, the wing inherently twists slightly causing a further increase in the angle of attack as the tip is approached. The first section of the wingtip extension is designed to take advantage of the bend-twist coupling terms and therefore twist in the opposite direction to the otherwise inherent response thus decreasing the angle of attack and prolonging flight prior to tip stall. This aspect of the design causes the tip to adapt without pilot interference. The culmination of these requirements results in the following stiffness matrices.

$$H = High$$

$$L = Low$$

$$\begin{bmatrix} N_x \\ N_y \\ N_{xy} \end{bmatrix} = \begin{bmatrix} H & H & L \\ H & H & L \\ L & L & L \end{bmatrix} \begin{bmatrix} \varepsilon_x^0 \\ \varepsilon_y^0 \\ \gamma_{xy}^0 \end{bmatrix} + \begin{bmatrix} L & L & L \\ L & L & L \\ L & L & L \end{bmatrix} \begin{bmatrix} \kappa_x \\ \kappa_y \\ \kappa_{xy} \end{bmatrix}$$

Equation 3.10

$$\begin{bmatrix} M_x \\ M_y \\ M_{xy} \end{bmatrix} = \begin{bmatrix} L & L & L \\ L & L & L \\ L & L & L \end{bmatrix} \begin{bmatrix} \varepsilon_x^0 \\ \varepsilon_y^0 \\ \gamma_{xy}^0 \end{bmatrix} + \begin{bmatrix} L & L & H \\ L & L & H \\ H & H & L \end{bmatrix} \begin{bmatrix} \kappa_x \\ \kappa_y \\ \kappa_{xy} \end{bmatrix}$$

Equation 3.11

A second Kevlar™ layer can be seen at the base of the lower honeycomb section (Figure 3.24). This provides elongation capability similar to the upper Kevlar™ layer which provides retraction capability.

3.2.4 Section 2: Positive Lift Area

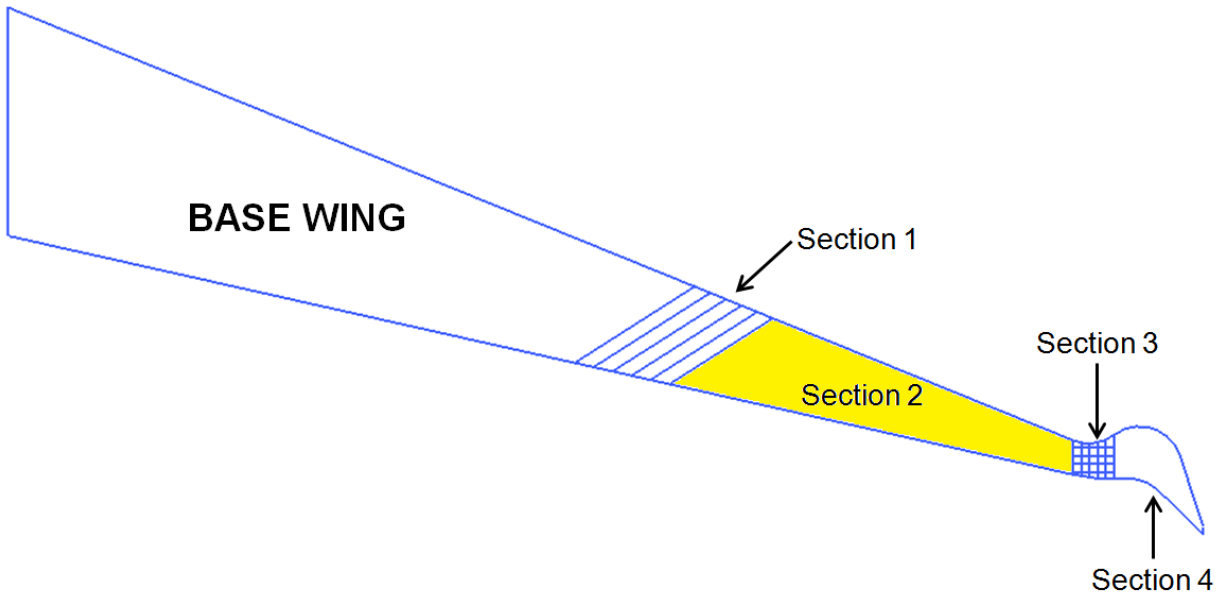

Figure 3.25: Wing Schematic with Section 2 in Yellow

The second section of the wingtip is present to provide positive lift. The outer mold line is designed similarly to a conventional wing but the internal structure varies. Similar to the first section, the second section has two honeycomb sections with a mid-plane actuator. The honeycomb sections are not pressure adaptive because this

section does not require deformation at different stages of the flight profile. The two section honeycomb and actuator internal structure was chosen to simplify the manufacturing and load transfer design of the second section.

The actuator of the second section is similar to that of the first section in that it needs low bending-extension coupling and bend-twist coupling, but it also needs low shear-extension coupling. This results in the following stiffness matrices for the second section actuator.

$$H = High$$

$$L = Low$$

$$\begin{bmatrix} N_x \\ N_y \\ N_{xy} \end{bmatrix} = \begin{bmatrix} H & H & L \\ H & H & L \\ L & L & L \end{bmatrix} \begin{bmatrix} \varepsilon_x^0 \\ \varepsilon_y^0 \\ \gamma_{xy}^0 \end{bmatrix} + \begin{bmatrix} L & L & L \\ L & L & L \\ L & L & L \end{bmatrix} \begin{bmatrix} \kappa_x \\ \kappa_y \\ \kappa_{xy} \end{bmatrix}$$

Equation 3.12

$$\begin{bmatrix} M_x \\ M_y \\ M_{xy} \end{bmatrix} = \begin{bmatrix} L & L & L \\ L & L & L \\ L & L & L \end{bmatrix} \begin{bmatrix} \varepsilon_x^0 \\ \varepsilon_y^0 \\ \gamma_{xy}^0 \end{bmatrix} + \begin{bmatrix} L & L & L \\ L & L & L \\ L & L & L \end{bmatrix} \begin{bmatrix} \kappa_x \\ \kappa_y \\ \kappa_{xy} \end{bmatrix}$$

Equation 3.13

3.2.5 Section 3: Transition Area

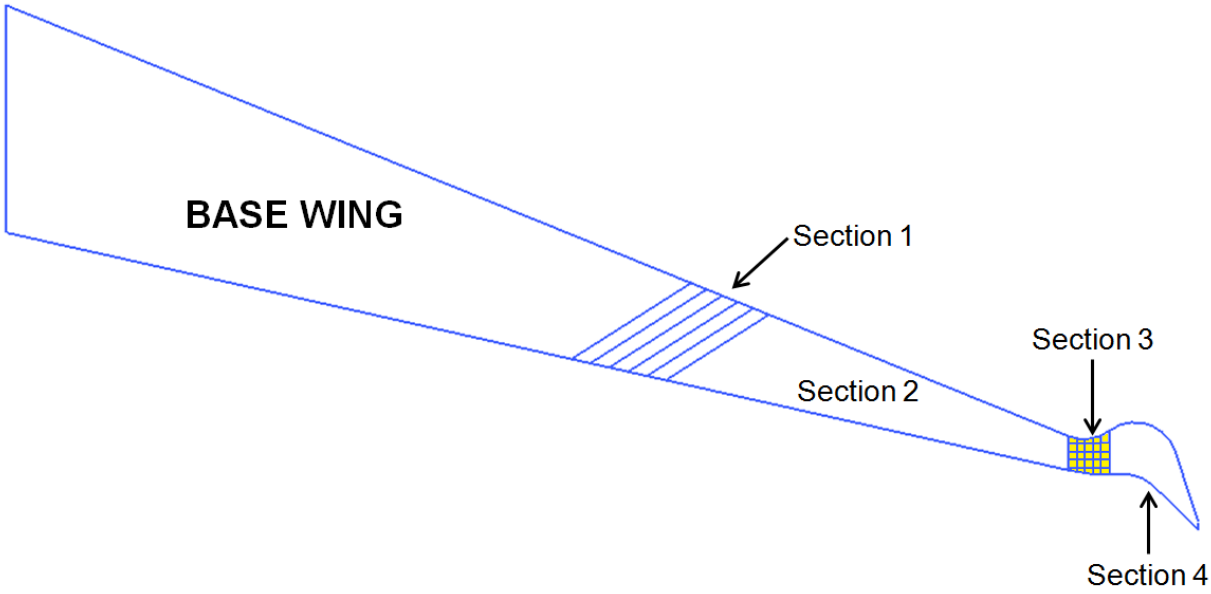

Figure 3.26: Wing Schematic with Section 3 in Yellow

The purpose of this area is to, essentially, “fly” the fourth section into the proper position depending on the flight conditions. The bend-twist coupling attributes enable the third section to adapt the angle of attack of the fourth section to meet the desired lifting attributes.

Similar to the first section, the third section adapts throughout the flight profile, but rather than adapt to the different flight phases, the third section adapts for the different flight conditions experienced during flight. Most commercial aircraft are designed with a system for trimming the aircraft which the pilot has control over. This system is important for adapting to the conditions that the aircraft must fly in such as varying speeds, varying altitude, and weight and balance changes. The third section of the wingtip, similar to the first section, has two pressure adaptive honeycomb sections and an actuator. The pressurization of the pressure adaptive honeycomb is

controlled by the pilot in this section allowing the shape of the honeycomb cells to be controlled thus controlling the shape of the structure. By controlling the shape of the third wingtip section, the fourth section is also controlled; hence when the angle of attack of the third section is reduced it is also reduced in the fourth section.

The actuator in the third section has a similar layup scheme to the first section in that it has bending-twist coupling properties. The stiffness matrices for the third section are shown below.

$$H = High$$

$$L = Low$$

$$\begin{bmatrix} N_x \\ N_y \\ N_{xy} \end{bmatrix} = \begin{bmatrix} H & H & L \\ H & H & L \\ L & L & L \end{bmatrix} \begin{bmatrix} \varepsilon_x^0 \\ \varepsilon_y^0 \\ \gamma_{xy}^0 \end{bmatrix} + \begin{bmatrix} L & L & L \\ L & L & L \\ L & L & L \end{bmatrix} \begin{bmatrix} \kappa_x \\ \kappa_y \\ \kappa_{xy} \end{bmatrix}$$

Equation 3.14

$$\begin{bmatrix} M_x \\ M_y \\ M_{xy} \end{bmatrix} = \begin{bmatrix} L & L & L \\ L & L & L \\ L & L & L \end{bmatrix} \begin{bmatrix} \varepsilon_x^0 \\ \varepsilon_y^0 \\ \gamma_{xy}^0 \end{bmatrix} + \begin{bmatrix} L & L & H \\ L & L & H \\ H & H & L \end{bmatrix} \begin{bmatrix} \kappa_x \\ \kappa_y \\ \kappa_{xy} \end{bmatrix}$$

Equation 3.15

3.2.6 Section 4: Negative Lift Area

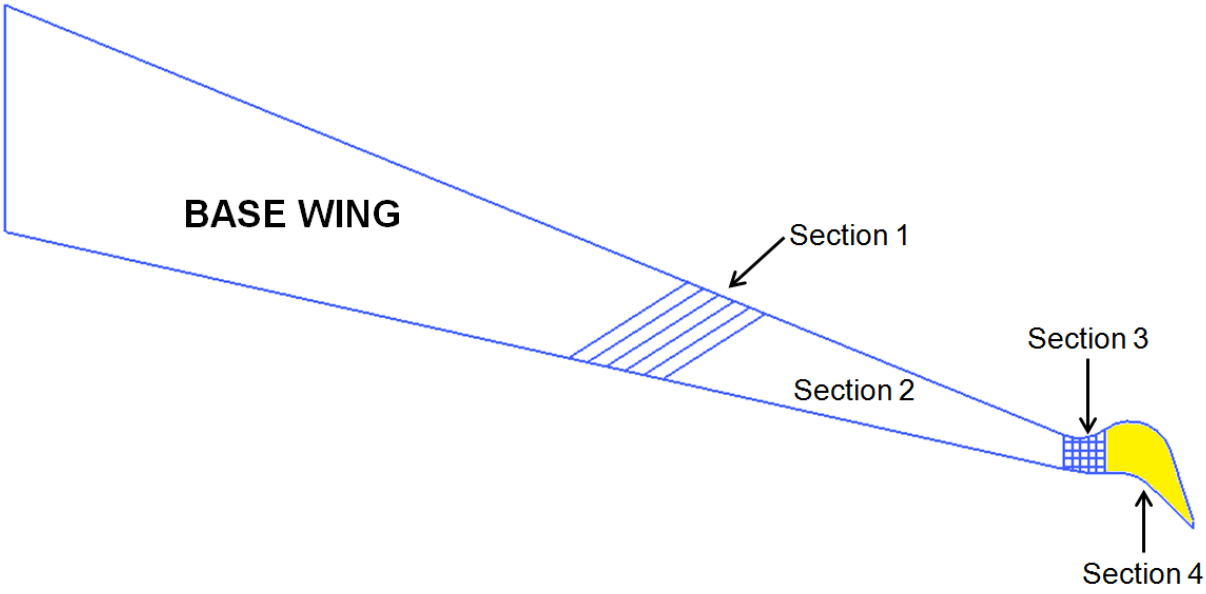

Figure 3.27: Wing Schematic with Section 4 in Yellow

The fourth section is of similar structure and shaping to the second section. The purpose of the fourth section is to provide downward lift to counteract the upward lift of the second section in terms of the bending moment at the root of the wingtip. The structure of this section is the same as the second section except for slight variation in the scheme of the actuator layup in that not as much structure is necessary because the fourth section has a lower loading than the second section.

4 Gust Alleviation

Gusts are a unique phenomenon which cannot be prevented during aircraft flight; the aircraft must be designed to handle them in an acceptable manner. FAR 25 requirements state that the V-n diagram must "be used in determining the airplane structural operating limitations as specified in Section 25.1501" [47]. The V-n diagram, as required by FAR 25 regulations, must have a positive limit no less than 2.5 for the maneuvering load factor, n, and -1 for the negative limit load factor at speeds up to V_C. From V_C to V_D, the load factor varies linearly until it reaches zero at V_D. The gust load factors are required to be met at three different design speeds: V_B, V_C, and V_D. These values are shown in Table 4.1 for a Boeing 737-400 [48].

Table 4.1: FAR 25 Requirements for Discrete Gust Velocities (derived)

Aircraft Design Speed	Gust Velocity	
	Altitude (0-20,000 feet)	Altitude (50,000 feet)
V_B	66 fps	38 fps
V_C	50 fps	25 fps
V_D	25 fps	12.5 fps
Flaps Extended	25 fps	-

Figure 4.1 and Figure 4.2 show the V-n diagrams accounting for gust loading with flaps retracted and extended [48]. The points plotted are coincident acceleration and speed measurements.

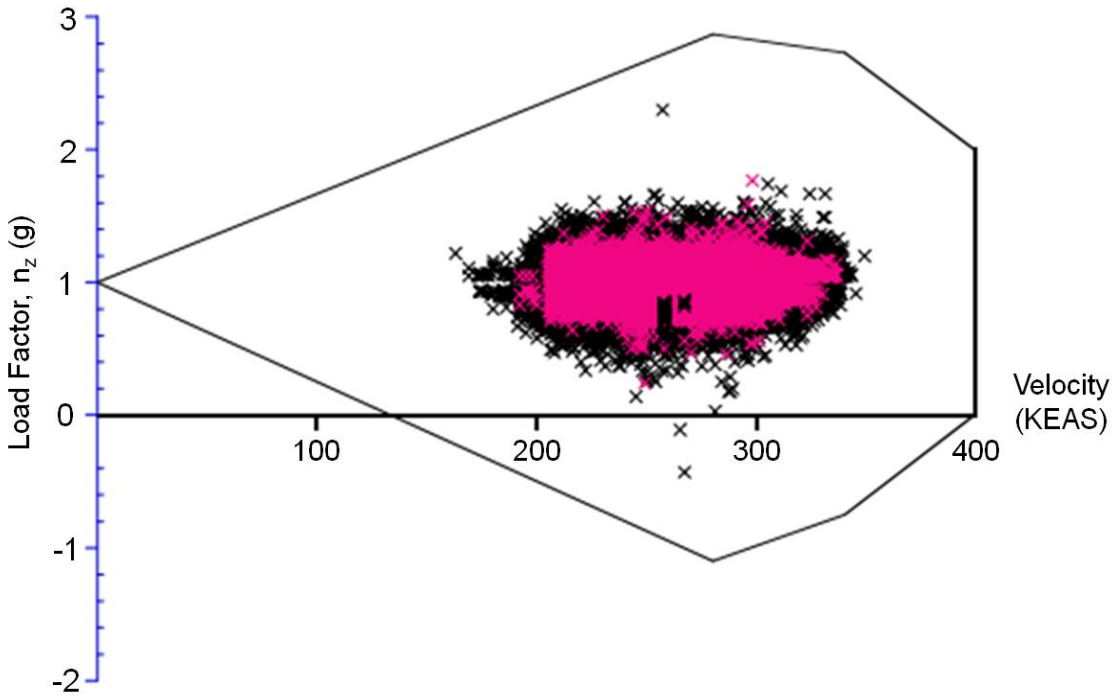

Figure 4.1: Coincident Gust Load Factor and Speed Diagram for 737-400, Flaps Retracted [48]

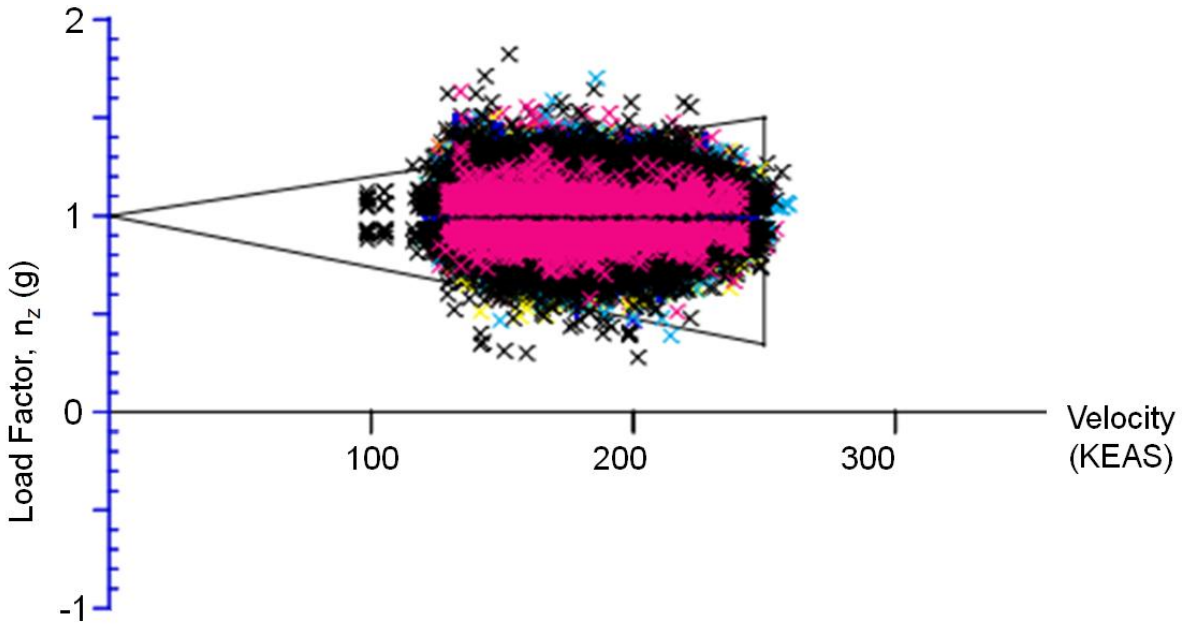

Figure 4.2: Coincident Gust Load Factor and Speed Diagram for 737-400, Flaps Extended [48]

It is seen in Figure 4.2 that a significant number of gust accelerations occurred outside the V-n diagram limits when the flaps were extended. With the addition of the Prandtl-tailored adaptive aerocompliant wingtip extension this would be exacerbated due to the increase in wing area. When the wing area of an aircraft is increased the area on which the gust acts increases which often times results in a rougher ride for passengers. The increased gust response also causes increased loading which would result in an even greater number of points in Figure 4.2 to be outside the V-n diagram ranges.

This provides an opportunity for the gust mitigation benefits for which the wingtip was designed. When the gust hits the wingtip, it acts as a force outside the predicted wing loading. This forces the pressurized honeycomb cells to retract or expand proportionally to the force which is applied whether it is a downward gust or upward gust. With the deformation of the cells, the wingtip essentially relieves the gust force because the pressurized honeycomb cells are unable to withstand the increased force. Once the gust passes, the wingtip will return to its pre-gust shape because the force which caused the honeycomb cell deformation is no longer present.

This gust alleviating design also prevents the wing root bending moment from surpassing the structural load carrying capacity of the base wing. This is shown in Figure 4.3 with a comparison between a conventional wing, a conventional winglet design added, and a Prandtl-tailored adaptive aerocompliant wingtip extension retrofitted on the same base wing.

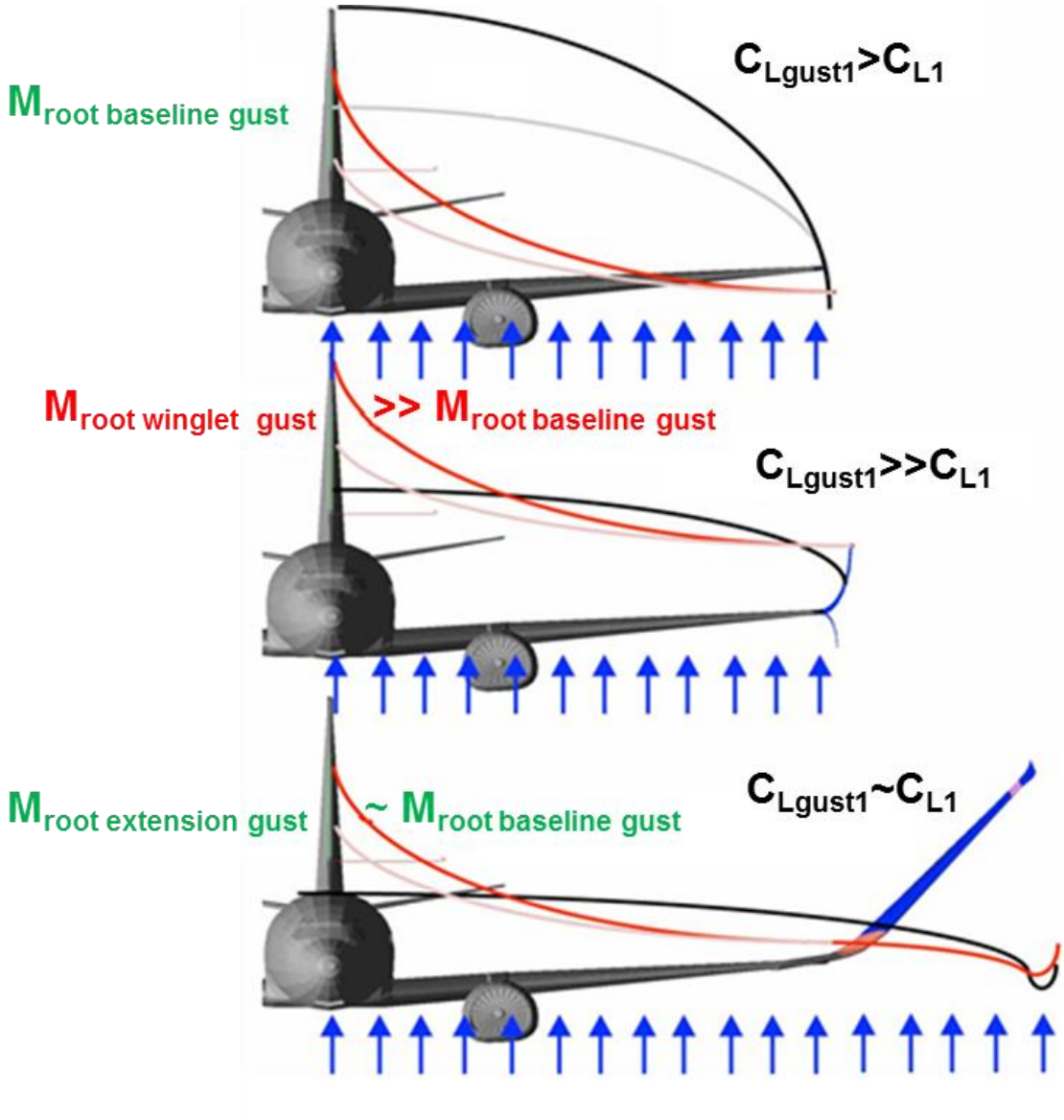

Figure 4.3: Gust Response Comparison for Conventional Wing (top), Conventional Winglet Retrofit (middle), Wingtip Extension Retrofit (bottom) [24]

Figure 4.5 shows a similar concept where the pressure adaptive honeycomb used in the wingtip is used in the trailing edge of a wing. When the gust force acts on the trailing edge it deforms in the same direction and relieves the added force. After the gust stops, it returns to the proper flying configuration. This can be compared to Figure 4.4 in which the wing has a flap system with no pressure adaptive honeycomb.

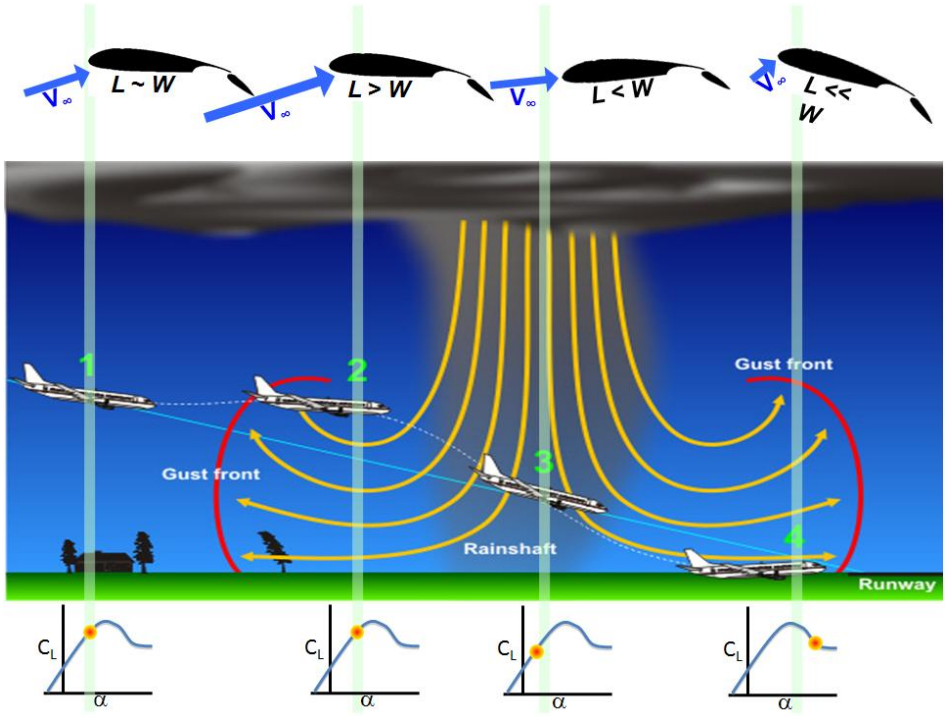

Figure 4.4: Flap System Gust Reaction Scenario [49]

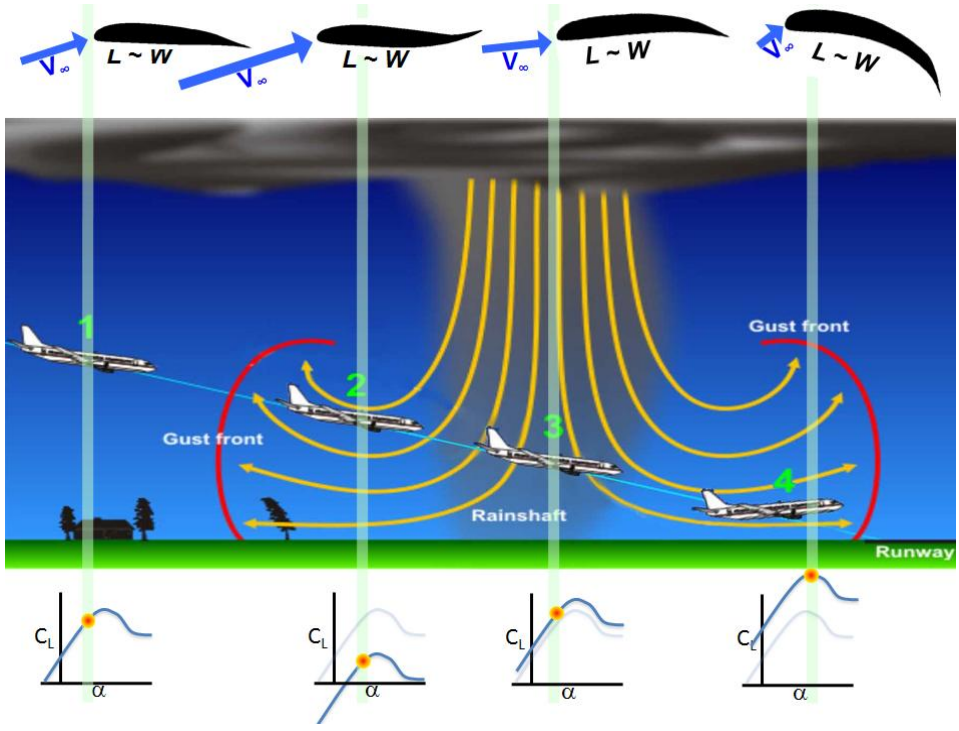

Figure 4.5: Pressure Adaptive Honeycomb Trailing Edge Gust Reaction Scenario [49]

As seen through a comparison of Figure 4.4 and Figure 4.5, the use of pressure adaptive honeycomb as a form of gust alleviation introduces a safety precaution in the form of flight into terrain due to gust field alleviation. The adaptability of the pressure adaptive honeycomb allows the aircraft to maintain a sustainable angle of attack and prevents stall near the gust front. Whereas in the scenario with the flap system, the airplane risks reaching an angle of attack which is not sustainable leading to the wing stalling and impact with terrain. This is of particular interest for takeoff and landing due to the close proximity to the ground.

Along with safety considerations, the gust alleviation properties of the pressure adaptive honeycomb allow for flights to take off and land even when weather conditions are less than optimal. Figure 4.5 shows that the aircraft is able to maintain the optimal flight path through the gust field rather than the volatile, unpredictable pattern shown in Figure 4.4.

5 Safety and Operational Considerations

A major concern with new concepts for commercial aircraft is safety. While certifying a new material is one obstacle to surmount, proving that its application in a new component is another obstacle entirely. This is why the Prandtl-tailored adaptive aerocompliant wingtip extension is a wingtip design and not a new base wing design. By starting with the base wing and maintaining the original technology which has been approved and tested, the wingtip only serves as a modification for improvement on what can already be attained. The wingtip is not a primary structure; it is a secondary structure in which a failure can take place and not cause immediate danger.

An additional safety feature within each honeycomb cell bladder is an over pressurization valve. The cells will be designed with a maximum pressurization and once that point is met the cells will release the excess air.

5.1 Ground Operations

Gate spacing and taxi are not the only limitations placed on wingspan. Hangar dimensions and storage are also a concern. Similar to the gate spacing requirements, the hangar places a hard limit on the wingspan of the aircraft but it places a height limitation as well.

Figure 5.1: Aircraft Approaching Hangar [50]

For this reason, although the layout of the wingtip is applicable to a variety of aircraft each application should be designed for that specific aircraft model to avoid overdesigning the wingtip, particularly the fold mechanism. Typically the highest point on a commercial aircraft is the vertical tail. This was used as the height limit from which the angle that the tip must be folded was attained. Without this limit, the fold may be designed as more robust than what is required resulting in pressure adaptive honeycomb cells being installed where conventional honeycomb could be installed, increasing cost and complexity.

Another consideration during ground operations is storage. The aircraft is not always in operation when it is outside where it is exposed to wind and gusts. Although the wing tip would be in its folded state during these times, variation in the air could cause wingtip movement. To avoid an unexpected unfolding of the wingtip extensions, a tie-down strap will be connected to each wingtip extension in Section 3. Since Section 2 and Section 4 taper into and out of Section 3, respectively, the straps, once

tightened, will stay secured to the wingtip extensions. The other end of each of these straps will be secured to the nose landing gear assembly. This is shown in Figure 5.2.

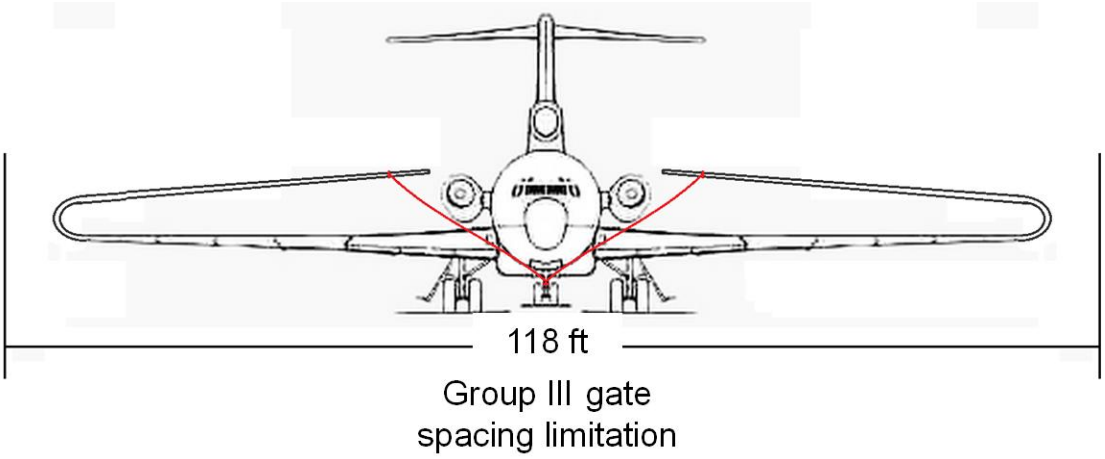

Figure 5.2: Wingtip Extension Storage Tie-Down Straps (red) and Gate Spacing Limit (Boeing 727) [20]

5.2 Takeoff and Landing Operations

During takeoff and landing the pressure adaptive honeycomb cells are to remain pressurized. To do this, air is routed from the engine and into the bladders within each cell. Once cruise altitude is reached the pressure at that altitude is used to maintain pressurization of the cells with the engine air only being used to make slight adjustments depending on the flight conditions.

5.3 Climb, Cruise, and Descent Operations

FAR 25 aircraft typically require a minimum of triple redundancy in all systems to reach the one failure in one trillion criterion for flight safety. Similar to this, the wingtip will be triply redundant as each pressurization bladder will be segmented into three

separate vessels. In the event that one of the three vessels losses pressurization, the remaining two vessels will be capable of overcoming the failed vessel.

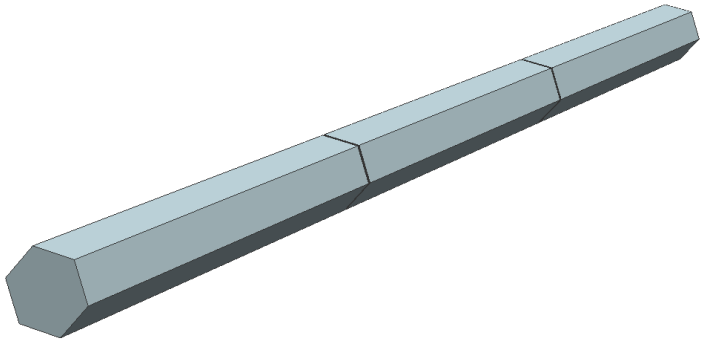

Figure 5.3: Three Section Honeycomb for Failure Redundancy

Additionally, each cell will have an over pressurization valve. During takeoff and landing the engine air is used to pressurize the cells to the desired level. Once the aircraft begins climbing the outside pressure will decrease causing an increase in the cell differential pressure if it is held constant. To ensure proper pressurization through these flight segments, the engine will continue to provide air to the honeycomb cells but the cells will simply release the air which is not needed. This manner of pressurization was chosen as a safety precaution in the event that a loss in altitude takes place. Once the cruise altitude is reached, the outside air pressure is used to maintain proper pressurization of the honeycomb cells with the engine air used only for adjustments.

5.3.1 Deflagration Line

Using the engine air as a pressurization method introduces safety concerns in the event of engine out operation. During cruise, the majority of the cell pressurization

is from the outside pressure differential therefore engine out will not have a significant impact. This is not the case for the climb and descent phase. If the engine malfunction causes a loss in air that prevents one segment of honeycomb from pressurizing properly, the wingtip would still be operational due to triple redundancy. If the engine malfunction causes a loss of two or more of the honeycomb segments, then the deflagration line can be used.

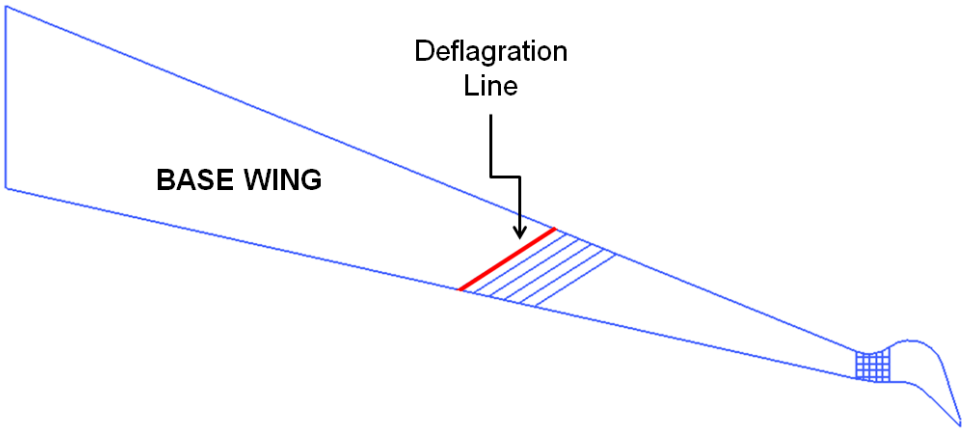

Figure 5.4: Deflagration Line Location

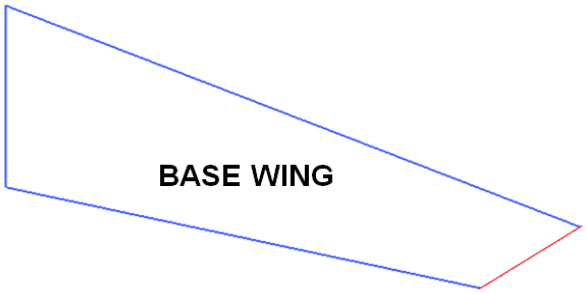

Figure 5.5: Wing Geometry Following Deflagration Line Usage

The deflagration line is a line installed in the wingtip root connection area which allows for the pilot to release the wingtip during flight. This is at the pilot's discretion and is only intended for use if the pilot deems the wingtip to be a hindrance to safe flight operation. If the deflagration line is blown, the wingtip is no longer attached to

the base wing and the base wing becomes the only operational lifting wing surface. This is acceptable since the base wing was already designed for the aircraft operation and is suitable for full operational flight. The release of the wingtip would be cause for an emergency landing but in the event of a transoceanic flight the nearest suitable landing site may be a considerable distance away. It this situation, the aircraft would be able to continue flying similar to an unmodified model simply with less efficient performance in comparison to the wingtip version.

5.3.2 Lightning Strike

Lightning strike is an important safety concern to consider. When an airplane is struck by lightning, components made of ferromagnetic material can become severely magnetized and electrical systems damaged. Important systems which risk damage include: electrically controlled fuel valves, power feeders, generators, and electrical distribution systems [51].

Safety precautions are taken in the design of the base wing for lightning strike occurrences. Zones are used to indicate how prone certain areas of the aircraft are to lightning strike. These zones are shown in Figure 5.6.

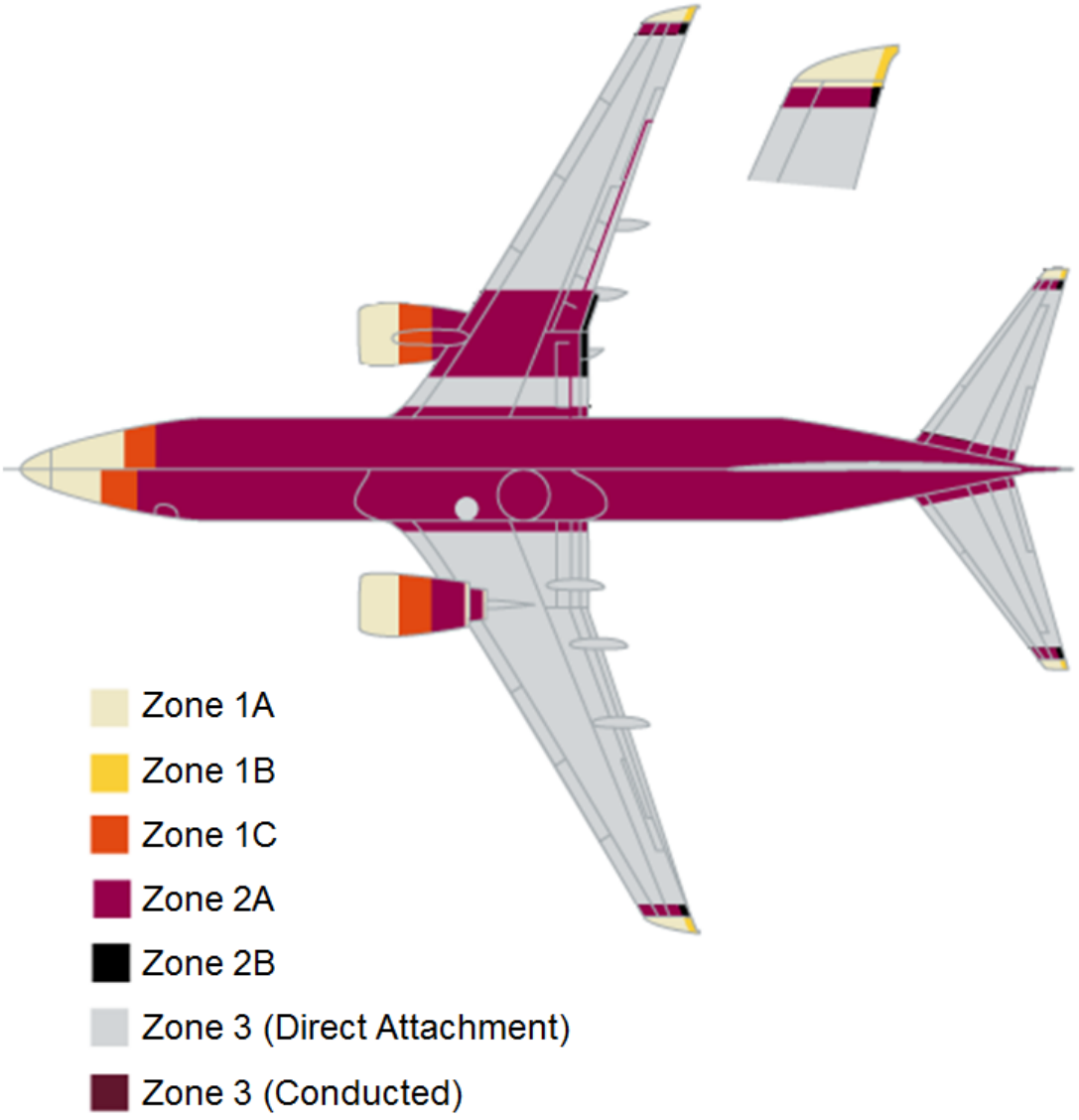

Figure 5.6: Lightning Strike Zones [51]

Zone 1: area likely affected by the initial attachment

Zone 2: area likely having a swept, or moving, attachment

Zone 3: area which may experience conducted current without actual attachment

Table 5.1: Lightning Strike Zone Definitions [51]

Zone	Description	Definition
1A	First return strike zone	Surfaces where first return is likely during lightning channel attachment, low expectation of hang on
1B	First return strike zone with long hang on	Surfaces where first return is likely during lightning channel attachment, low expectation of hang on
1C	Transition zone for first return strike	Surfaces where first return strike of reduced amplitude is likely during lightning channel attachment, low expectation of hang on
2A	Swept strike zone	Surfaces where first return of reduced amplitude strike is likely during lightning channel attachment, low expectation of hang on
2B	Swept strike zone with long hang on	Surfaces where lightning channel carry subsequent return strike is likely to be swept, high expectation of hang on
3	Strike locations other than Zone 1 and 2	Surfaces not in Zone 1A, 1B, 1C, 2A, 2B where attachment of lightning channel is unlikely, surfaces between other zones and/or conduct substantial electrical current between direct or swept strike attachment points

A few methods of lightning strike protection which are currently used on metal aircraft include wire bundle shields and ground straps. For composite structure, wire mesh, aluminum spray coating, embedded metallic wire, diverter strips, coated glass fabric, and bonded aluminum foil.

For the Prandtl-tailored adaptive aerocompliant wingtip extension, a wire mesh will be laid up within the composite skin of the wingtip. This will distribute the electrical current through the top layer and prevent electromagnetic energy which is above a satisfactory level from entering the aircraft's internal spaces and negatively impacting the systems.

5.3.2.1 Lightning Strike Test

Although a wire mesh will be used within the composite skin of the aircraft, it is necessary to test the performance of the pressure adaptive honeycomb when subjected to a lightning strike. To do this a wing section was manufactured with a foam core and pressure adaptive honeycomb trailing edge actuator. This layout is shown in Figure 5.7.

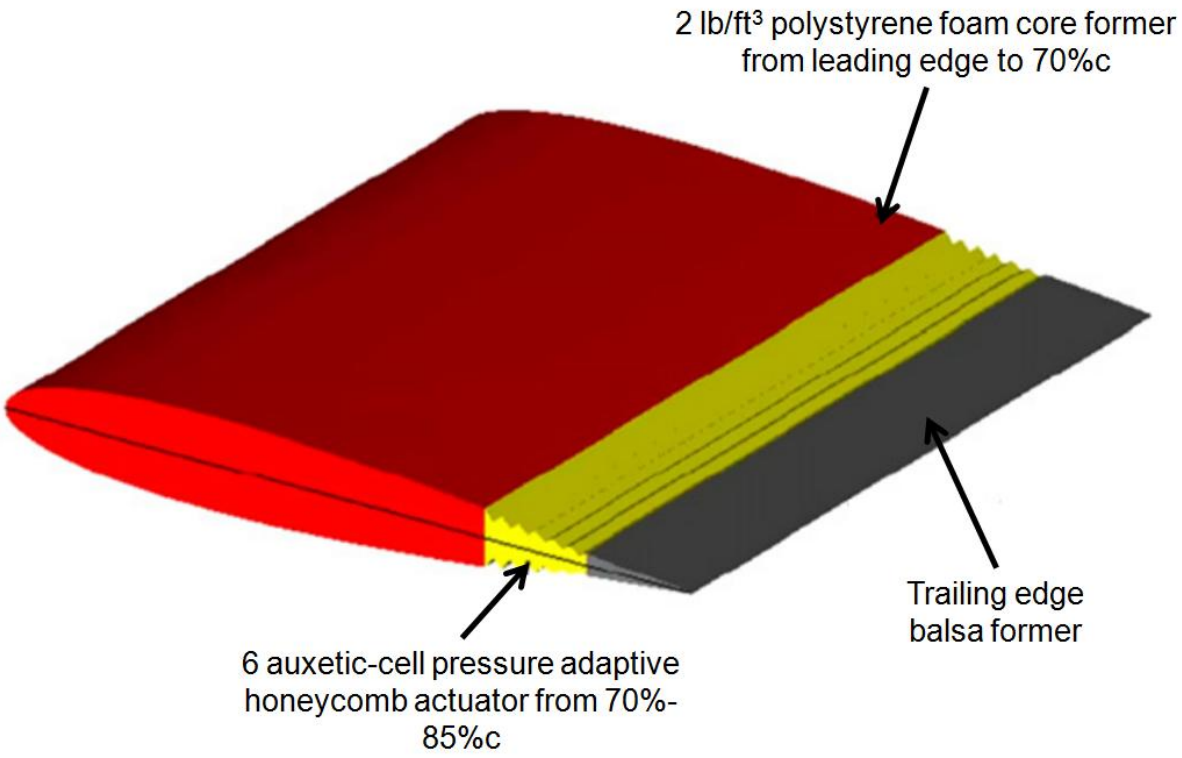

Figure 5.7: Lightning Strike Test Model Layout [49]

Using the Transportation Research Institute's Lightning Strike Test Range, a full strike run was completed. Two series of shots were run under the following conditions: 58% humidity, 22 degrees Celsius, and 100.6 kPa atmospheric pressure [49]. The test setup is shown in Figure 5.8.

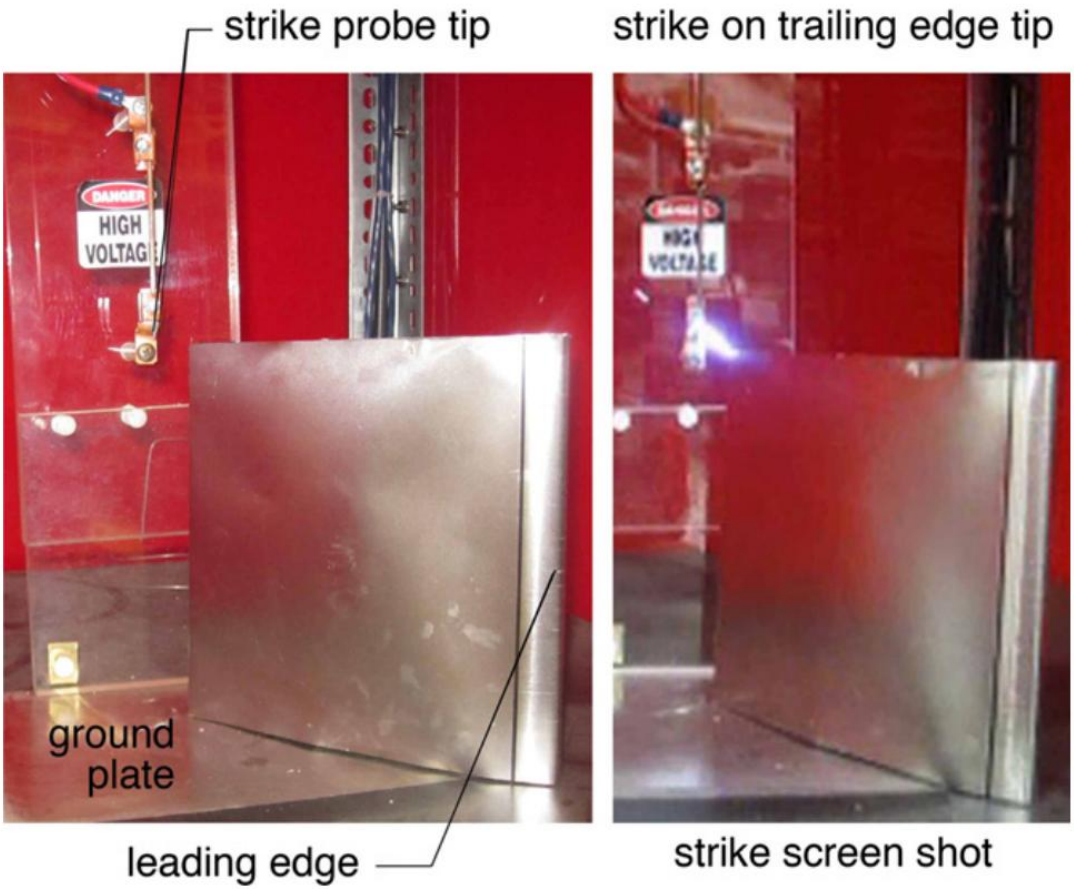

Figure 5.8: Setup of Wing Section Model during Lightning Strike Testing [49]

The skin over the actuator is a 3 mil aluminum sheet which allows deformation through the use of sliding panels resulting in the expansion and contraction of the skin surface [49]. During the first series of shots it was determined that the skin panels have a tendency to spot weld themselves together preventing further cycles. Following this discovery, the model was disassembled and the skin panels were cleaned and refinished. Then a 25 μm thick Teflon layer was applied to the skin surface. A second series of shots was completed. Following the addition of the Teflon coating, no complications were encountered which prevented the proper functioning of the trailing edge actuator. The second series of shots were run up to 256 kV of voltage and 280 A of current.

6 Analytical Proof of Concept Demonstration of Wingtip Extension

To prove the benefits of the conceptual wingtip outlined in the previous chapters, a proof of concept was performed analytically to verify the performance improvements. The aircraft chosen for this analysis was a Boeing 727-200. This was due to the availability of technical information in public sources and while there are still 727-200s still in-service, they are no longer in production rendering this study minimally controversial.

The analysis began with a market analysis to determine whether the preliminary predicted benefits were justifiable and marketable. Then fifteen different wingtip shapes were designed and analyzed based on their aerodynamic performance. This performance was then compared to the base model airplane performance from which a final judgment was made as to the value which these wingtips add to an aircraft.

6.1 Preliminary Market Analysis

The Boeing 727 line was a successful mid-size, narrow body jet which was designed to service high-altitude airports while maintaining an acceptable fuel efficiency level. The first flight of the 727 was in 1963 after which over 1,800 have been built with some still in service as converted freighters.

While the 727 market provides a good basis from which to judge the viability of the conceptual wingtip, the entire commercial market must be considered because the theory which supports this design is applicable to nearly all commercial aircraft. For this reason, the fuel consumption and revenue hours flown by United States passenger and cargo flights were compared from 2000 to 2013 to evaluate the trends

industry is following. Then the effects of increasing wing span were estimated using Class I methods [52].

6.1.1 Commercial Industry

The Research and Innovative Technology Administration (RITA) Bureau of Transportation Statistics tracks commercial air traffic revenue hours and fuel consumption for United States air carrier passenger and cargo services [53]. This data was gathered from 2000 to 2013, combining passenger and cargo hours for a combined revenue hour value which is equivalent to the hours that an aircraft is airborne. From the revenue hour and fuel consumption values gathered for each year, the change in each was calculated for one year increments. This resulted in the trend lines shown in Figure 6.1. The change in fuel efficiency was calculated by finding the difference between the change in revenue hours and the change in fuel consumption.

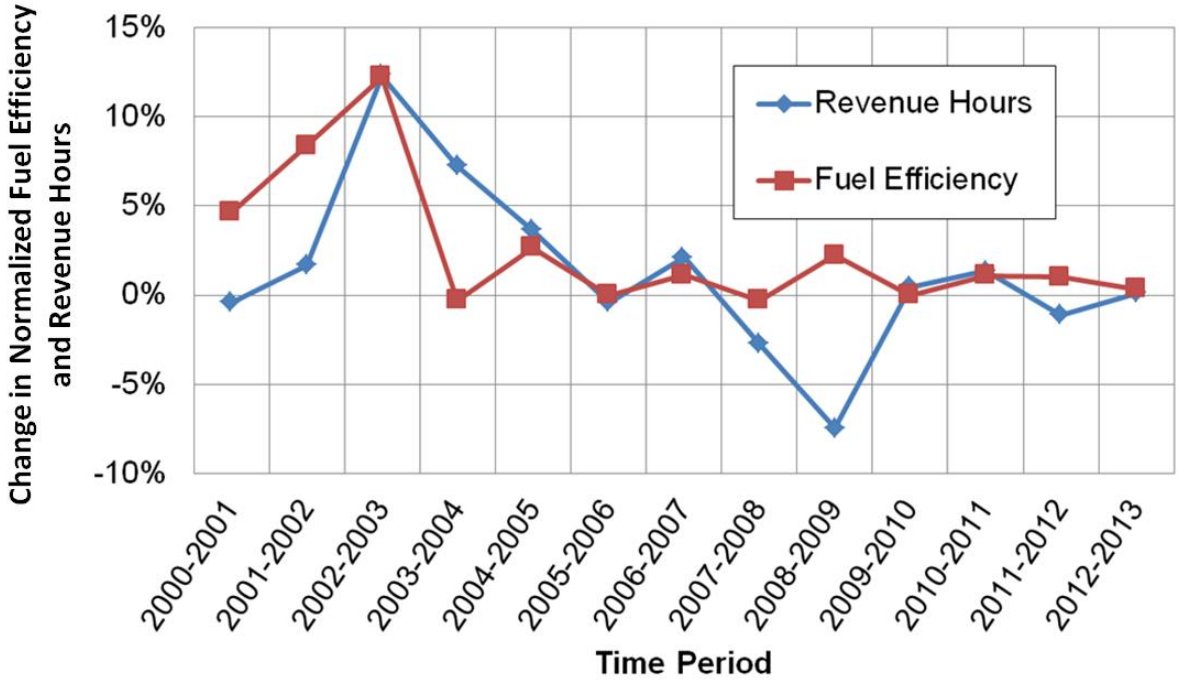

Figure 6.1: Fuel Efficiency and Revenue Hours Trend

[Data from Ref. 53]

This chart shows a fluctuation in revenue hours seen over the 13 year period. This variability shows the volatility of the commercial industry. Of significant note is the sharp decline in revenue hours from 2007 until 2009. The significance of this is revealed when it is compared to the change in fuel efficiency. When the change in revenue hours declines steeply, the change in fuel efficiency increases. This relation is seen from 2003 to 2005 except the revenue hours are increasing during this time, merely at a slower rate. Over this 13 year period it can be seen that an emphasis may be placed on fuel efficiency improvements in years where the revenue hours are not increasing from the previous year.

Another factor which drives improvements in fuel efficiency is fuel prices. A comparison was made between total fuel consumption cost and the cost of one gallon

of fuel. From the trends shown in Figure 6.2 it is clear that the total amount spent on fuel each year follows the changes in fuel costs very closely.

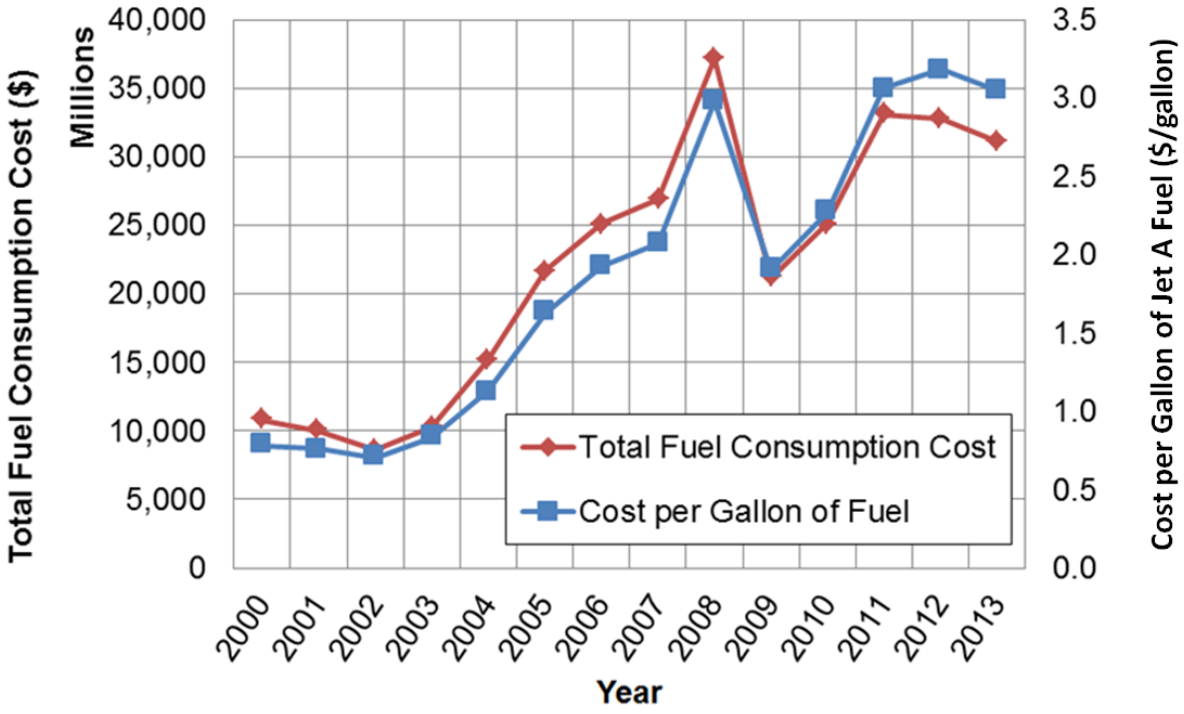

Figure 6.2: Total Fuel Consumption Cost and Cost of Fuel Trend Comparison [Data from Ref. 53]

Again, 2009 is a significant year. During this time the trend lines switch with the cost of fuel increasing slightly faster than the total fuel consumption cost. Comparing this to Figure 6.1 where the revenue hours are increasing along with the fuel efficiency from 2009 to 2011 it can be seen that when there is a significant increase in fuel prices the push for improved fuel efficiency continues.

6.1.2 Benefits of Increased Span

Due to reduced induced drag, increased span has several important benefits for the performance of an aircraft the first of which is an increase in the lift-to-drag ratio if properly designed. This can be shown using several basic aerodynamic principles. To begin the following relations are considered:

$$\frac{L}{D} \equiv \frac{C_L}{C_D}$$

Equation 6.1 [54]

$$C_D = C_{D_0} + C_{D_i}$$

Equation 6.2 [54]

$$C_{D_i} = \frac{{C_L}^2}{\pi A e}$$

Equation 6.3 [54]

$$C_L = \frac{2L}{\rho V^2 S}$$

Equation 6.4 [54]

$$A = \frac{b^2}{S}$$

Equation 6.5 [54]

During the cruise segment of a flight, the aircraft is designed to fly at the maximum lift-to-drag ratio to achieve the best performance possible. This results in the following equations:

$$C_D = \frac{2{C_L}^2}{\pi A e}$$

Equation 6.6 [54]

$$\frac{L}{D} = \frac{\pi b^2 e \rho V^2}{4L}$$

Equation 6.7

Figure 6.3 shows the correlation between span and lift-to-drag ratio assuming all other variables are held constant. This is overly simplified seeing as a span change affects the Oswald efficiency factor as well as the weight of the aircraft, which is equivalent to the lift.

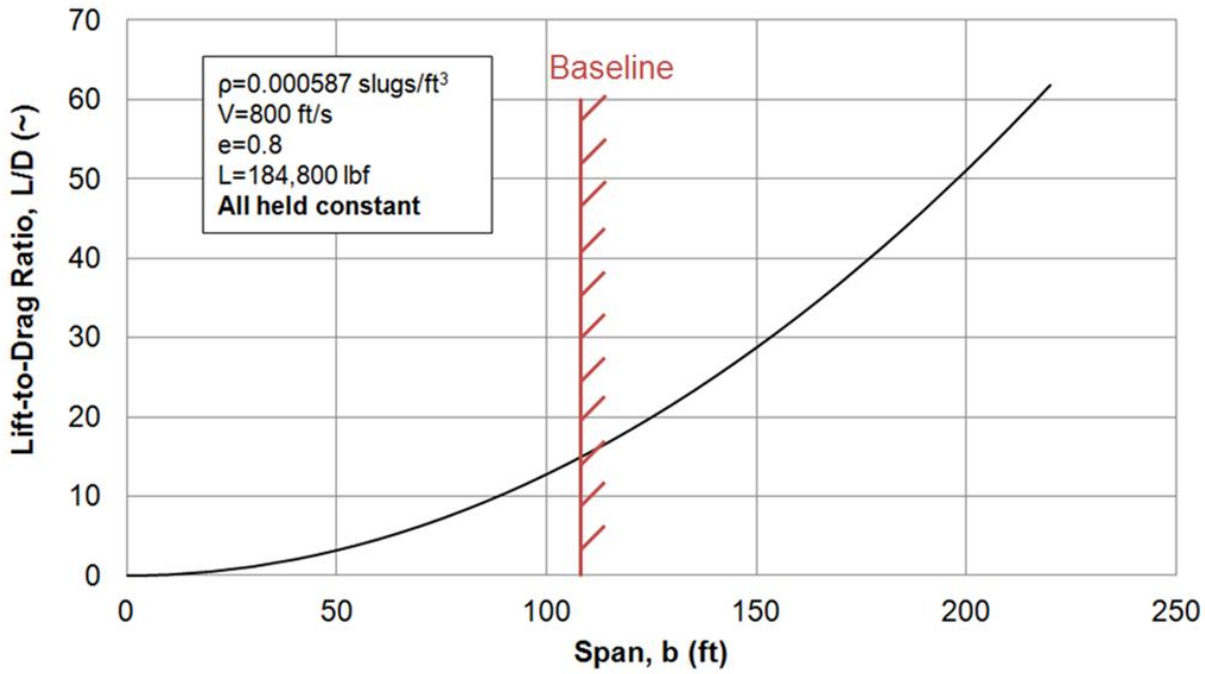

Figure 6.3: Hypothetical 727-200 Wing Modification Effects (Lift-to-Drag Ratio)

While the lift-to-drag ratio of an aircraft is a strong indicator of performance, it is also important to show the benefits airlines can take advantage of like range and lifting capability. From the calculated lift-to-drag ratio values, range can be determined quite easily using the Breguet range equation (Eq. 6.8). This was done for a jet aircraft since the goal market for this analytical proof of concept is the commercial jet transport industry.

$$R = \frac{V}{c_j}\frac{L}{D}\ln\left(\frac{W_i}{W_{i+1}}\right)$$

Equation 6.8 [52]

From this equation, it is seen that the range of the aircraft is directly proportional to the lift-to-drag ratio if all other variable are held constant. This is shown in Figure 6.4.

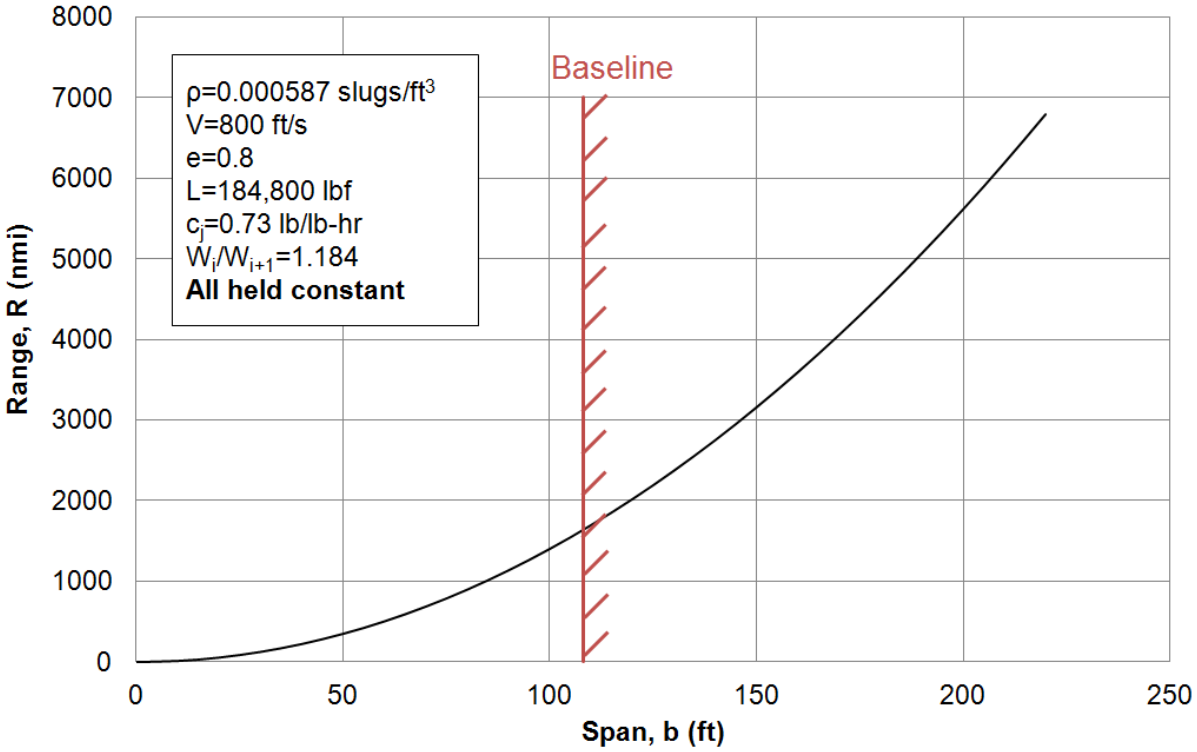

Figure 6.4: Hypothetical 727-200 Wing Modification Effects (Range)

This shows that there is enormous benefit to be had from a span increase. While some of the range increase will be lost due to weight increase, it is assumed through proper design the range benefit will outweigh the incremental weight increase for a reasonable span increase.

6.2 Wingtip Shape

When looking at the benefits of adding a wingtip extension, the aerodynamics as well as the weight and structure must be considered. As the span of the wing grows, the structure will have increased loads which it must carry. To carry these increased loads, the structure must be increased causing a weight increase. This is shown by Torenbeek's Method for calculating the wing weight for a commercial transport airplane (Eq. 6.9).

$$W_W = 0.0017 W_{MZF} \left(\frac{b}{\cos \Lambda_{1/2}} \right)^{0.75} \left[1 + \frac{6.3 \cos \Lambda_{1/2}}{b} \right]^{1/2} (n_{ult})^{0.55} \left(\frac{bS}{t_r W_{MZF} \cos \Lambda_{1/2}} \right)^{0.30}$$

Equation 6.9 [55]

This shows that the estimated wing weight is directly proportional to the span of the wing meaning a balance must be struck between an increase in span and an increase in wing weight to make the wingtip worthwhile.

A limitation was placed on the span increase for the design of the wingtip which was attained by the hangar height and fold mechanism limitations. For the aircraft to be stored in current hangars, the vertical tail height cannot be surpassed. The folding mechanism allows for the wingtip to be folded but the fuselage provides a hard limit for how far down this fold can be taken. For this study only one folding mechanism was considered, therefore the hangar height and folding limit led to a span growth limitation of one span length, or a doubling of the original span. This is shown in Figure 6.5.

Figure 6.5: Largest Wingtip Extension with One Fold [20]

To provide a full view of the capabilities of the Prandtl-tailored adaptive aerocompliant wingtip extension shape, five different spans were chosen in equal span increase increments. Each of these spans was then segmented into three partitions; the first being the transition-folding area and positive lifting area, the second being the second transition area, and the third being the negative lifting area. The three segment geometry is shown in Figure 6.6 by the red line with the design geometry in blue.

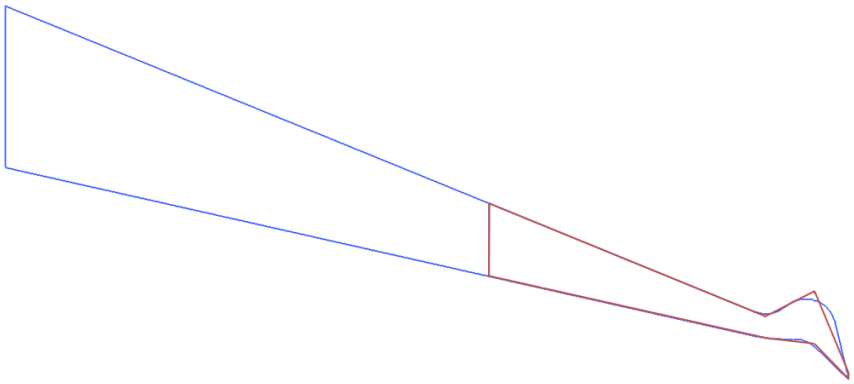

Figure 6.6: Actual Geometry (blue), Analyzed Geometry (red)

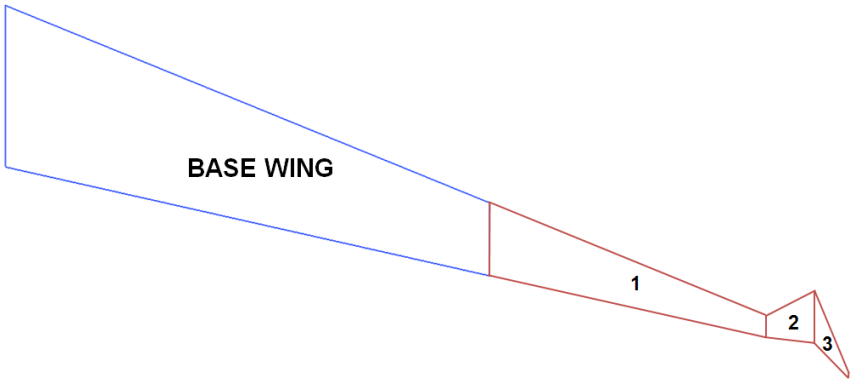

Figure 6.7: Wingtip Extension Partition Locations

The partitions were designed in this manner to assist in simplifying the input data required to run the aerodynamic analysis models while still maintaining a reasonable level of approximation to the designed wingtip extension.

To keep as many characteristics of the wingtip partitions invariable, the dihedral, sweep, and taper were kept constant at each of the five span increments. The span of each partition was determined as a percentage of the total wingtip span with the first, second, and third partition consisting of 50%, 10%, and 40% of the total wingtip extension span, respectively. These span percentages were used for all five wingtip extension span lengths.

Since one of the design assumptions made was that the total lifting capability of the wing remained constant, the twist of partitions 2 and 3 were varied as well as the cruise angle of attack. This also allowed for the moment at the wingtip root to be minimized avoiding overstressing of the base wing tip.

The layout of each of the five wingtips can be seen in the figures below along with the shaping characteristics of each partition. The shaping characteristics give the inputs necessary for completion of the Tornado analysis. Appendix A walks through a sample Tornado analysis with each input screen shown.

Table 6.1: Inputs for Wingtip 1

	Partition		
Characteristic	1	2	3
Γ	1.1 deg	1.1 deg	1.1 deg
b	5.4 ft	1.1 ft	4.3 ft
Λ	32 deg	-45 deg	57 deg
λ	0.546	4	0.3
ε_i	-1 deg	0	-8.6 deg
ε_o	0	-8.6 deg	-8.6 deg
$\propto_{cruise}$	2.7 deg		

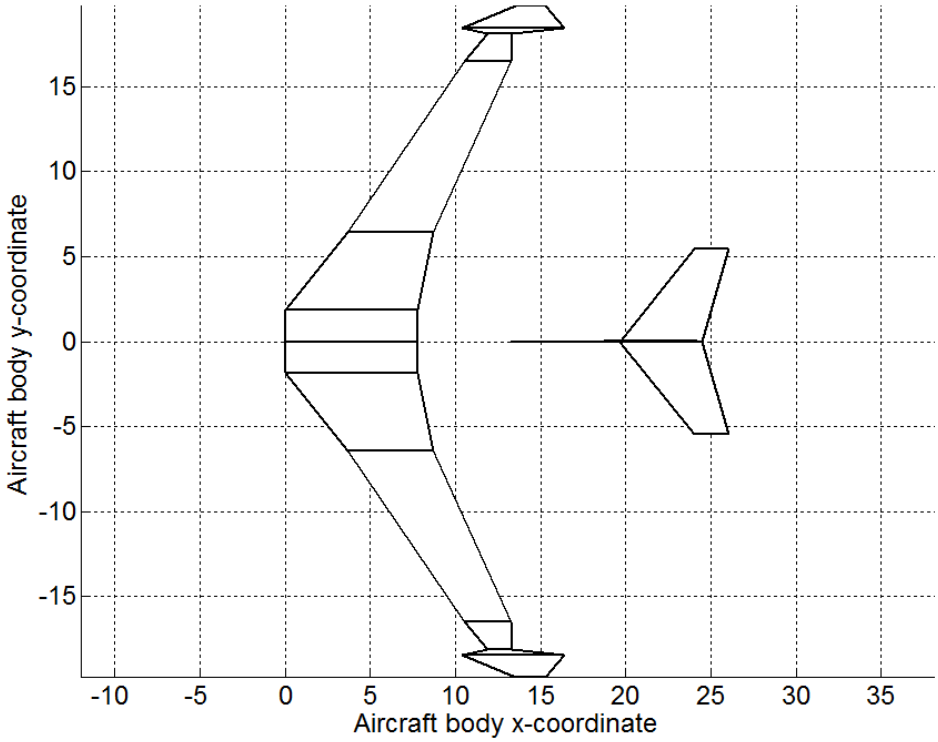

Figure 6.8: Wingtip 1 Geometry

Table 6.2: Inputs for Wingtip 2

	Partition		
Characteristic	1	2	3
Γ	1.1 deg	1.1 deg	1.1 deg
b	10.8 ft	2.2 ft	8.6 ft
Λ	32 deg	-45 deg	57 deg
λ	0.546	4	0.3
ε_i	-1 deg	0	-8.6 deg
ε_o	0	-8.6 deg	-8.6 deg
$\propto_{cruise}$	2.6 deg		

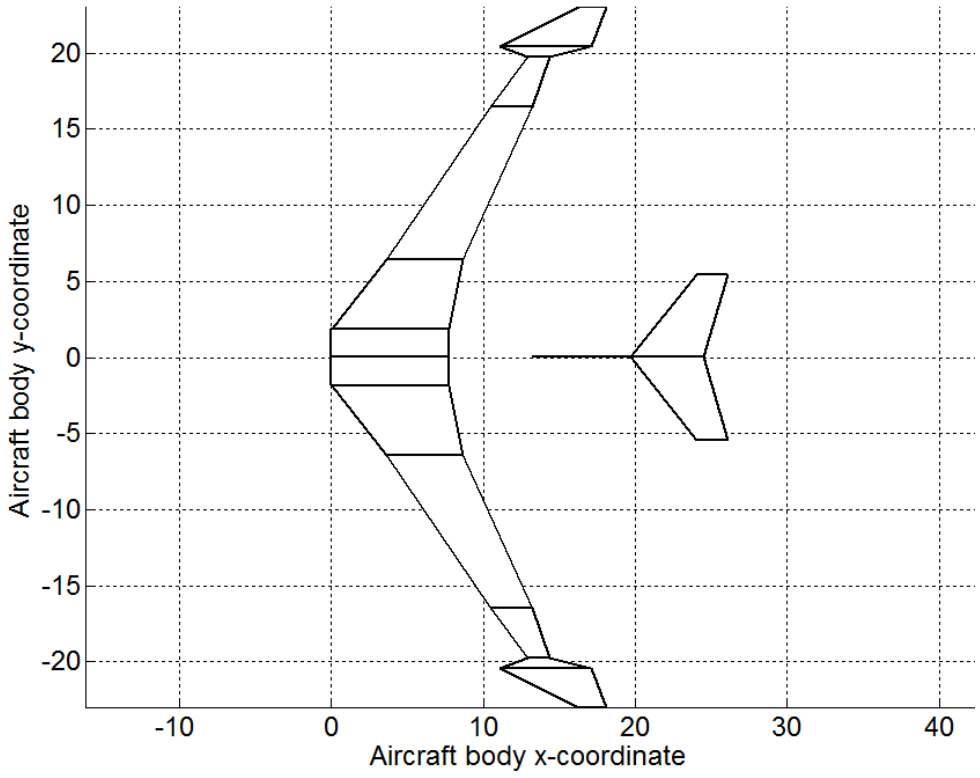

Figure 6.9: Wingtip 2 Geometry

Table 6.3: Inputs for Wingtip 3

	Partition		
Characteristic	1	2	3
Γ	1.1 deg	1.1 deg	1.1 deg
b	16.2 ft	3.3 ft	12.9 ft
Λ	32 deg	-45 deg	57 deg
λ	0.546	4	0.3
ε_i	-1 deg	0	-8 deg
ε_o	0	-8 deg	-8 deg
$\propto_{cruise}$	2.5 deg		

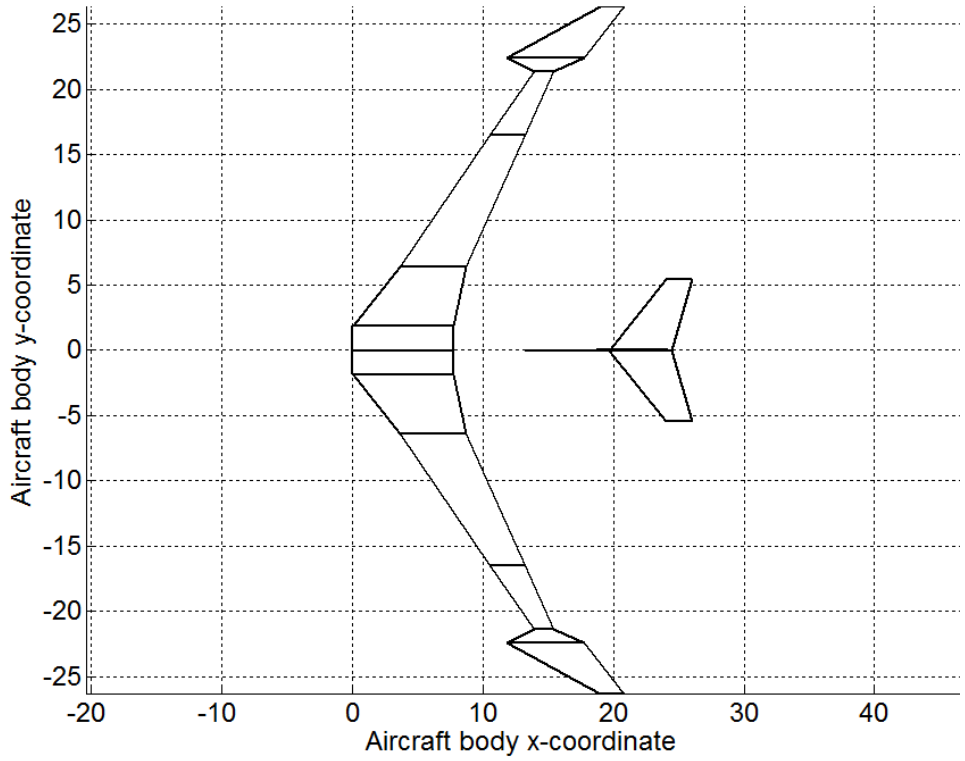

Figure 6.10: Wingtip 3 Geometry

Table 6.4: Inputs for Wingtip 4

	Partition		
Characteristic	1	2	3
Γ	1.1 deg	1.1 deg	1.1 deg
b	21.6 ft	4.4 ft	17.2 ft
Λ	32 deg	-45 deg	57 deg
λ	0.546	4	0.3
ε_i	-1 deg	0	-7.2 deg
ε_o	0	-7.2 deg	-7.2 deg
$\propto_{cruise}$	2.3 deg		

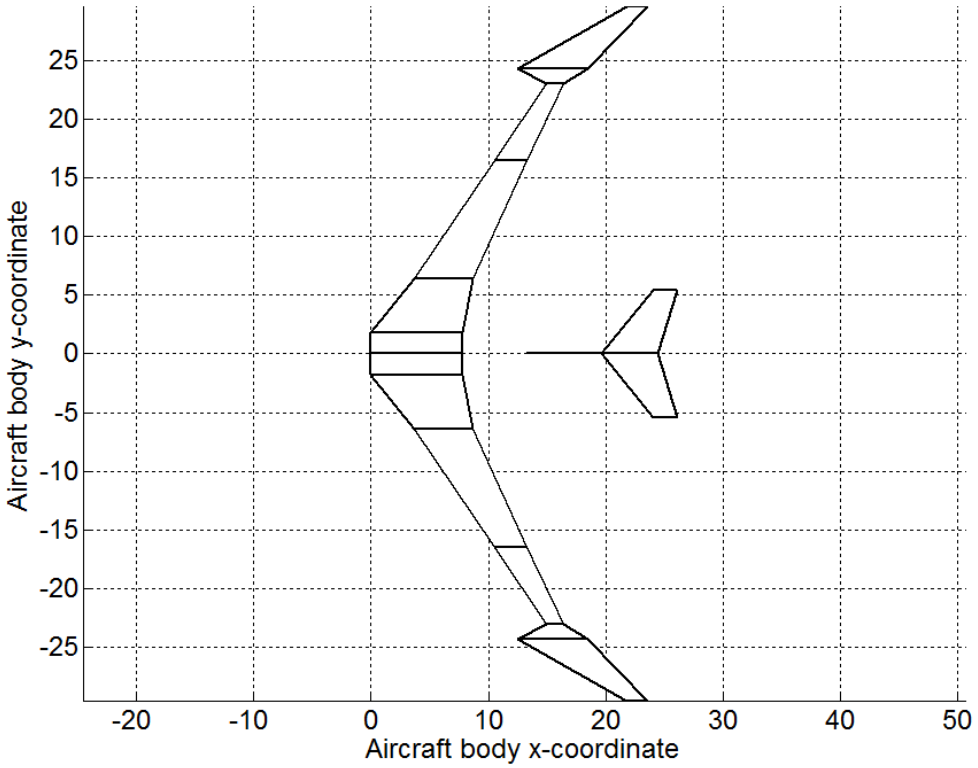

Figure 6.11: Wingtip 4 Geometry

Table 6.5: Inputs for Wingtip 5

	Partition		
Characteristic	1	2	3
Γ	1.1 deg	1.1 deg	1.1 deg
b	27.2 ft	5.4 ft	21.6 ft
Λ	32 deg	-45 deg	57 deg
λ	0.546	4	0.3
ε_i	-1 deg	0	-6.6 deg
ε_o	0	-6.6 deg	-6.6 deg
$\propto_{cruise}$	2.2 deg		

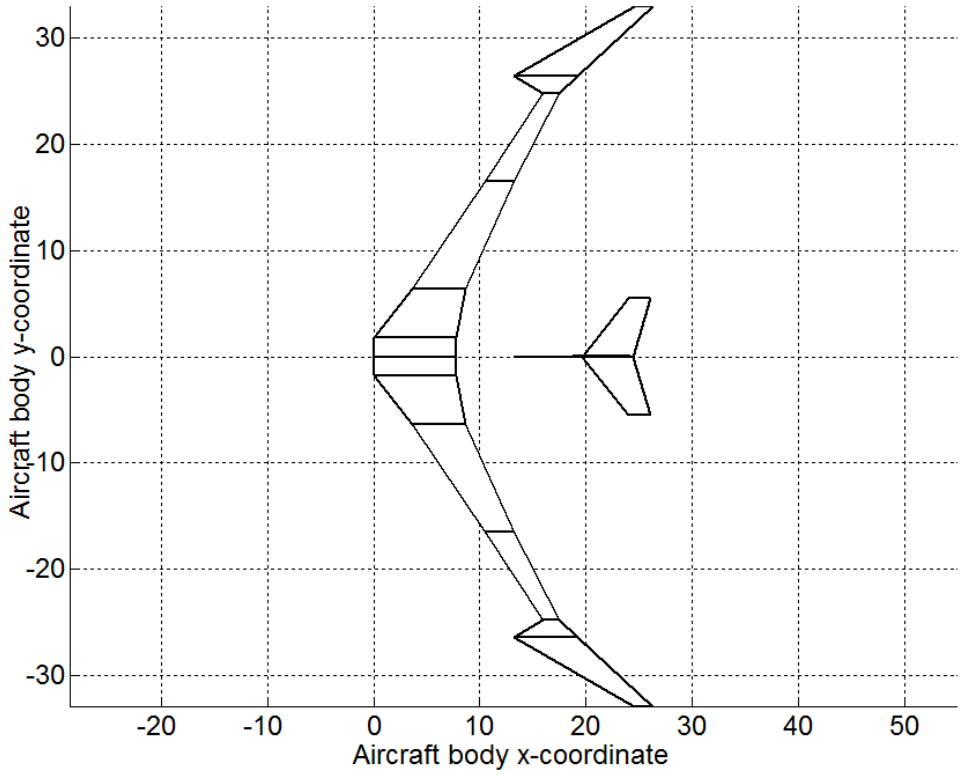

Figure 6.12: Wingtip 5 Geometry

6.3 Wingtip Weight Estimation

There are significant differences between the weight of a wingtip and the weight of a wing. Typically, the loading of a wingtip is much less than that of the wing because the moments transferred through it are less. For this reason, the wing weight equations found in Reference 57 were not used. A weight estimation was made based on weight data published by Aviation Partners, Inc., the manufacturers of many currently used winglets for commercial aviation such as the winglets for the Hawker 800 and 800XP, Falcon 2000, 900, and 50, and Boeing 737, 757, 767, and BBJ.

a) 

b) 

c) 

Figure 6.13: a) Hawker 800XP, b) Falcon 50, c) Boeing 737 [56]

The winglet data for the 737-700 was used to make the weight estimation due to the similarity in the aircraft size to the 727. This estimation was done through the extrapolation of a volumetric density estimation. Based on the dimensions given by Aviation Partners, Inc. the volume was estimated for the 737-700 winglet. Using the weight given for this particular winglet, the volumetric density was calculated. The

volumes of the newly designed wingtips were then calculated. Multiplying these volumes by the 737-700 winglet volumetric density resulted in the estimated wingtip weight. These weights are shown in Table 6.6.

Table 6.6: Wingtip Extension Weight Estimation

Wingtip	$b_{wing+extension}$ (ft)	$S_{extension}$ (ft^2)	$W_{extension}$ (lbf)
1	130	211	1,606
2	151	422	1,898
3	173	633	2,161
4	195	843	2,394
5	216	1,056	2,599

6.4 Wingtip Extension Performance

The performance analysis for the wingtips was completed using two methods. The first was Roskam's Class I analysis outlined in Reference 54 in which the wingtip shape and weight is used to calculate the lift-to-drag ratio. The second method used a vortex lattice code, Tornado [57], to simulate the cruise condition flight of the wing and wingtip which was then used to generate a drag polar plot resulting in the calculation of the lift-to-drag ratio. The Tornado code has been proven to be accurate through the simulation of a Cessna 172. The output generated by Tornado was compared to flight test data released by Cessna [58]. With the results from Tornado, the estimations using the first method from Reference 54 were verified and then used to calculate the range attainable during the cruise segment of the flight profile.

6.4.1 Vortex Lattice Method Lift-to-Drag Ratio Estimation

The Tornado code is based around the theory outlined in Reference 59 with modifications to allow a three-dimensional solution [60]. One of these modifications was the extension of horseshoe vortex theory into the vortex-sling concept. The vortex-sling concept has a segmented vortex line for each panel which starts far behind the aircraft. It then moves to the trailing edge of the wing, upstream to the quarter chord line of the specific panel, across the panel, and then downstream once more in an analogous manner.

The Tornado models were set up to operate at the cruise conditions for a 727-200. The resulting induced drag polars are shown in Figure 6.14 through Figure 6.18.

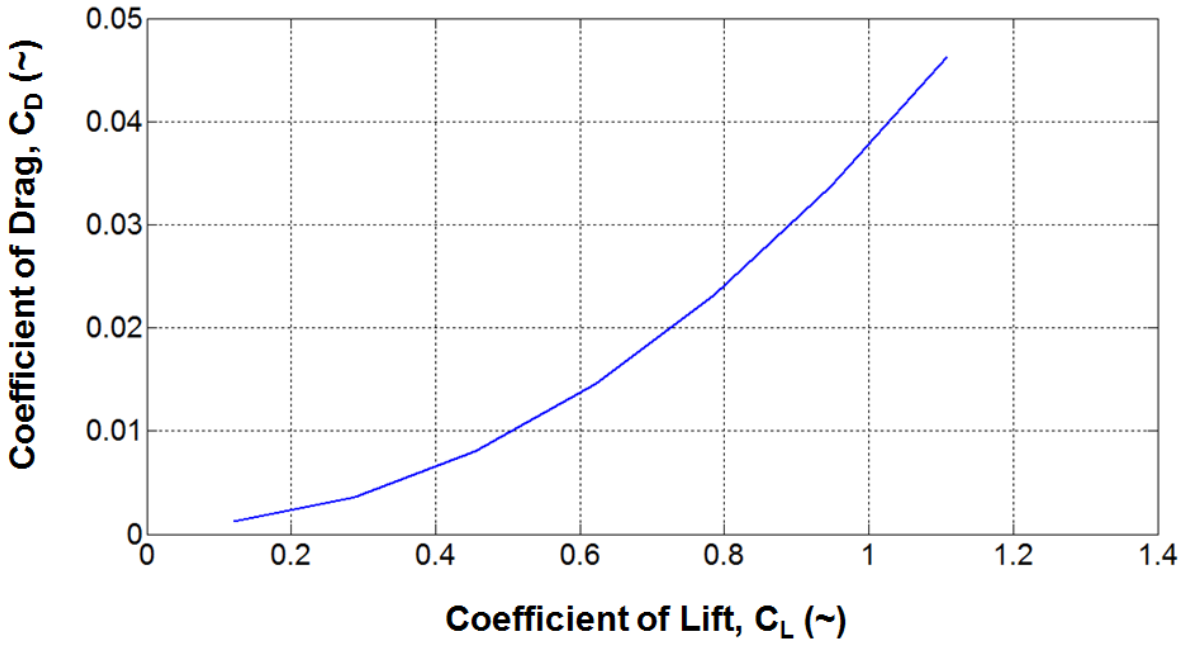

Figure 6.14: Wingtip 1 Induced Drag Polar

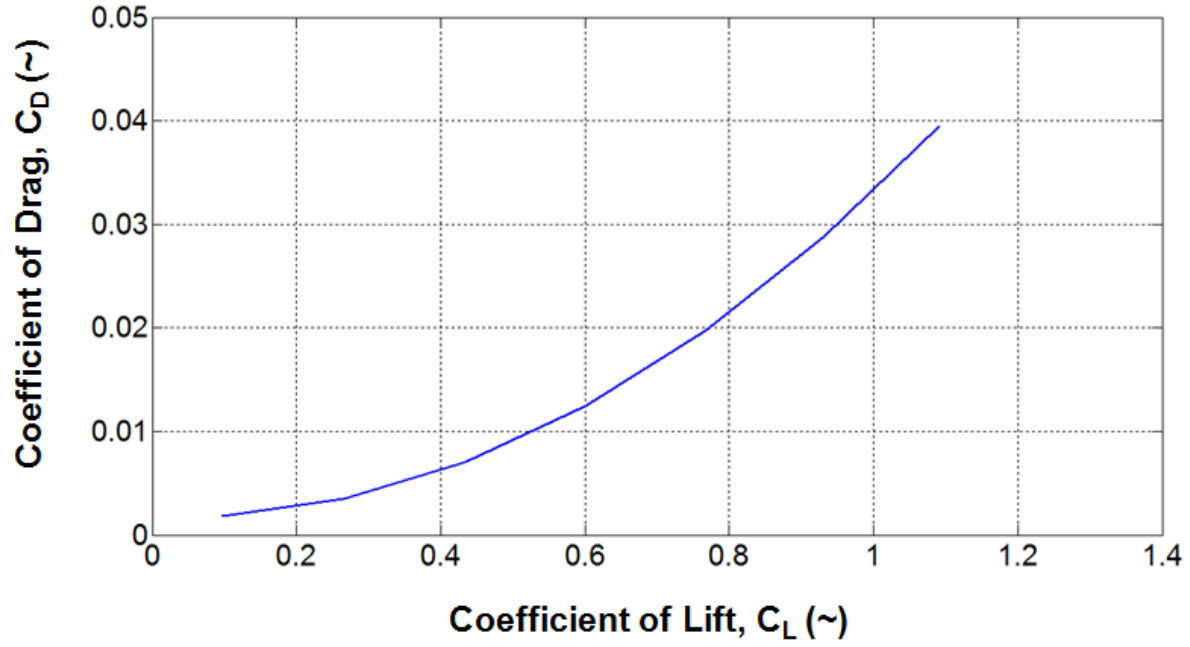

Figure 6.15: Wingtip 2 Induced Drag Polar

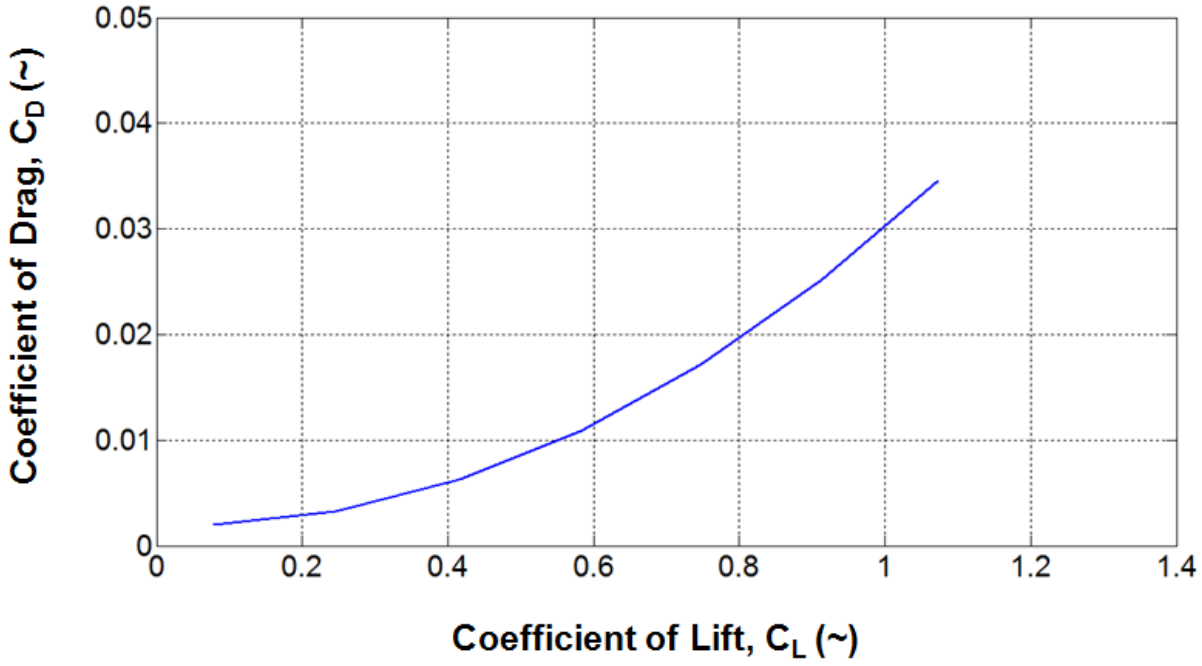

Figure 6.16: Wingtip 3 Induced Drag Polar

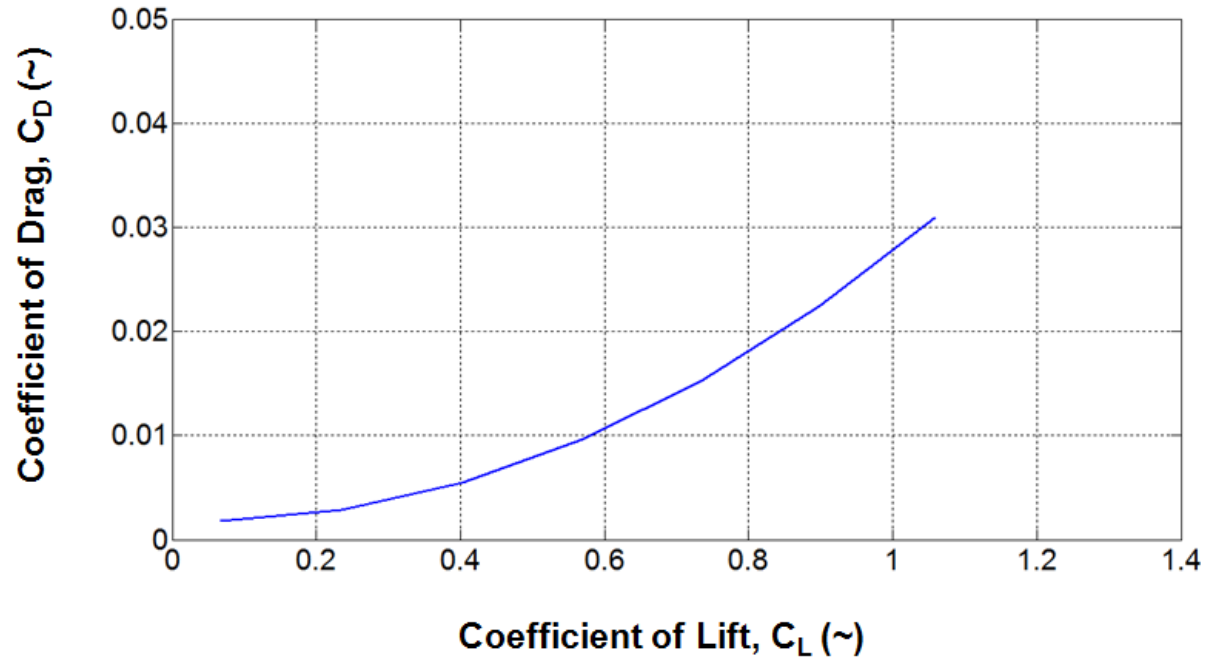

Figure 6.17: Wingtip 4 Induced Drag Polar

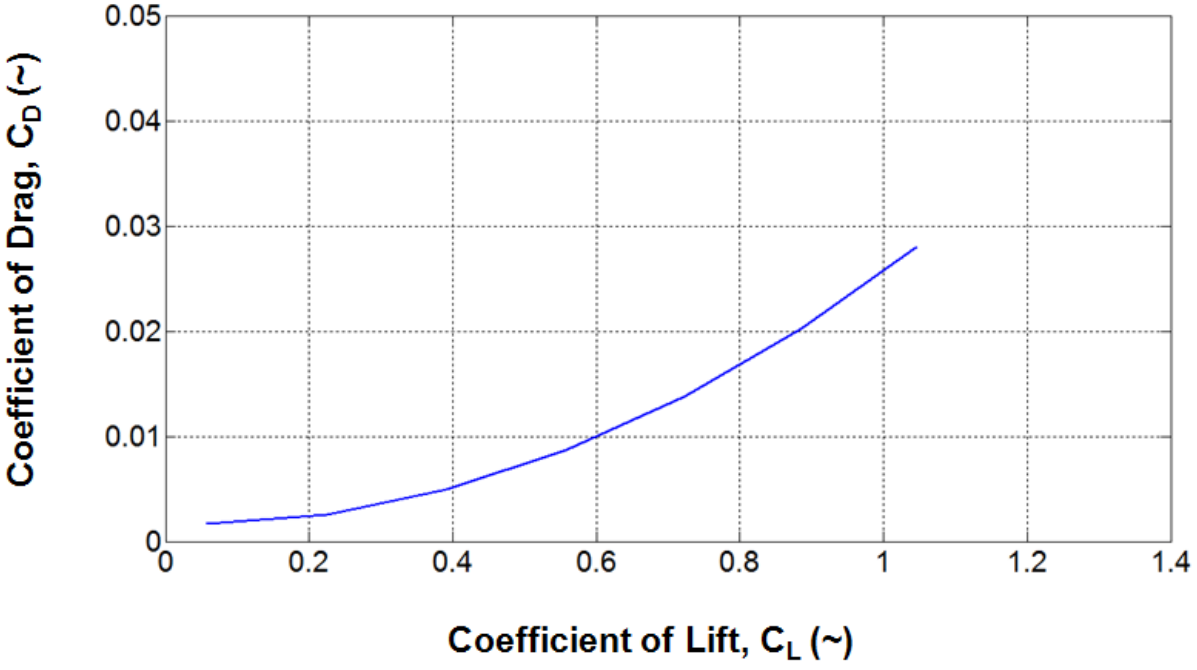

Figure 6.18: Wingtip 5 Induced Drag Polar

This representation of the drag does not, however, account for the parasitic drag component (Eq. 6.10). To estimate this drag element, the wingtip area was found. From this value, the wetted area and equivalent parasite area, f, were found. The equivalent parasite area was estimated using Figure 5.20 from Reference 63.

$$C_{D_0} = \frac{f}{S}$$

Equation 6.10 [61]

The parasitic drag was then added to the induced drag term generated by Tornado producing the total drag term. The final drag polar lines are shown in Figure 6.19 along with the calculated lift-to-drag ratio term for each wingtip.

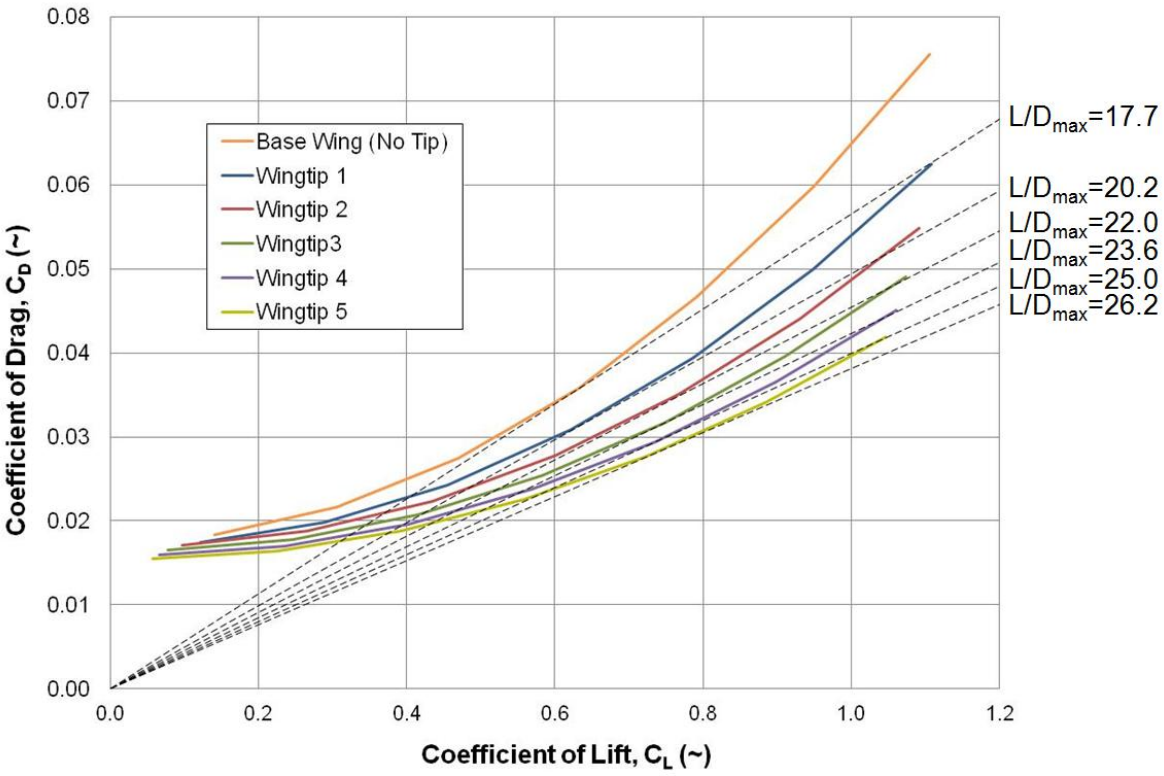

Figure 6.19: Drag Polar with Lift-to-Drag Ratios

Figure 6.19 shows that the maximum lift-to-drag ratio point varies based on the wingtip extension design. Each of these points were used to plot the trend line for the maximum lift-to-drag ratio as the wingtip extension span is changed following the design philosophy used for the five designs. This line is shown in Figure 6.20 (black) with the maximum lift-to-drag ratio points from the five wingtip extension designs used to generate the trend line.

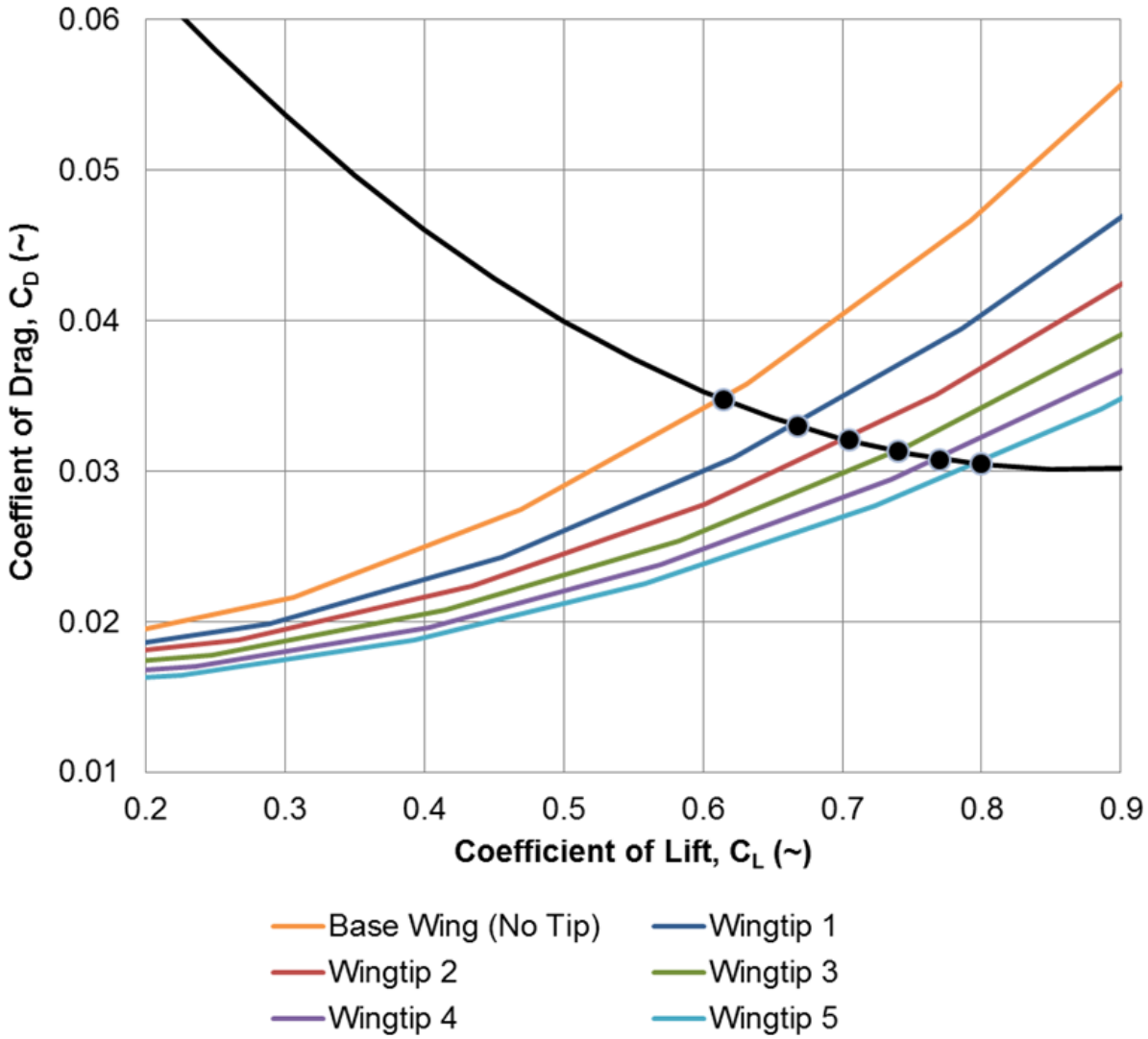

Figure 6.20: Maximum Lift-to-Drag Ratio Trend Line (black)

Using the maximum lift-to-drag ratio trend line (Figure 6.20), it is possible to relate the maximum lift-to-drag ratio to a wingspan ratio. The wingspan ratio used for this comparison was the total span, base wing and wingtip extension, to the base wing span. This comparison is shown in Figure 6.21.

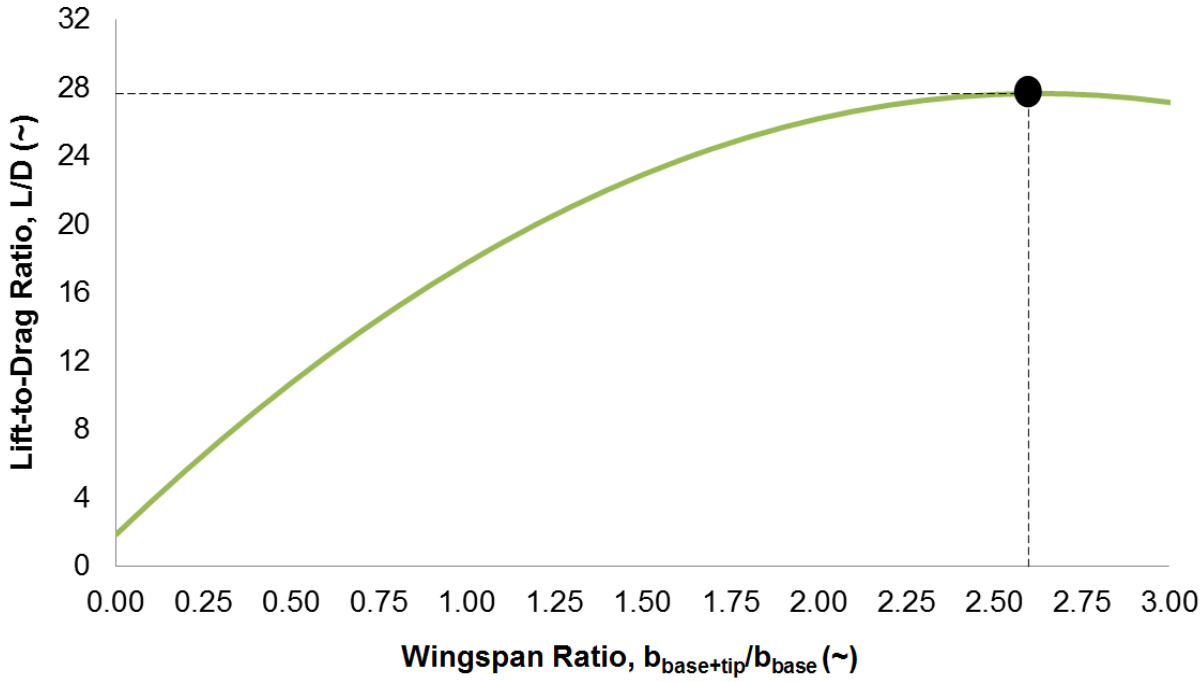

Figure 6.21: Maximum Lift-to-Drag Ratio Related to Wingtip Extension Span

Figure 6.21 reveals an estimated wingtip extension span which maximizes the lift-to-drag ratio term for the Boeing 727 family of aircraft. This value is shown by the dashed line with a wingspan ratio of approximately 2.6 and a lift-to-drag ratio of nearly 28. This is important for future studies as this study limited the wingspan growth due to the wingtip extension to double the original base wing due to only one folding section being used.

6.4.2 Roskam Method Lift-to Drag Ratio Estimation

The drag polars created using Tornado allow for a comparison to be made between the five wingtips at the original cruise conditions. In changing the wing aerodynamically through the addition of a wingtip extension, the optimal cruise conditions may change. An analysis of the optimal cruise conditions, in the form of speed and altitude, was completed using two basic aerodynamic principles, shown below:

$$C_L = \frac{2W}{\rho V^2 S}$$

Equation 6.11 [54]

$$\frac{L}{D} \equiv \frac{C_L}{C_{D_0} + \frac{{C_L}^2}{\pi A e}}$$

Equation 6.12 [54]

Substituting Equation 6.11 into Equation 6.12 gives the following relationship:

$$\frac{L}{D} = \frac{2W}{C_{D_0} \rho V^2 S} + \frac{\pi A e \rho V^2 S}{2W}$$

Equation 6.13

The lift-to-drag ratios found using Tornado were used to find the Oswald's efficiency factor, e, by sweeping through values of e until the maximum lift-to-drag ratio term using Roskam's method [54] corresponded to that put out by Tornado [57] at the original cruise conditions. Various cruise altitudes and speeds were swept through to find which combination resulted in the maximum lift-to-drag ratio. From the lift-to-drag ratio values, the range can be calculated using the Breguet range equation (Eq. 6.8) for each of the wingtips. The results are shown in Figure 6.22 through Figure 6.27.

These results do not account for powerplant efficiency changes due to altitude and speed variation or compressibility effects.

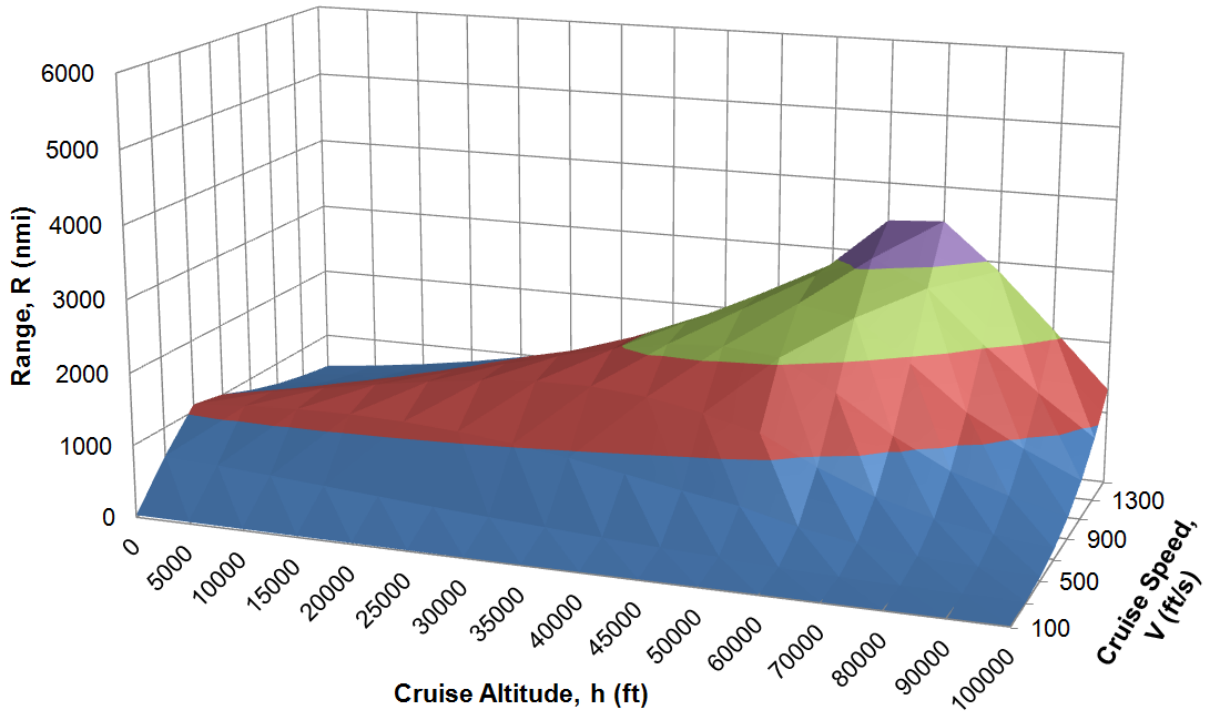

Figure 6.22: Cruise Condition Sweep: Base Wing

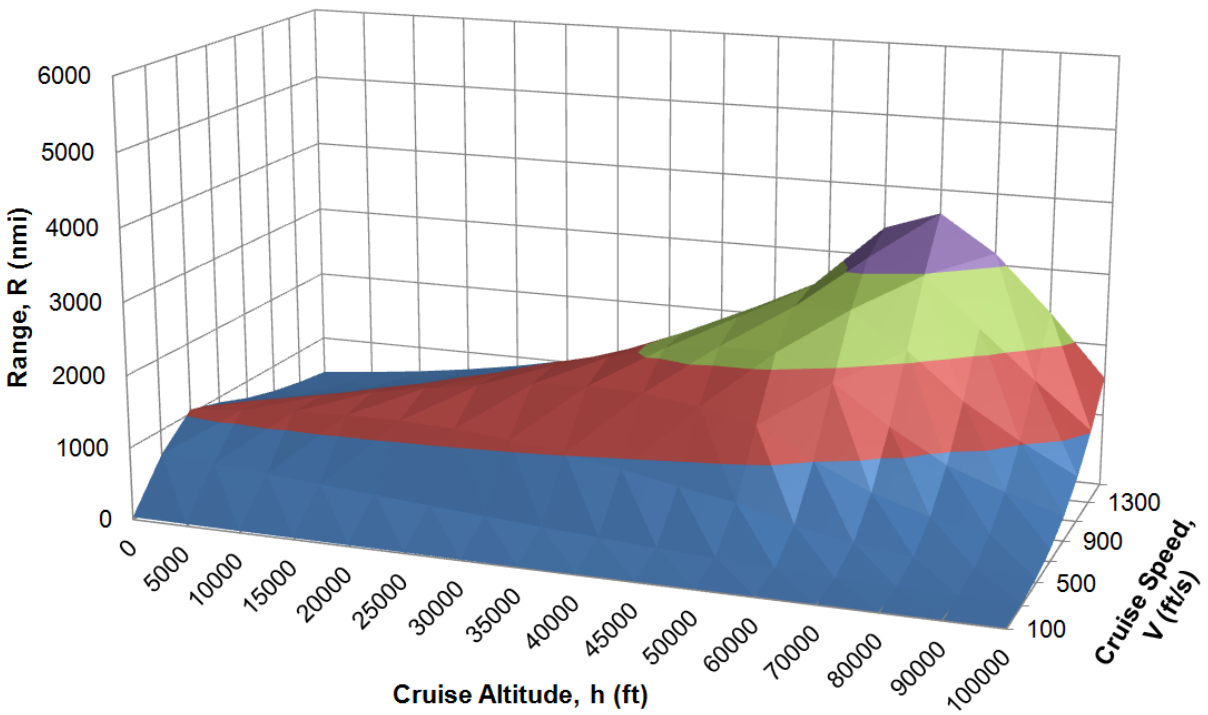

Figure 6.23: Cruise Condition Sweep: Wingtip 1

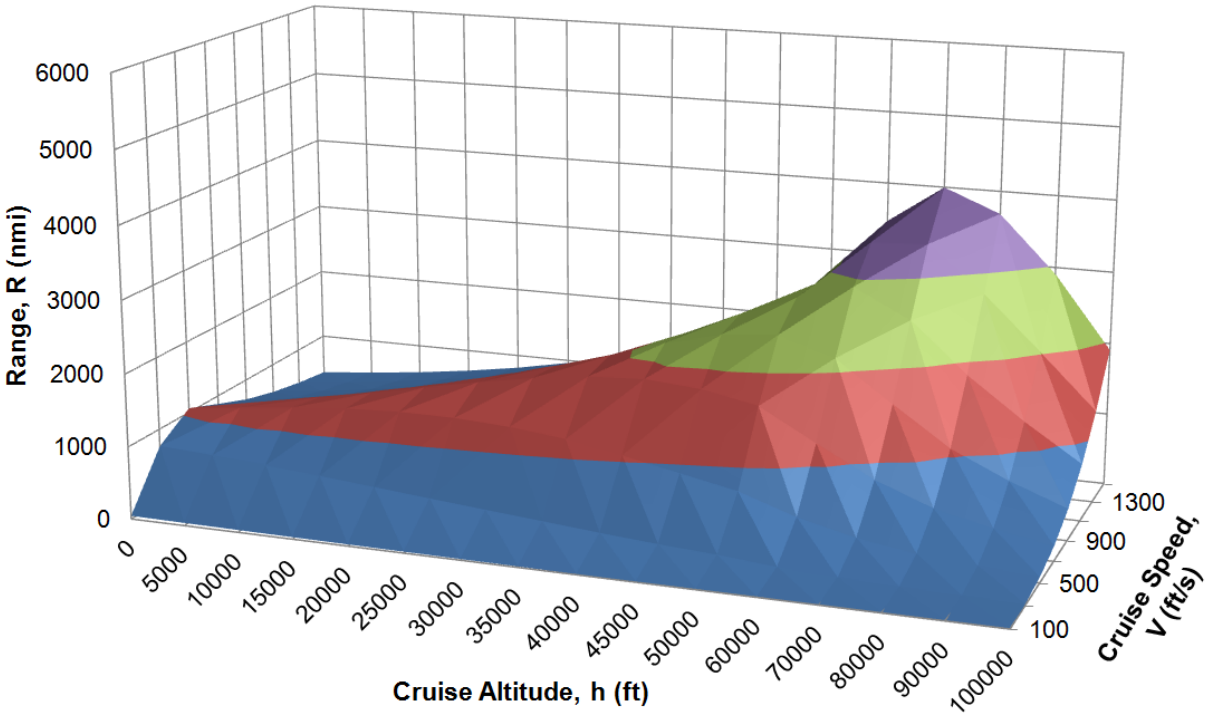

Figure 6.24: Cruise Condition Sweep: Wingtip 2

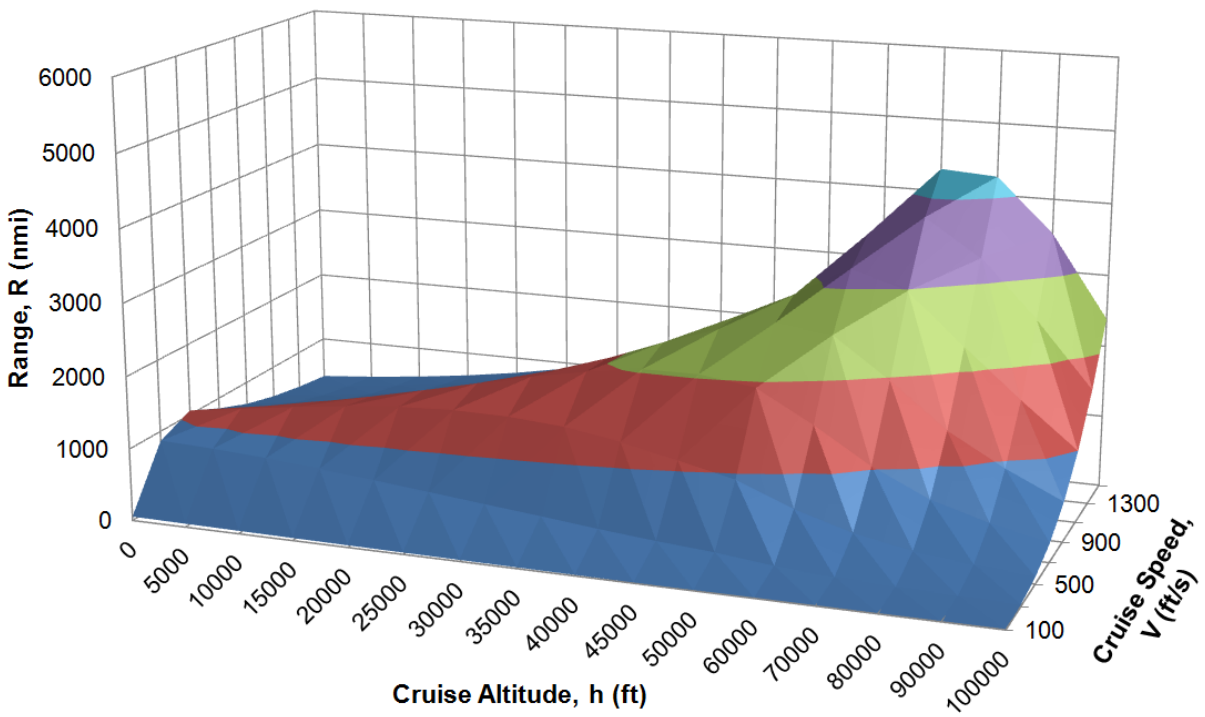

Figure 6.25: Cruise Condition Sweep: Wingtip 3

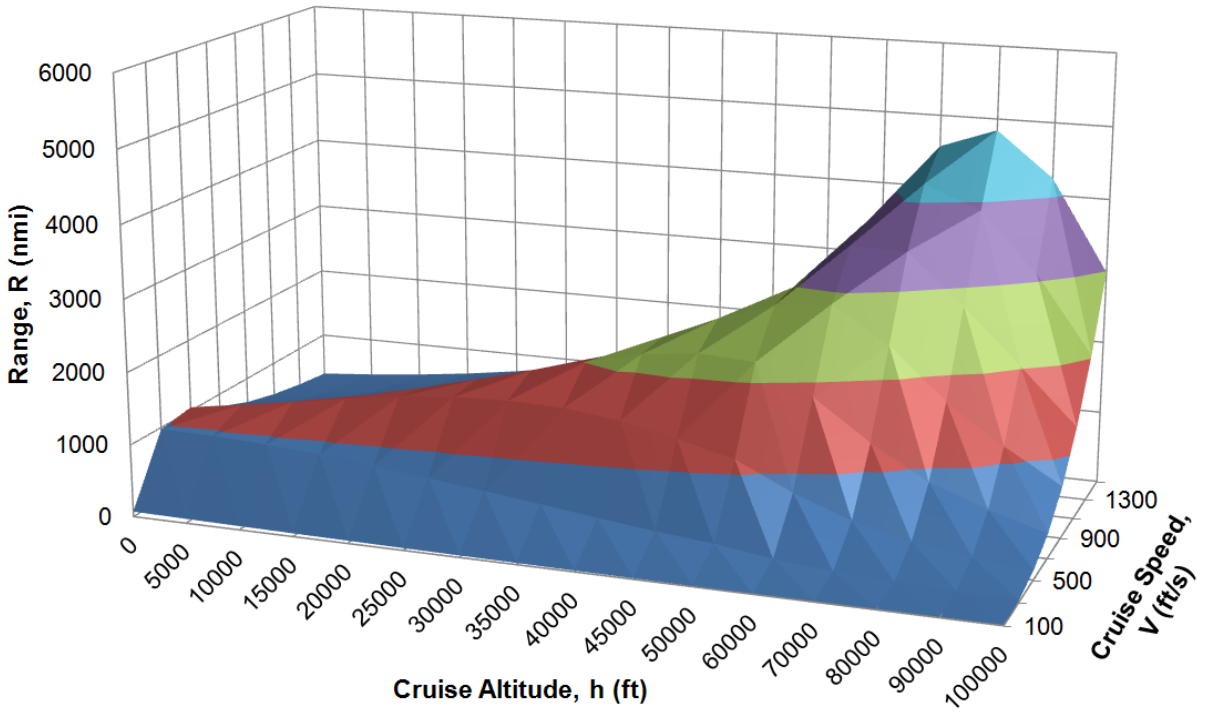

Figure 6.26: Cruise Condition Sweep: Wingtip 4

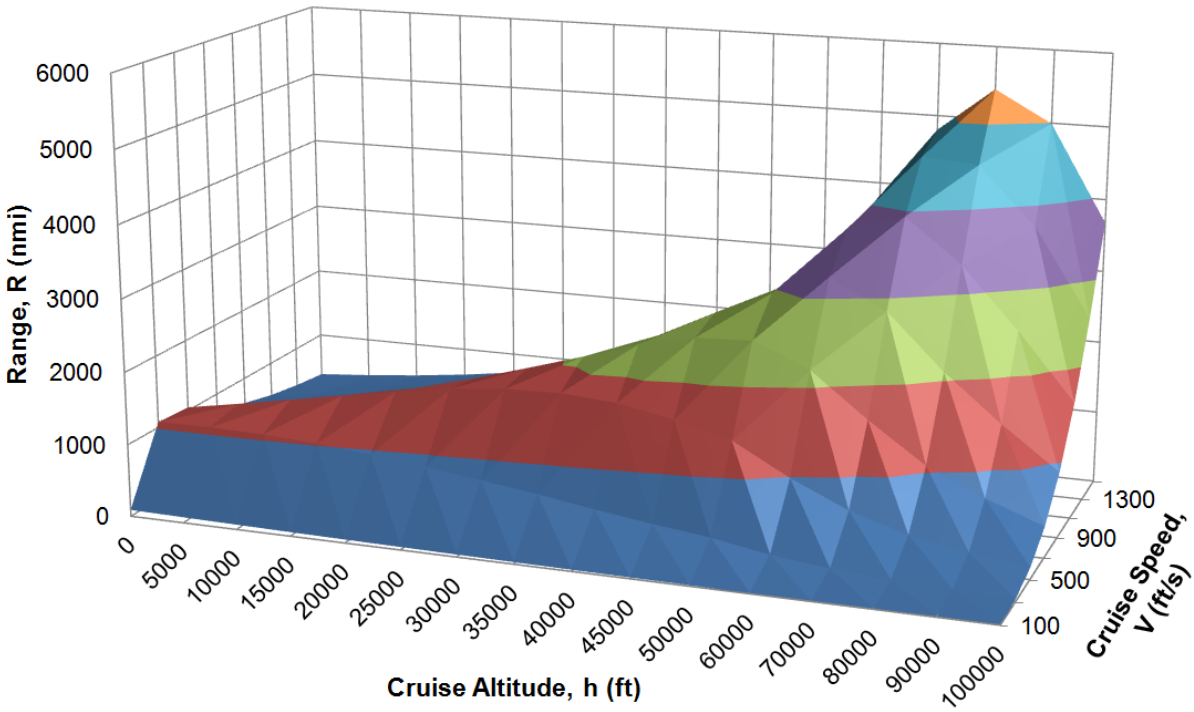

Figure 6.27: Cruise Condition Sweep: Wingtip 5

Comparison of the above graphs shows that the maximum range for each wingtip is at the maximum cruise speed but varying altitude. While it is acceptable to fly slightly over the designed cruise speed of an aircraft, it is ill advised to fly significantly over for extended periods. This can cause excessive strain on the structure, increased fatigue, and reduce the power plant efficiency. For this reason, the cruise speed was held constant for the aircraft with only the altitude being varied. This is shown in Figure 6.28 with the engine efficiency and cruise speed held constant.

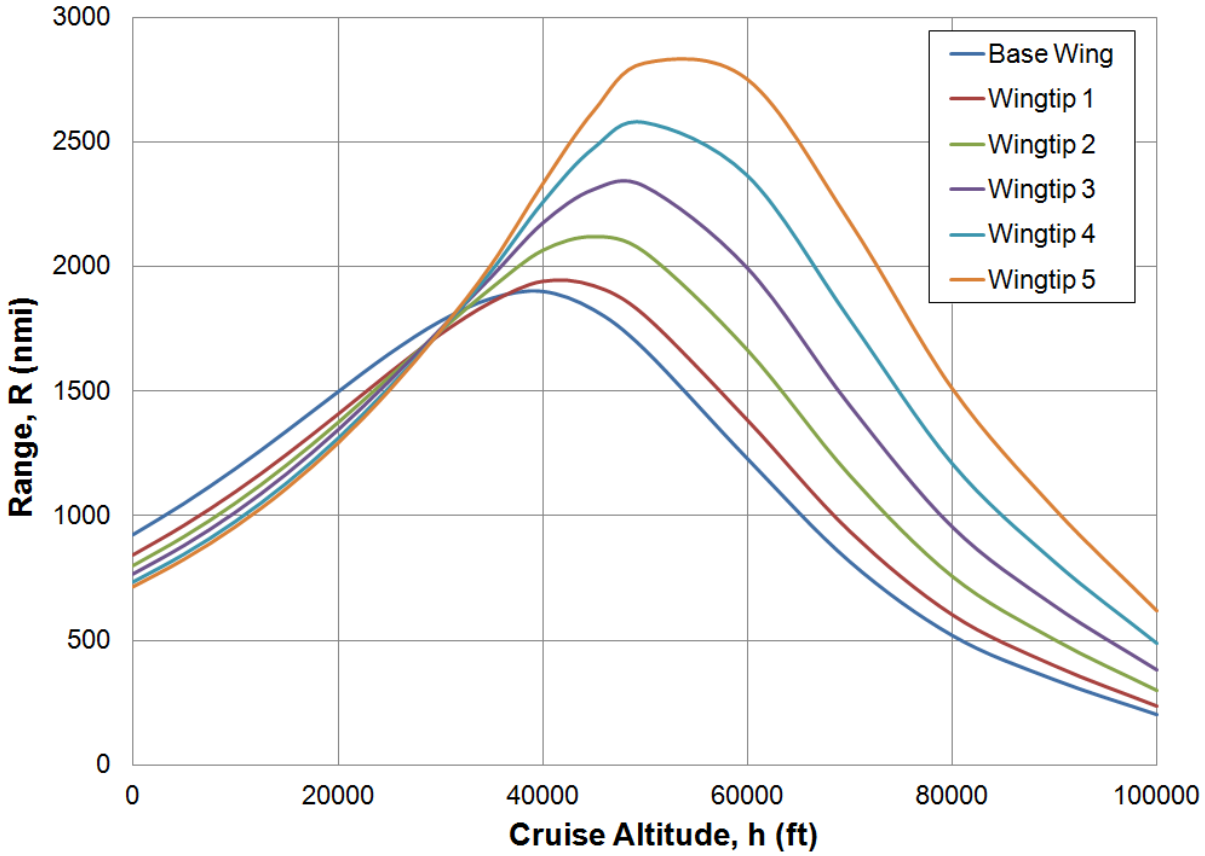

Figure 6.28: Altitude Sweep for Constant Cruise Speed

It is seen that the optimal cruise altitude is pushed higher to maximize the range as the wingspan grows. The maximum range during cruise for each of the wingtip extensions and the base wing are listed in the table below along with the respective cruise altitude. Each of these ranges is based on a Mach 0.82 cruise speed.

Table 6.7: Design Cruise Altitude and Resulting Ferry Range

Wingtip	Cruise Altitude (ft)	Range (nmi)	Percentage Range Improvement (%)
No Tip	40,000	1,900	Baseline
1	40,000	1,940	2%
2	45,000	2,118	11%
3	50,000	2,320	22%
4	50,000	2,576	36%
5	50,000	2,815	48%

6.4.3 Structural Analysis

As was stated previously, one wingtip design decision was to minimize the moment at the wingtip root to limit the moment transferred into the base wing tip. This was done by counteracting the upward lift generated near the wingtip extension root with the downward lift from the wingtip extension tip. The bending moment and shear force diagrams for the base wing compared to each wingtip extension design are shown in Figure 6.29 through Figure 6.38.

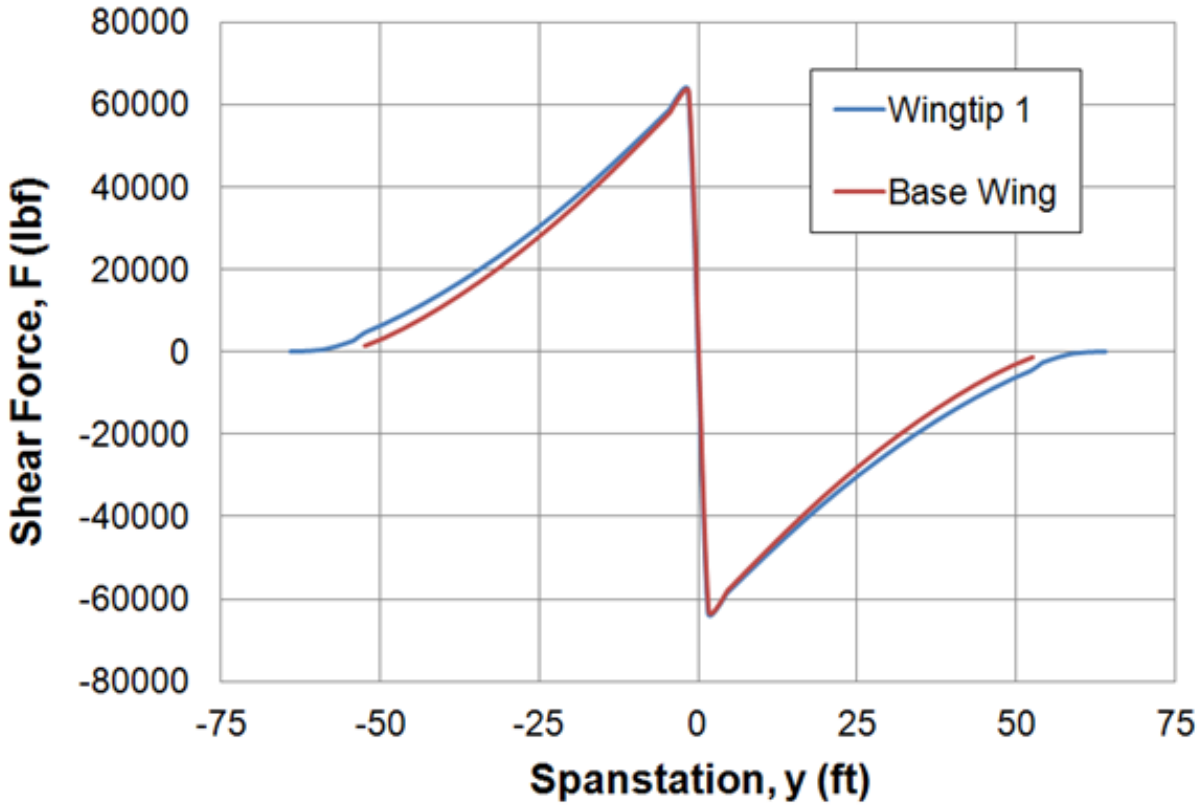

Figure 6.29: Shear Force on Wing and Wingtip 1

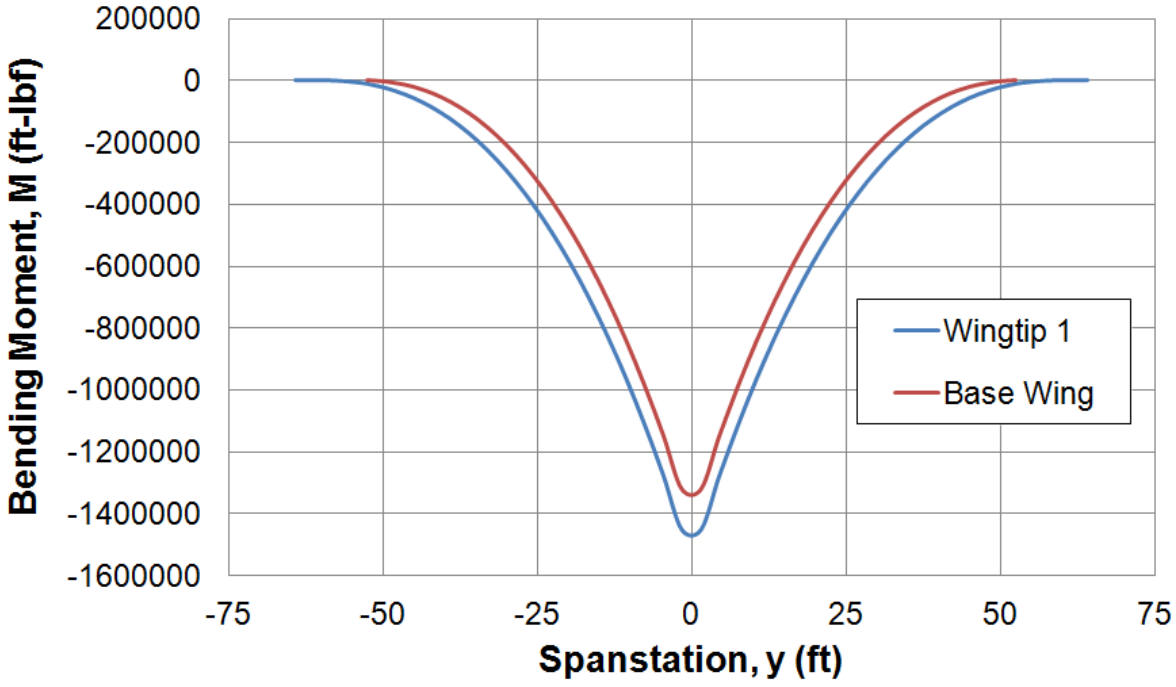

Figure 6.30: Bending Moment on Wing and Wingtip 1

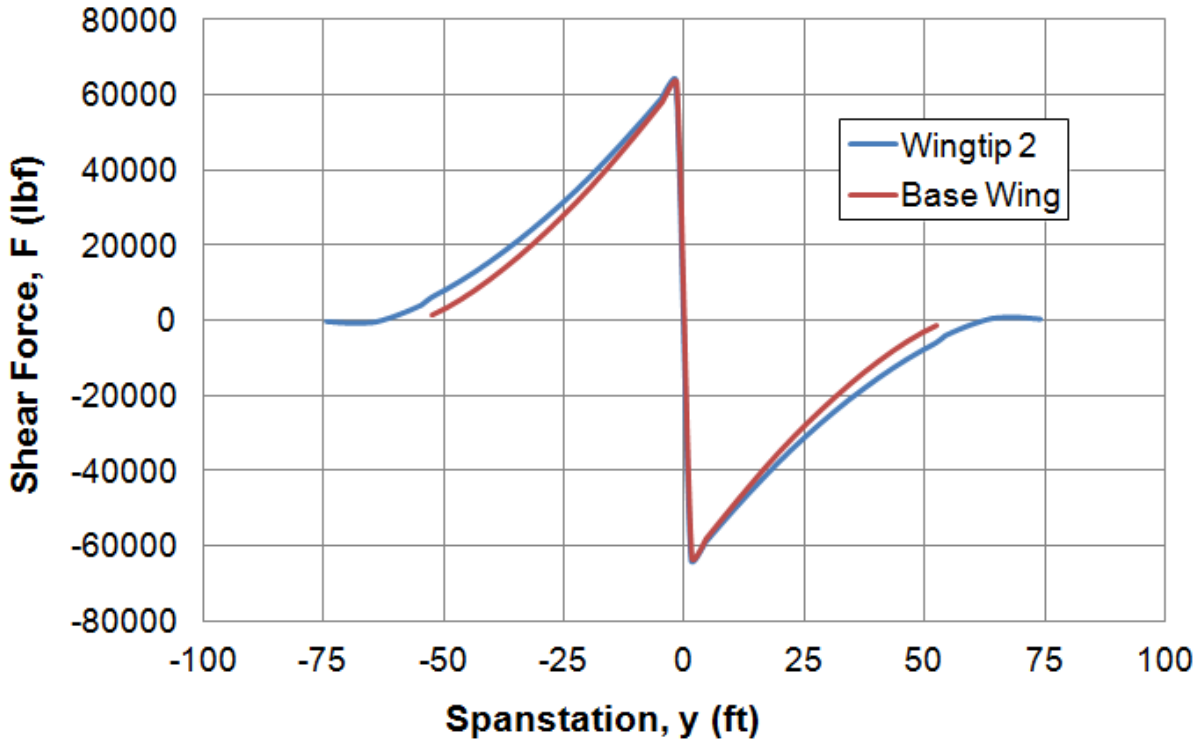

Figure 6.31: Shear Force on Wing and Wingtip 2

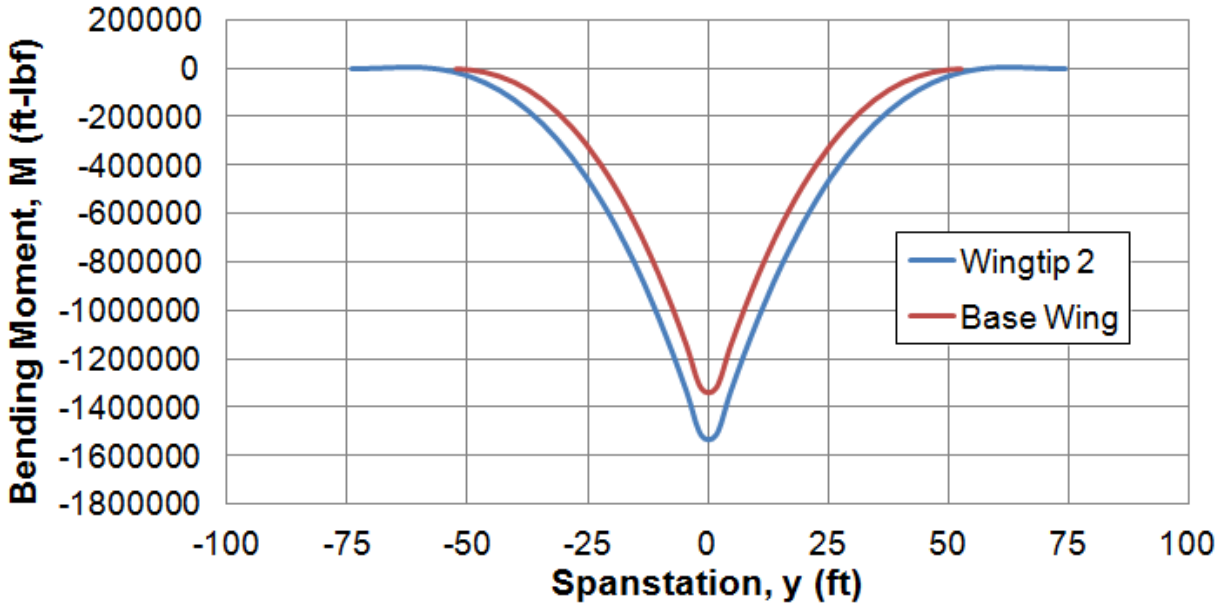

Figure 6.32: Bending Moment on Wing and Wingtip 2

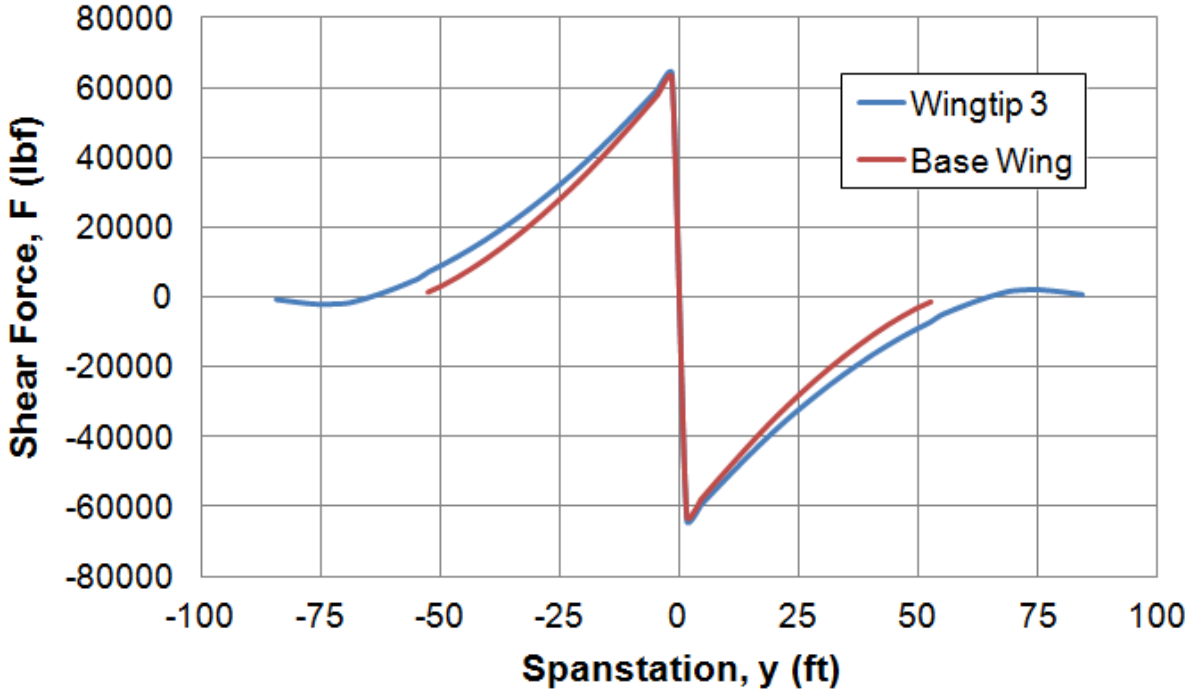

Figure 6.33: Shear Force on Wing and Wingtip 3

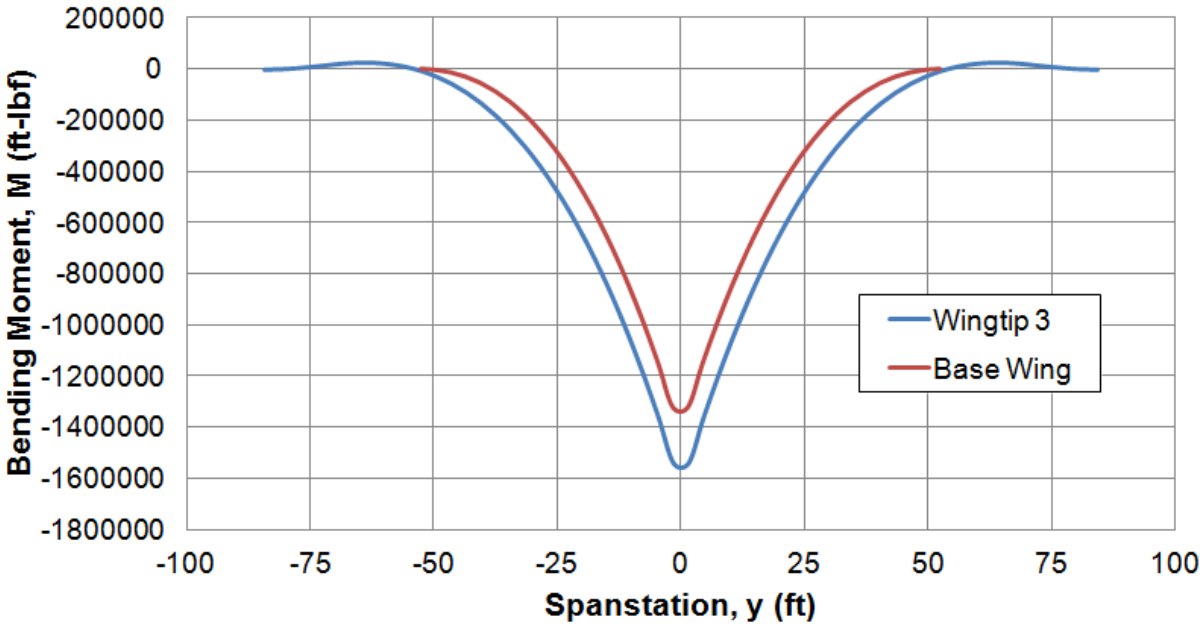

Figure 6.34: Bending Moment on Wing and Wingtip 3

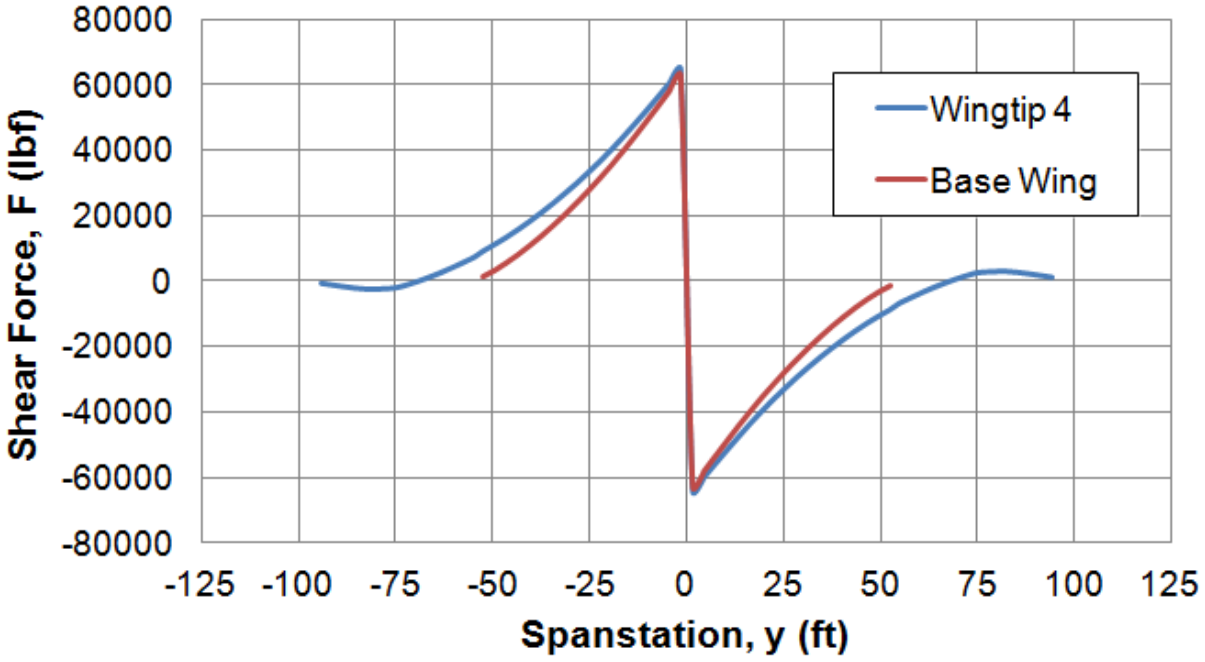

Figure 6.35: Shear Force on Wing and Wingtip 4

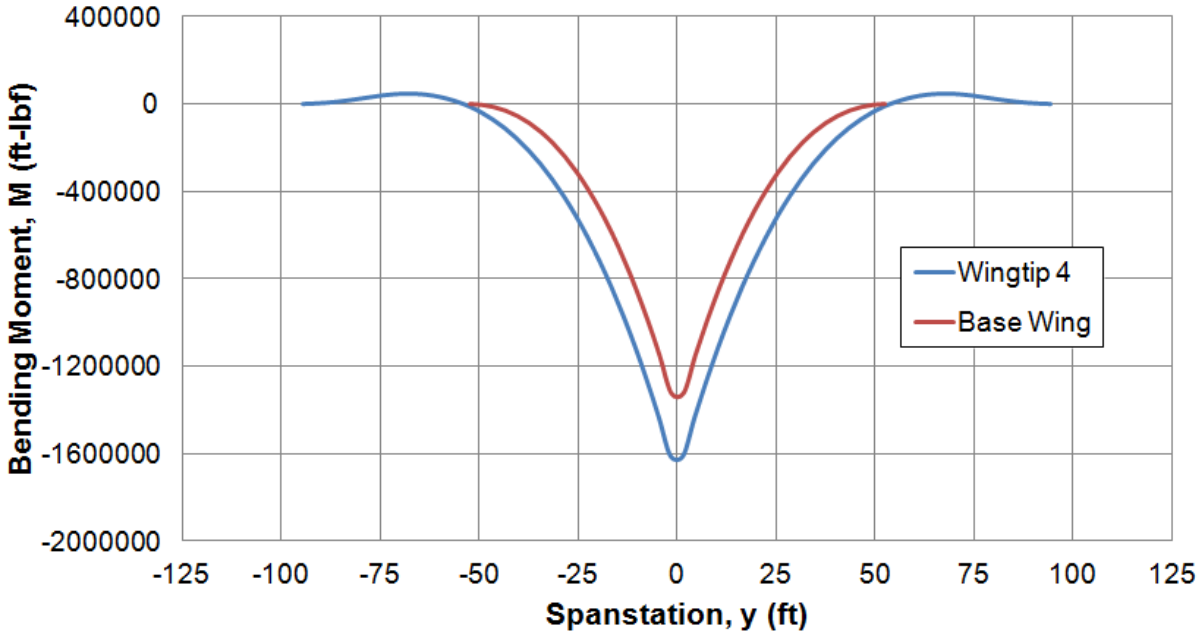

Figure 6.36: Bending Moment on Wing and Wingtip 4

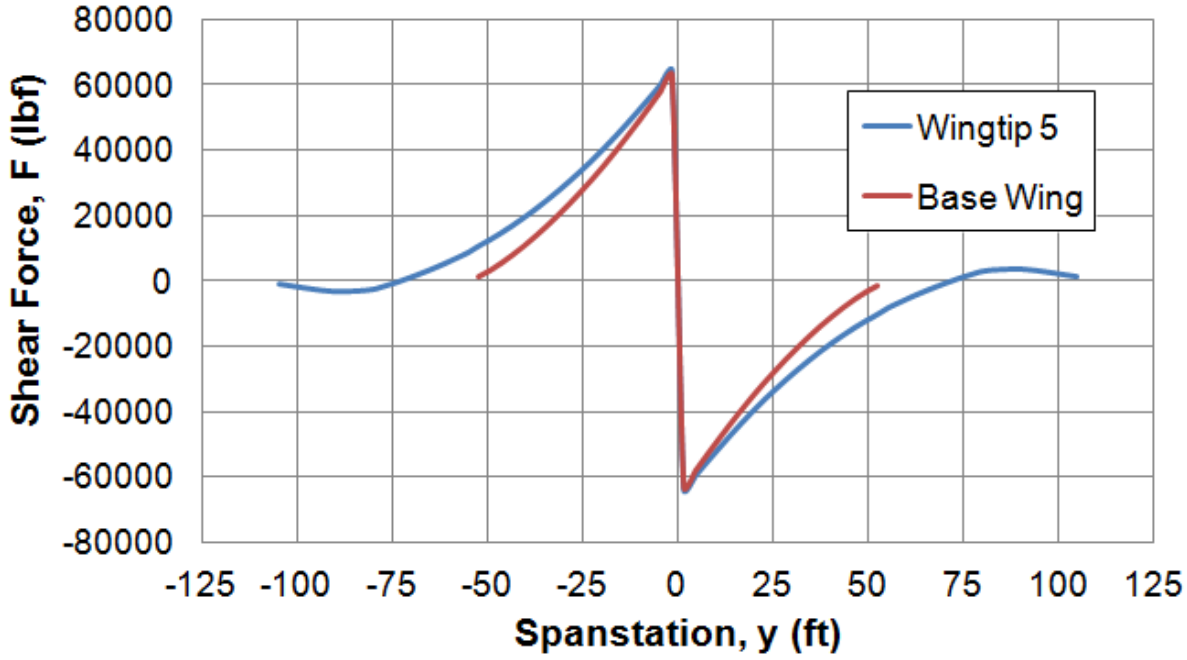

Figure 6.37: Shear Force on Wing and Wingtip 5

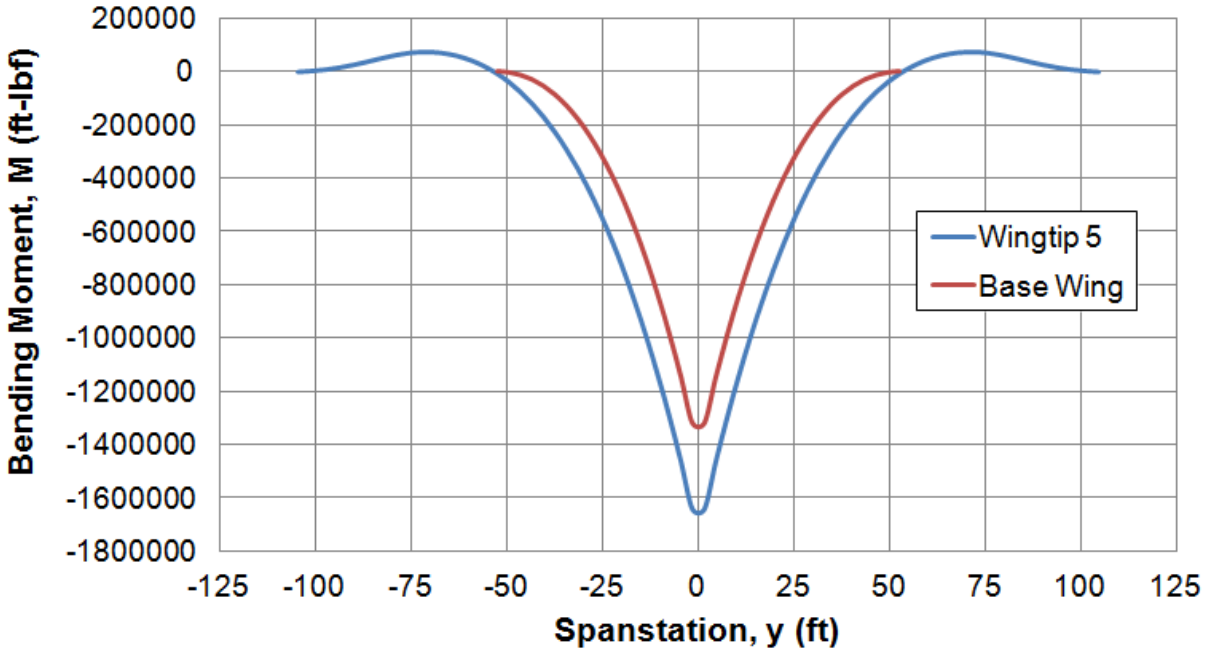

Figure 6.38: Bending Moment on Wing and Wingtip 5

6.4.4 Marketability Improvement

With an increase in fuel efficiency there are a couple benefits which airlines will see. The first being a reduction in fuel consumption, a recurring cost which makes up a significant portion of the lifecycle cost of an aircraft. With the addition of the largest span wingtip (wingtip 5), the range of the 727-200 was increased by 48%. This means that the airline could save nearly half the money which would be spent on fuel. This extrapolated over the life of the aircraft equates to substantial savings.

Another advantage to the increased range is the opening of new city pairs. Figure 6.39 shows the range circles of the original 727-200 (inner circles) along with the range circles of the 727-200 with wingtip 5 (outer circles).

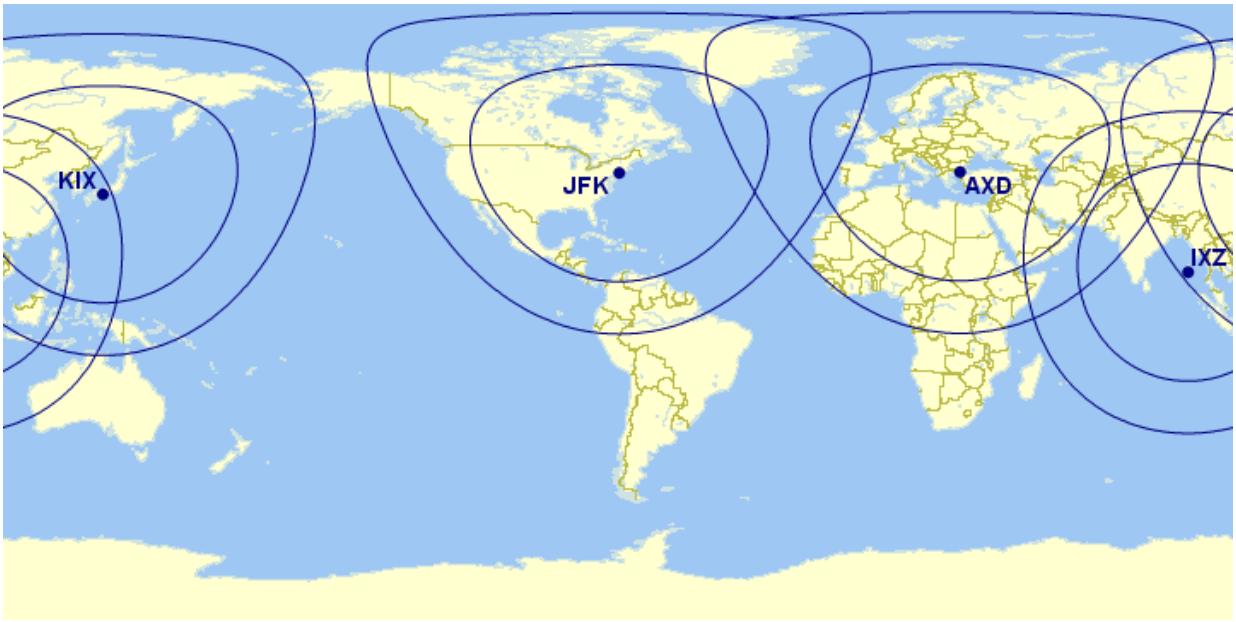

Figure 6.39: Airports with Still-Air Range Circles [62]

With the range increase from the wingtip, the aircraft can fly all domestic flights within the United States and Canada and reach part of South America; all routes within Europe can be serviced.

Even though more city pairs are attainable with the improved range capability, the current city pairs will still be operated. In flying the same paths, aircraft operators will see significant fuel cost savings. Fuel is a recurring cost to operators meaning that these fuel savings will be incurred over the lifespan of the aircraft. Figure 6.40 shows the cost of fuel as a percentage of cash operating expenses. From the aerodynamic analysis performed, a 48% fuel burn reduction was applied to estimate the cost of fuel as a percentage of the cash operating expense to operate the same aircraft with the addition of the wingtip 5 design. This does not take into account the acquisition and installation cost of the wingtip extension or maintenance.

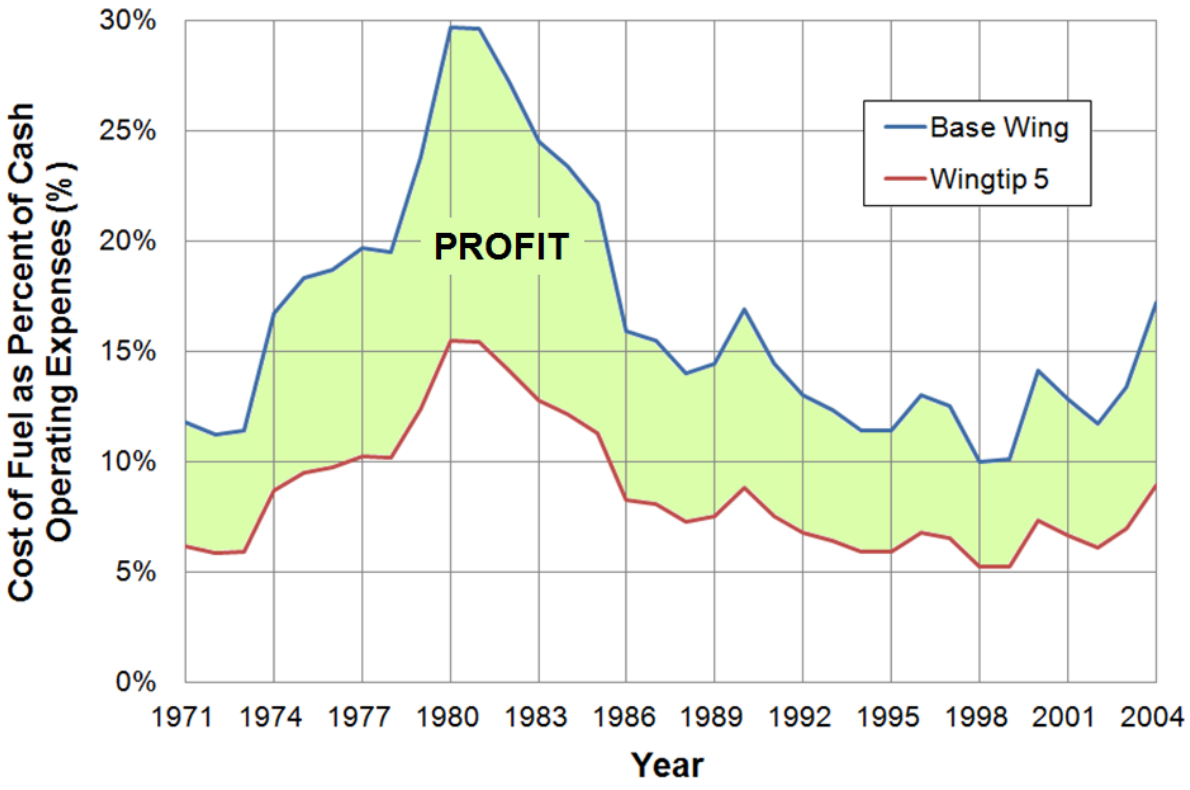

Figure 6.40: Fuel Cost as Percentage of Cash Operating Expenses for Base Wing and Wingtip 5 [Data from Ref. 63]

If aircraft operators install and operate the wingtip 5 design without changing other economic factors, such as consumer expenditure or wages, the difference in the cost of fuel as a percentage of cash operating expenses between the baseline aircraft and the aircraft with the wingtip 5 design retrofit is pure profit to the operator. This profit is shown in green in Figure 6.40. This, again, does not take acquisition, installation, or maintenance costs into account.

7 Conclusions and Recommendations

The results from the study completed are summarized in Section 7.1 with the recommendations for future work explained in Section 7.2

7.1 Conclusions

The following benefits were found through a preliminary analysis when Prandtl-tailored adaptive aerocompliant wingtip extensions are retrofitted on a Boeing 727-200:

- Significant increase in the maximum lift-to-drag ratio
    - Percent increase over baseline aircraft
        - Wingtip 1 L/D increase: 14%
        - Wingtip 2 L/D increase: 24%
        - Wingtip 3 L/D increase: 33%
        - Wingtip 4 L/D increase: 41%
        - Wingtip 5 L/D increase: 48%
- Increased mission range with no additional fuel usage, opening more city pairs
    - Percent increase over baseline aircraft
        - Wingtip 1 range increase: 2% @ 40,000 ft
        - Wingtip 2 range increase: 11% @ 40,000 ft
        - Wingtip 3 range increase: 22% @ 45,000 ft
        - Wingtip 4 range increase: 36% @ 50,000 ft
        - Wingtip 5 range increase: 48% @ 50,000 ft

- Substantial reduction in fuel consumption leading to reduction in direct operating cost
- Reduction in airframe fatigue due to gust alleviation
- Dispatch rate improvement due to performance improvement in adverse weather conditions

One consideration in the design of the wingtip extension was the challenges in certifying new technology. For this reason, only FAR 25 certified materials were used in the design along with triple redundancy in the honeycomb structure.

The philosophy used behind the design of the Boeing 727-200 Prandtl-tailored adaptive aerocompliant wingtip extension follows basic principles which can be applied to nearly all aircraft by simply modifying the outer mold line dimensions. The design of the wingtip extension also serves as a stepping stone for changing the way that future base wings are designed. After the wingtip extension retrofit is successfully proven for in-service aircraft, the design of wings in their base form could be revolutionized to follow the same philosophy and therefore improve the performance not only when a wingtip extension retrofit is added but also the simplest base model.

7.2 Recommendations

This thesis represents the first phase of this study. It is recommended that phases two through five be conducted to properly prove this concept. Within these phases, a wind tunnel model should be built to verify the following:

- Aerodynamic performance

- Performance of the pressure adaptive honeycomb in its pressurized and depressurized state
- Gust alleviation properties
- Fatigue of the folding mechanism
- Fatigue of the base wing due to the increase in loading

Following the wind tunnel tests, full-scale flight test verification should be completed. This will ensure that the results found through the wind tunnel tests are acceptable and the wingtip extension design is a viable and safe retrofit for commercial aircraft.

8 References

1. Gray, Carroll. "John J. Montgomery 1858-1911." *Flying Machines*. 1998. Web. 24 June 2014.

2. Benson, Tom. "Wright Brothers' Wing Warping." *NASA*. NASA, 2014. Web. 24 June 2014.

3. Gaunt, Brian. "Makhonine MAK 10- 1931." *Virtual Aircraft Museum*. N.p., Aug. 2008. Web. 24 June 2014.

4. Anon., "Factsheets : Bell X-5." *National Museum of the US Air Force*. N.p., Oct. 2013. Web. 24 June 2014.

5. Page, R. *Aircraft Engineering and Aerospace Technology*. Bradford: MCB UP. Print.

6. Dunbar, Brian. "North American Aviation XB-70 Valkyrie." *NASA*. NASA, 2014. Web. 24 June 2014.

7. Hansen, James R. *The Bird Is on the Wing: Aerodynamics and the Progress of the American Airplane*. College Station: Texas A & M UP, 2004. Print.

8. Hoerner, Sighard F. *Aerodynamic Shape of the Wing Tips*. Wright Patterson Air Force Base, Dayton, Ohio: U.S. Air Force, Air Materiel Command, 1949. Print.

9. Anon., "ZODIAC XL Design & Construction - WINGS - Kit Plane." *ZODIAC XL Design & Construction - WINGS - Kit Plane*. Zenith Aircraft Company, 30 Sept. 2013. Web. 10 June 2014.

10. Dunbar, Brian. "Aviation Pioneer Richard T. Whitcomb." *NASA*. NASA, Oct. 2009. Web. 24 June 2014.

11. Curry, Marty. "KC-135 EC79-11481: KC-135A in Flight - Closeup of Winglet with Attached Tufts." *KC-135 EC79-11481: KC-135A in Flight - Closeup of Winglet with Attached Tufts*. NASA, 6 Feb. 2002. Web. 12 June 2014.

12. Barber, R. “Technical Notes to NASA Dryden Tech Director.” 17 April 1980. Memos.

13. Padfield, R. "First Learjet 28 Still Awesome." *Aviation International News*. EPIC®, Dec. 2013. Web. 24 June 2014.

14. Larson, Jonathan. "A Producer Class Hero Is Something to Be." *Real Economics*. N.p., 25 Aug. 2013. Web. 12 June 2014.

15. Pingstone, Adrian. "Learjet 60 on Climb-out." N.p., 1 Dec. 2006. Web. 10 June 2014.

16. Anon., "767-400ER Flight Testing." *767-400ER Flight Testing*. N.p., n.d. Web. 12 June 2014.

17. Anon., "Aviation Partners Blended Winglet Performance Enhancement System." *Aviation Partners Inc- Seattle WA*. N.p., n.d. Web. 24 June 2014.

18. Anon., "Winglets On A Light Twin? — Tech Ops Forum | Airliners.net." *Winglets On A Light Twin? — Tech Ops Forum | Airliners.net*. 2 Oct. 2009. Web. 24 June 2014.

19. Kunz, David. "Snow//The FRA Experience. VIE-FRA VvOn LH." *The Wings of the Web*. N.p., 30 Jan. 2012. Web. 12 June 2014.

20. Leibowitz, Bruce. "3 Engines on the Tail." *Flightline Aviation Media*. N.p., n.d. Web. 12 June 2014.

21. Ursache, Narcis M., Tomas Melin, Askin T. Isikveren, and Michael I. Friswell. *Morphing Winglets for Aircraft Multi-phase Improvement*. Tech. no. 2007-7813. AIAA, 2007. Print.

22. Gatto, A., F. Mattioni, and M. I. Friswell. "Experimental Investigation of Bistable Winglets to Enhance Wing Lift Takeoff Capability." *Journal of Aircraft - 46(2):647 - PDF (AIAA)*. Journal of Aircraft, Mar.-Apr. 2009. Web. 8 Apr. 2014.

23. Falcao, Luis, Alexandra Gomes, and Afzal Suleman. *Design and Analysis of and Adaptive Wingtip*. Tech. no. 2011-2131. AIAA, Apr. 2011. Web. 16 Mar. 2014.

24. Barrett, R. *Passively Dynamic Prantdl-Tailored Aerocompliant δ_3 PAH Wingtip Extension Study for the AMC Fleets*. Tech. Print.

25. Stephenson, Brent. "Pelagic Fun." Weblog post. *B1RDER: The Birding Blog of Brent Stephenson*. N.p., 15 Nov. 2012. Web. 10 June 2014.

26. Anon., "Black Browed Albatross Flying." Weblog post. N.p., 19 Sept. 2011. Web. 10 June 2014.

27. Anon., "Pterosaurs." *Biology of Extinct Animals*. N.p., 21 Nov. 2007. Web. 10 June 2014.

28. Shyamal, L. "Flight Silhouettes." N.p., 1 Dec. 2007. Web. 15 May 2014.

29. Prandtl, Ludwig. "About Smallest Induced Drag of A[n Air Plane] Wing."*Zeitschrift Fur Flugtechnik Und Motorluftschiffahrt* (1933): 305-06. Web.

30. Baals, Donald D., and William R. Corliss. *Wind Tunnels of NASA*. Washington, D.C.: NASA, 1981.

31. Barber, R. “Technical Notes to NASA Dryden Tech Director.” 1979-1980. Memos.

32. Anon., "Typical Mission Profile." *737NG Range Assets*. The Boeing Company, 2006. Web. 24 June 2014.

33. Anon., "Boeing Commercial Aircraft- Design Groups/Codes (FAA & ICAO)." (2014). *Airport Compatibility*. The Boeing Company. Web. 24 June 2014.

34. Anon., "Charlotte Douglas Airport Aerial View." City of Charlotte, 2013. Web. 8 June 2014.

35. Leishman, J. Gordon. *Principles of Helicopter Aerodynamics*. Cambridge: Cambridge UP, 2000. Print.

36. Anon., "Elite UK Forces." *Royal Marines Photos - Lynx Helicopter*. N.p., n.d. Web. 24 June 2014.

37. Defense Industry Daily Staff. "From VH-71 to VXX: The Future of US Presidential Helicopters." *Defense Industry Daily RSS News*. Defense Industry Daily, 7 May 2014. Web. 24 June 2014.

38. Johnson, Wayne. *Helicopter Theory*. New York: Dover Publications, 1994. Print.

39. Parsch, Andreas. "Raytheon (Philco/General Electric) AAM-N-7/GAR-8/AIM-9 Sidewinder." *Raytheon AIM-9 Sidewinder*. 2008. Web. 24 June 2014.

40. Anon., "The Sidewinder Missile." *The Home Shop Machinist and Machinist's Workshop*. Web. 24 June 2014.

41. Curry, Marty. "X-29 at High Angle of Attack with Smoke Generators." *X-29 FSW Photo Gallery*. Dryden Flight Research Center, 2002. Web. 24 June 2014.

42. Anon., "History of Aerodynamics and Aircraft Design." *Scientists and Friends*. 2007. Web. 24 Mar. 2014.

43. Vos, Roelof, and Ron Barrett. "Mechanics of Pressure-adaptive Honeycomb and Its Application to Wing Morphing." *Smart Materials and Structures* 20.9 (2011): 094010. Web.

44. Vos, Roelof, and Ron Barrett. "Pressure Adaptive Honeycomb: A New Adaptive Structure for Aerospace Applications." *Sensors and Smart Structures Technologies for Civil, Mechanical, and Aerospace Systems* (2010).

45. Anon., “Comparison of eaps with other actuator technologies,” in [ndeaa.jpl.nasa.gov/nasa-nde/lommas/eap/], SRI International and DARPA (Accessed: May 30 2009).

46. Jones, Robert M. *Mechanics of Composite Materials*. Washington: Scripta Book, 1975. Print.

47. Anon., "FAA Federal Aviation Regulations (FARS, 14 CFR)." *FAR Part § 25.333: Flight Maneuvering Envelope*. 1996. Web. 7 Apr. 2014.

48. Rustenburg, John, Donal Skinn, and Daniel O. Tipps. *Statistical Loads Data for Boeing 737-400 Aircraft in Commercial Operations*. Washington, D.C.: Federal Aviation Administration, Office of Aviation Research, 1998. Web.

49. Barrett, R., and C. Barrett. "Biomimetic FAA-certifiable, Artificial Muscle Structures for Commercial Aircraft Wings." *Smart Materials and Structures* 23.7 (2014). Web.

50. Brown, David P. "Photos of ANA's First Boeing 787 Dreamliner in Special Livery." *Airline Reporter*. N.p., 7 Aug. 2011. Web. 16 May 2014.

51. Sweers, Greg, Bruce Birch, and John Gokcen. "Lightning Strikes: Protection, Inspection, and Repair." The Boeing Company, 2012. Web. 24 June 2014.

52. Roskam, Jan. *Preliminary Sizing of Airplanes*. Lawrence, Kansas: DARcorporation, 2005. Print.

53. Anon., "BTS | Air Carrier Traffic Statistics." *Research and Innovative Technology Administration Bureau of Transportation Statistics*. Web. 19 Jan. 2014.

54. Lan, C. Edward, and Jan Roskam. *Airplane Aerodynamics and Performance*. Ottawa, Kansas: DARcorporation, 1981. Print.

55. Roskam, Jan. *Component Weight Estimation*. Lawrence, Kansas: DARcorporation, 2005. Print.

56. *Aviation Partners Inc.* Aviation Partners, n.d. Web. 24 Jan. 2014. <http://www.aviationpartners.com/>.

57. Melin, Tomas. "Tornado." *Tornado, the Vortex Lattice Method.* Redhammer Consulting Ltd, 2010. Web. 23 June 2014.

58. L.L Leisher et al, Stability derivatives of Cessna aircraft, Cessna Aircraft company. 1957.

59. Moran, J "Computational Fluid Dynamics", Weily&Sons, 1984

60. Melin.T, Tornado, a vortex lattice MATLAB implementation for Linear Aerodynamic Wing applications", Masters thesis, Royal Institute of Technology (KTH),Sweden, December 2000.

61. Roskam, Jan. *Preliminary Calculation of Aerodynamic, Thrust and Power Characteristics*. Lawrence, Kansas: DARcorporation, 2005. Print.

62. Swartz, Karl L. "Great Circle Mapper." *Great Circle Mapper*. N.p., 1996. Web. 24 June 2014.

63. Aerospace Research Center Aerospace Industries Association of America, Inc. *Aerospace Facts and Figures 2005-2006*. Arlington, Virginia: Aerospace Industries Association of America, 2005. Print.

A. Appendix A: Tornado Example Analysis

User inputs: green
Directions: blue
Tornado prompts: black

The program is started by typing and executing:
>Tornado
which will prompt the main menu to appear.

```
_____________________________________________________________
 TORNADO  Version 135  Release version
 build 2010 03 20 14:07 UTC
 Main Menu
_____________________________________________________________
Input operations.
        [1]. Aircraft geometry setup
        [2]. Flight condition setup
        [3]. Change rudder setting
        [4]. Move reference point

Lattice operations.
        [5]. Generate lattice.

Computation operations.
        [6]. Processor access

Post processing and interactive operations.
        [7]. Post processing, Result/Plot functions
        [8]. Keyboard access

Auxiliary operations.
        [10]. About / Release Info
        [100]. Help files
        [0]. Exit Tornado

        Please enter choice from above:
```

The user navigates through the program by selecting the number next to the desired function and entering it in the prompt area. This input should be entered in either a numerical format or string format. When a yes or no question is prompted, the user enters 0 for no and 1 for yes.

The inputs for analyzing the first wingtip extension design are shown below:

```
Input operations.
        [1]. Aircraft geometry setup
        [2]. Flight condition setup
        [3]. Change rudder setting
        [4]. Move reference point

Lattice operations.
```

[5]. Generate lattice.

Computation operations.
[6]. Processor access

Post processing and interactive operations.
[7]. Post processing, Result/Plot functions
[8]. Keyboard access

Auxiliary operations.
[10]. About / Release Info
[100]. Help files
[0]. Exit Tornado

Please enter choice from above: 1

---

[1]. Define new geometry
[2]. Load geometry
[3]. Edit current geometry
[4]. Save current geometry

[5]. Define blunt body data (for friction drag est).

[0]. Back / up menu

Please enter choice from above: 2

B727_100-2.mat
B727_100.mat
B747-400.mat
B747_200.mat
B_47B.mat
B_52A.mat
Bo_CRJ900-2.mat
Bo_CRJ900.mat
Bo_GEX-2.mat
Bo_GEx-3.mat
Bo_GEx.mat
C.mat
delta70.mat
ellipse.mat
safir9.mat
B707_320B-2.mat
B707_320B-3.mat
B707_320B.mat
Le_45-2.mat
Le_45-3.mat
Le_45-4.mat
Me262.mat
P51Da.mat
SQR.mat
TCR1.mat
TCR4.mat
TCRTM.mat
X31.mat
airfoil
delta.mat
L_45.mat
L_C141B.mat
L_C5A.mat

Load file: B727_100-2

Input operations.

[1]. Aircraft geometry setup
[2]. Flight condition setup
[3]. Change rudder setting
[4]. Move reference point

Lattice operations.

[5]. Generate lattice.

Computation operations.

[6]. Processor access

Post processing and interactive operations.

[7]. Post processing, Result/Plot functions
[8]. Keyboard access

Auxiliary operations.

[10]. About / Release Info
[100]. Help files
[0]. Exit Tornado

Please enter choice from above: 1

---

[1]. Define new geometry
[2]. Load geometry
[3]. Edit current geometry
[4]. Save current geometry

[5]. Define blunt body data (for friction drag est).

[0]. Back / up menu

Please enter choice from above: 3

Number of wings are: 3
Number of partition per wing are : 3 1 1

---

[1] Add Wing
[2] Remove Wing

[3] Add partition to a wing
[4] Remove partition from a wing

[5] View wing data

[6] Edit wing/partition data

[7] Plot Geometry

[0] Back / up menu

Please enter choice from above: 3

Partition will be added at wingtip
Add partition to wing no: 1

Number of wings are: 3
Number of partition per wing are: 4 1 1

---

[1] Add Wing
[2] Remove Wing

[3] Add partition to a wing
[4] Remove partition from a wing

[5] View wing data

[6] Edit wing/partition data

[7] Plot Geometry

[0] Back / up menu

Please enter choice from above: 3

Partition will be added at wingtip
Add partition to wing no: 1

Number of wings are :3
Number of partition per wing are :5 1 1

---

[1] Add Wing
[2] Remove Wing

[3] Add partition to a wing
[4] Remove partition from a wing

[5] View wing data

[6] Edit wing/partition data

[7] Plot Geometry

[0] Back / up menu

Please enter choice from above: 3

Partition will be added at wingtip
Add partition to wing no: 1

Number of wings are :3
Number of partition per wing are :6 1 1

---

[1] Add Wing
[2] Remove Wing

[3] Add partition to a wing
[4] Remove partition from a wing

[5] View wing data

[6] Edit wing/partition data

[7] Plot Geometry

[0] Back / up menu

Please enter choice from above: 6

Edit wing no: 1
Edit partition no: 4

Global entries

Reference point position:	5.6233	0	0.09722
[18] Center of gravity position:	5.1807	0	0.09722

Wing specific entries

[1] Wing Symmetric:	1		
[2] Apex coordinates:	0	0	0
[3] Base chord:	7.77		

Partition specific entries

[4] Dihedral:	0
[5] Partition half-span:	0
[6] Partition sweep:	0
[7] Partition taper:	0
[8] Partition inner airfoil:	0
[9] Partition outer airfoil:	0
[10] Partition inner twist:	0
[11] Partition outer twist:	0
[12] Partition flapped:	0
[13] Flap chords (Parts) :	0
[14] Flaps deflect symmetric:	0
[15] No. of chord-wise panels:	0
[16] No. of span-wise panels:	0
[17] No. of flap-chord panels:	0
[19] Panel Distribution:	1

[0] EXIT

Edit Menu Item [1-19]:

The final wingtip extension user inputs for wingtip 1 are shown below:

Partition specific entries

Partitions half-span:	1.828	4.571	10.056
	1.65	0.33	1.32
Partitions sweep:	0	0.57643	0.55858
	0.55858	-0.785	1
Partitions Dihedral:	0	0.019199	0.019199
	0.019199	0.019199	0.019199
Partitions taper:	1	0.647	0.546
	0.546	4	0.3
Partitions inner airfoil:	N651012.DAT	N651012.DAT	N651012.DAT
	N651012.DAT	N651012.DAT	N651012.DAT
Partitions outer airfoil:	N651012.DAT	N651012.DAT	N651012.DAT
	N651012.DAT	N651012.DAT	N651012.DAT
Partition inner twists:	0.0524	0.05236	0
	-0.01745	0	-0.15

Partition outer twists:	0.0524	0	-0.01745	
	0	-0.15	-0.15	
Partition flapped:	0	0	0	
	0	0	0	
No. Chord-wise panels:		5	5	5
		5	5	5
No. Span-wise panels:		2	5	11
		13	1	3
No. Flap-chord panels:		0	0	0
		0	0	0
Panel distribution:		1	1	1
		1	1	1
Flap setting:		0	0	0
		0	0	0

The flight condition will be set up next.

[1]. Aircraft geometry setup
[2]. Flight condition setup
[3]. Change rudder setting
[4]. Move reference point

Lattice operations.
[5]. Generate lattice.

Computation operations.
[6]. Processor access

Post processing and interactive operations.
[7]. Post processing, Result/Plot functions
[8]. Keyboard access

Auxiliary operations.
[10]. About / Release Info
[100]. Help files
[0]. Exit Tornado

Please enter choice from above: 2

---

[1]. Define new state
[2]. Load state
[3]. Save current state

[4]. Change angle of attack

[0]. Back / up menu

Please enter choice from above: 1

Alpha [deg]: 2.7
Beta [deg]: 0
Roll angular velocity [deg/s]: 0
Pitch angular velocity [deg/s]: 0
Yaw angular velocity [deg/s]: 0
Angle of attack time derivative, (Alpha_dot), [deg/s]: 0
Angle of sideslip time derivative, (Beta_dot), [deg/s]: 0

****
Enter which type of speed you wish to enter:

International units:

[1]. True airspeed (TAS) at SSL [m/s]
[2]. True airspeed (TAS) at altitude [m/s, m]
[3]. Equivalent airspeed (EAS) at altitude [m, m/s]
[4]. Calibrated air speed (CAS) at altitude [m, m/s]
[5]. Mach number at altitude [-, m]

Imperial Units:

[6]. True airspeed (TAS) at altitude [kts, ft]
[7]. Equivalent airspeed (EAS) at altitude [kts, ft]
[8]. Calibrated air speed (CAS) at altitude [kts, ft]
[9]. Mach number at altitude [-, ft]

Type of speed selection: 9

Mach number [-]: 0.82
+++

Altitude [ft]: 40000

Caution, only use this option if you are sure, really sure, what you are doing.
Apply Prandtl-Glauert Correction [0 1]: 0

---

[1]. Aircraft geometry setup
[2]. Flight condition setup
[3]. Change rudder setting

[4]. Move reference point

Lattice operations.
[5]. Generate lattice.

Computation operations.
[6]. Processor access

Post processing and interactive operations.
[7]. Post processing, Result/Plot functions
[8]. Keyboard access

Auxiliary operations.
[10]. About / Release Info
[100]. Help files
[0]. Exit Tornado

Please enter choice from above: 5

****
Which type of method to use:

[0] = Freestream following wake, Tornado method
[1] = Fixed wake, standard VLM method

Type of lattice selection: 0

---

[1]. Aircraft geometry setup
[2]. Flight condition setup
[3]. Change rudder setting
[4]. Move reference point

Lattice operations.
[5]. Generate lattice.

Computation operations.
[6]. Processor access

Post processing and interactive operations.
[7]. Post processing, Result/Plot functions
[8]. Keyboard access

Auxiliary operations.
[10]. About / Release Info
[100]. Help files
[0]. Exit Tornado

Please enter choice from above: 6

Low order solutions:
[1]. Static computation at selected state.
[2]. Sequential state parameter sweep menu:

High order methods:
[3]. Trimmed aircraft polar point.
[4]. Trimmed pitch sweep, polar.
[5]. Unsteady, acceleration free, time coefficients only.
[6]. Unsteady, acceleration free, all inviscous coefficients.

Auxillary operations:
[7]. Viscous Drag Estimation Methods Menu:
[8]. Grid convergence study.
[9]. Find stall angle of attack.
[10]. Find alpha at prescribed CL.
[11]. Compute static margin.

[0]. Cancel / up menu.

Enter choice from above please: 1
Enter Job IDentity tag (JID): wingtip1

Solution started, please wait.

Solution available in output/wingtip1-Cx

This generates the static state data for assumed cruise conditions. The output data can be opened as follows:

[1]. Aircraft geometry setup
[2]. Flight condition setup
[3]. Change rudder setting
[4]. Move reference point

Lattice operations.
[5]. Generate lattice.

Computation operations.
[6]. Processor access

Post processing and interactive operations.
[7]. Post processing, Result/Plot functions
[8]. Keyboard access

Auxiliary operations.

[10]. About / Release Info
[100]. Help files
[0]. Exit Tornado

Please enter choice from above: 7

---

[1]. Clear plots
[2]. Geometry plot

Solution plots

[3]. Static state
[4]. Parameter sweep sub menu
[5]. Unsteady state, time coefficients only
[6]. Unsteady state, all coefficients

Viscous drag estimation plots

[7]. Plot wing system zero lift drag estimation
[8]. Plot body friction drag estimation

Post processing computations

[9]. Perform a trefftz plane analysis, (experimental)
[10]. Export simple state results to textfile

[0]. Back / up menu

Please enter choice from above: 3

Available static solution result files are:

Cx.mat
wingtip1-Cx.mat
C-Cx.mat

Enter JID to plot: wingtip1

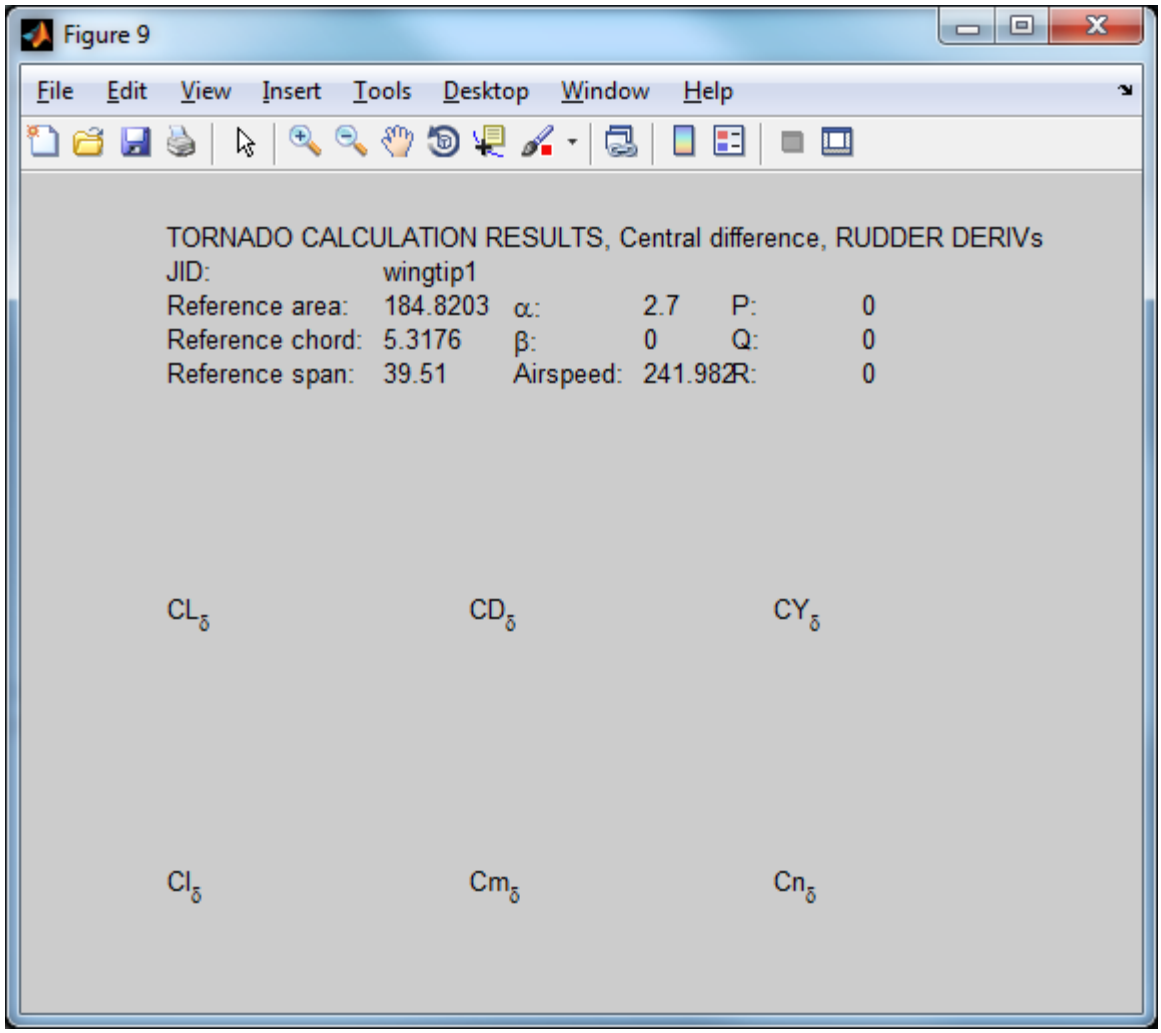
Figure 9
File Edit View Insert Tools Desktop Window Help
TORNADO CALCULATION RESULTS, Central difference, RUDDER DERIVs
JID: wingtip1
Reference area: 184.8203 α: 2.7 P: 0
Reference chord: 5.3176 β: 0 Q: 0
Reference span: 39.51 Airspeed: 241.982 R: 0
CLδ CDδ CYδ
Clδ Cmδ Cnδ

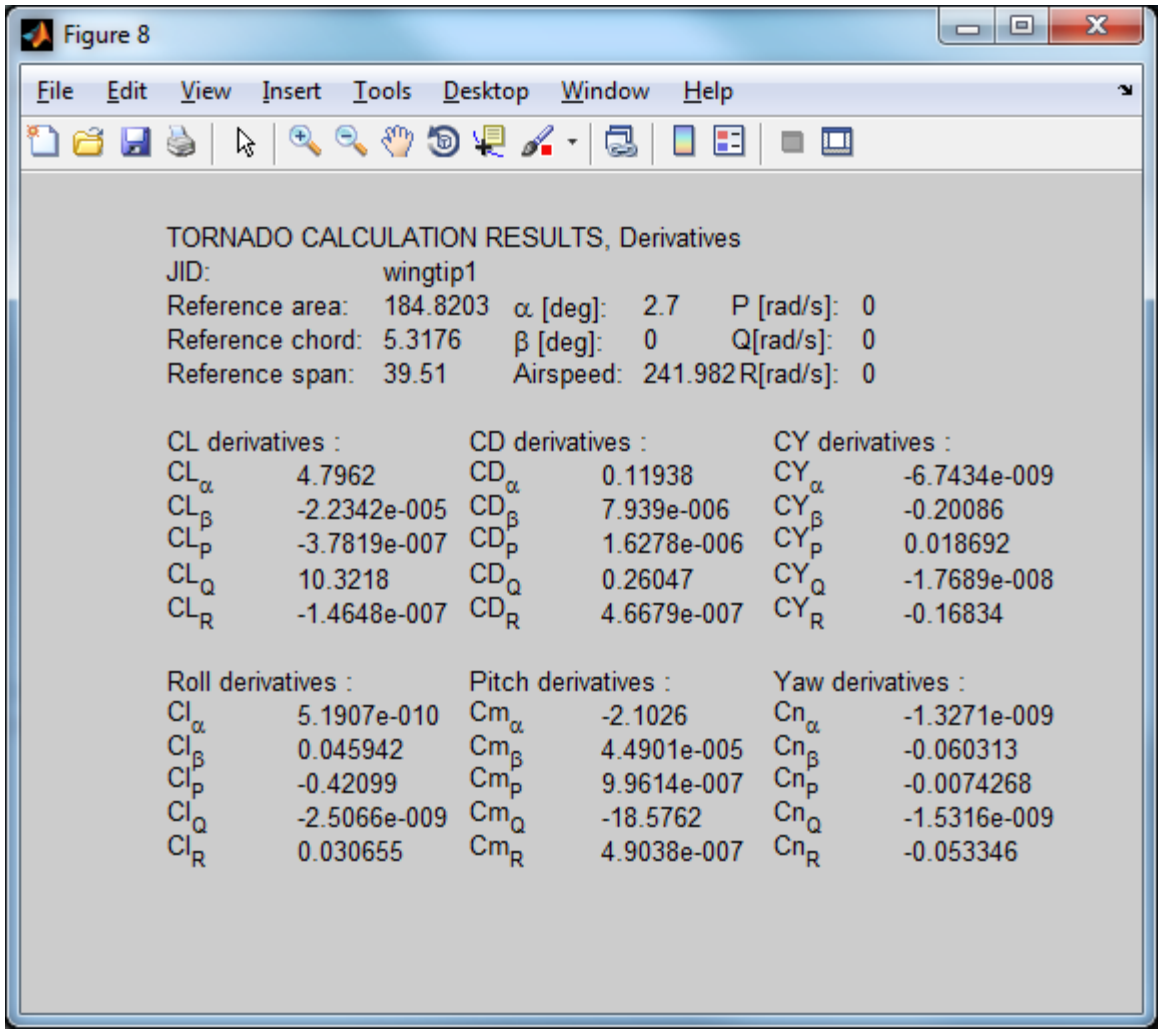
Figure 8
File Edit View Insert Tools Desktop Window Help
TORNADO CALCULATION RESULTS, Derivatives
JID: wingtip1
Reference area: 184.8203 α [deg]: 2.7 P [rad/s]: 0
Reference chord: 5.3176 β [deg]: 0 Q[rad/s]: 0
Reference span: 39.51 Airspeed: 241.982 R[rad/s]: 0
CL derivatives :
CLα 4.7962
CLβ -2.2342e-005
CLP -3.7819e-007
CLQ 10.3218
CLR -1.4648e-007
CD derivatives :
CDα 0.11938
CDβ 7.939e-006
CDP 1.6278e-006
CDQ 0.26047
CDR 4.6679e-007
CY derivatives :
CYα -6.7434e-009
CYβ -0.20086
CYP 0.018692
CYQ -1.7689e-008
CYR -0.16834
Roll derivatives :
Clα 5.1907e-010
Clβ 0.045942
ClP -0.42099
ClQ -2.5066e-009
ClR 0.030655
Pitch derivatives :
Cmα -2.1026
Cmβ 4.4901e-005
CmP 9.9614e-007
CmQ -18.5762
CmR 4.9038e-007
Yaw derivatives :
Cnα -1.3271e-009
Cnβ -0.060313
CnP -0.0074268
CnQ -1.5316e-009
CnR -0.053346

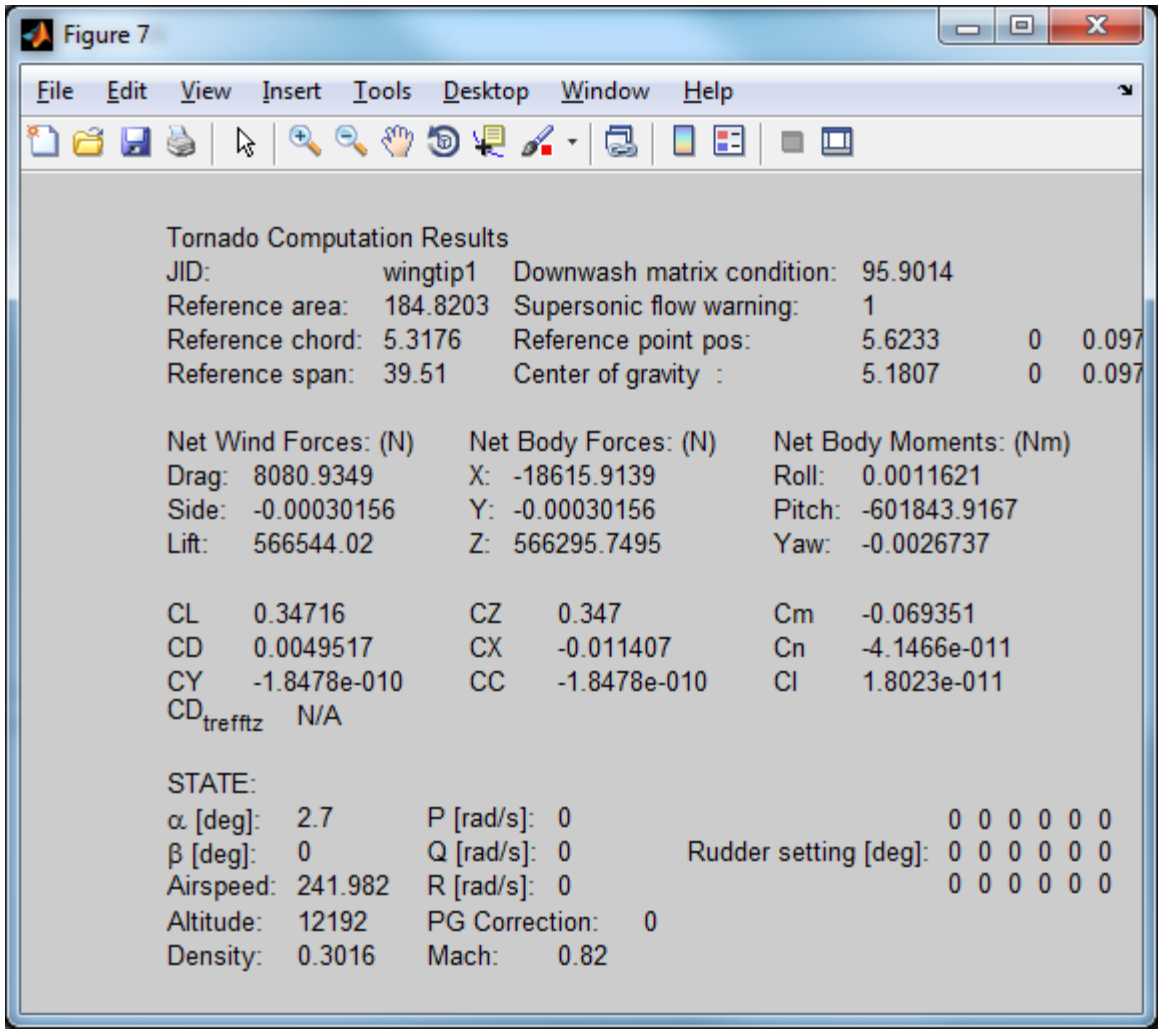
Figure 7
File Edit View Insert Tools Desktop Window Help
Tornado Computation Results
JID: wingtip1 Downwash matrix condition: 95.9014
Reference area: 184.8203 Supersonic flow warning: 1
Reference chord: 5.3176 Reference point pos: 5.6233 0 0.097
Reference span: 39.51 Center of gravity : 5.1807 0 0.097
Net Wind Forces: (N) Net Body Forces: (N) Net Body Moments: (Nm)
Drag: 8080.9349 X: -18615.9139 Roll: 0.0011621
Side: -0.00030156 Y: -0.00030156 Pitch: -601843.9167
Lift: 566544.02 Z: 566295.7495 Yaw: -0.0026737
CL 0.34716 CZ 0.347 Cm -0.069351
CD 0.0049517 CX -0.011407 Cn -4.1466e-011
CY -1.8478e-010 CC -1.8478e-010 Cl 1.8023e-011
CD trefftz N/A
STATE:
α [deg]: 2.7 P [rad/s]: 0
β [deg]: 0 Q [rad/s]: 0 Rudder setting [deg]: 0 0 0 0 0 0
Airspeed: 241.982 R [rad/s]: 0 0 0 0 0 0 0
Altitude: 12192 PG Correction: 0
Density: 0.3016 Mach: 0.82

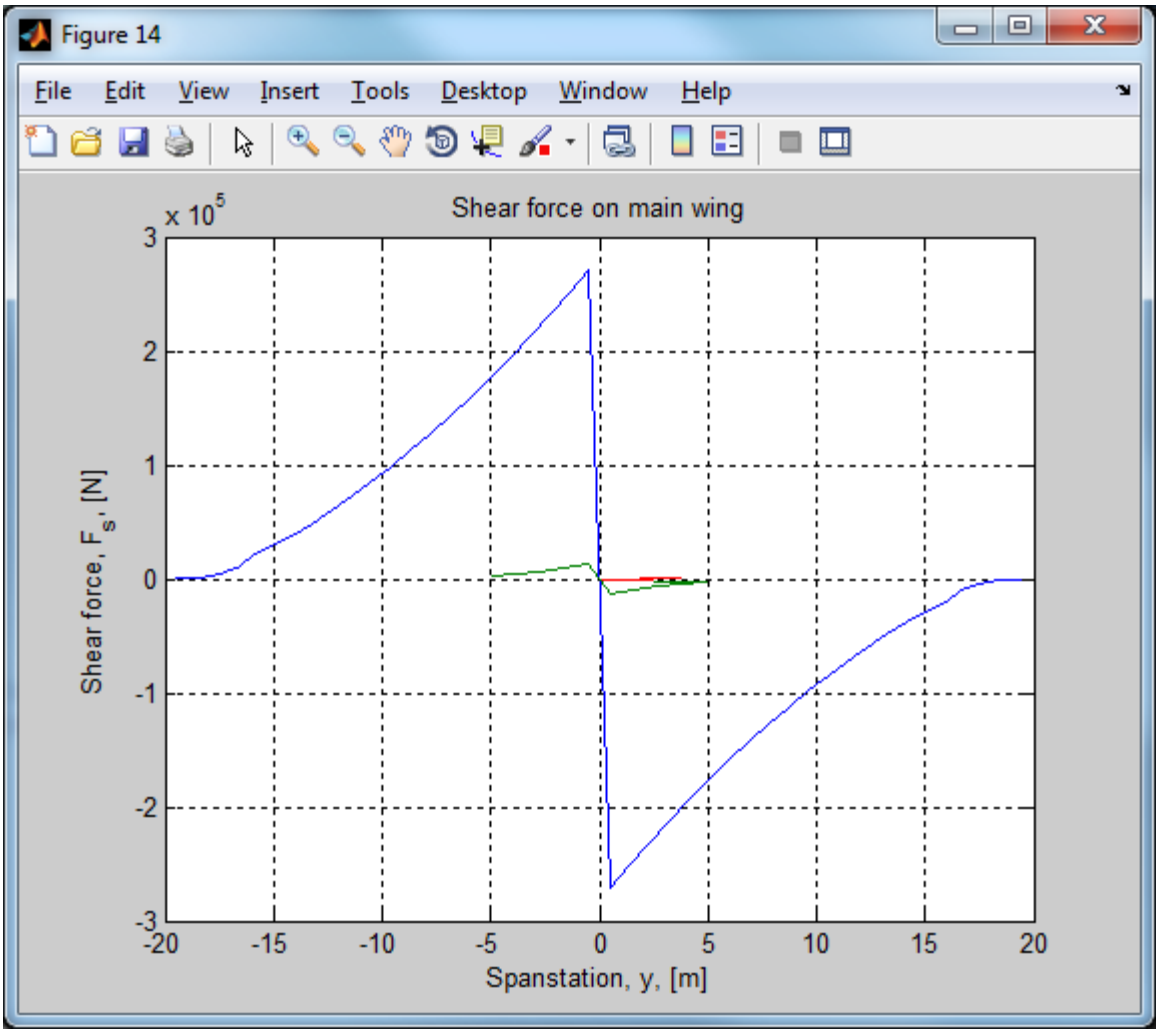
Figure 14
File Edit View Insert Tools Desktop Window Help
Shear force on main wing
x 10^5
Shear force, F_s, [N]
Spanstation, y, [m]
3
2
1
0
-1
-2
-3
-20
-15
-10
-5
0
5
10
15
20

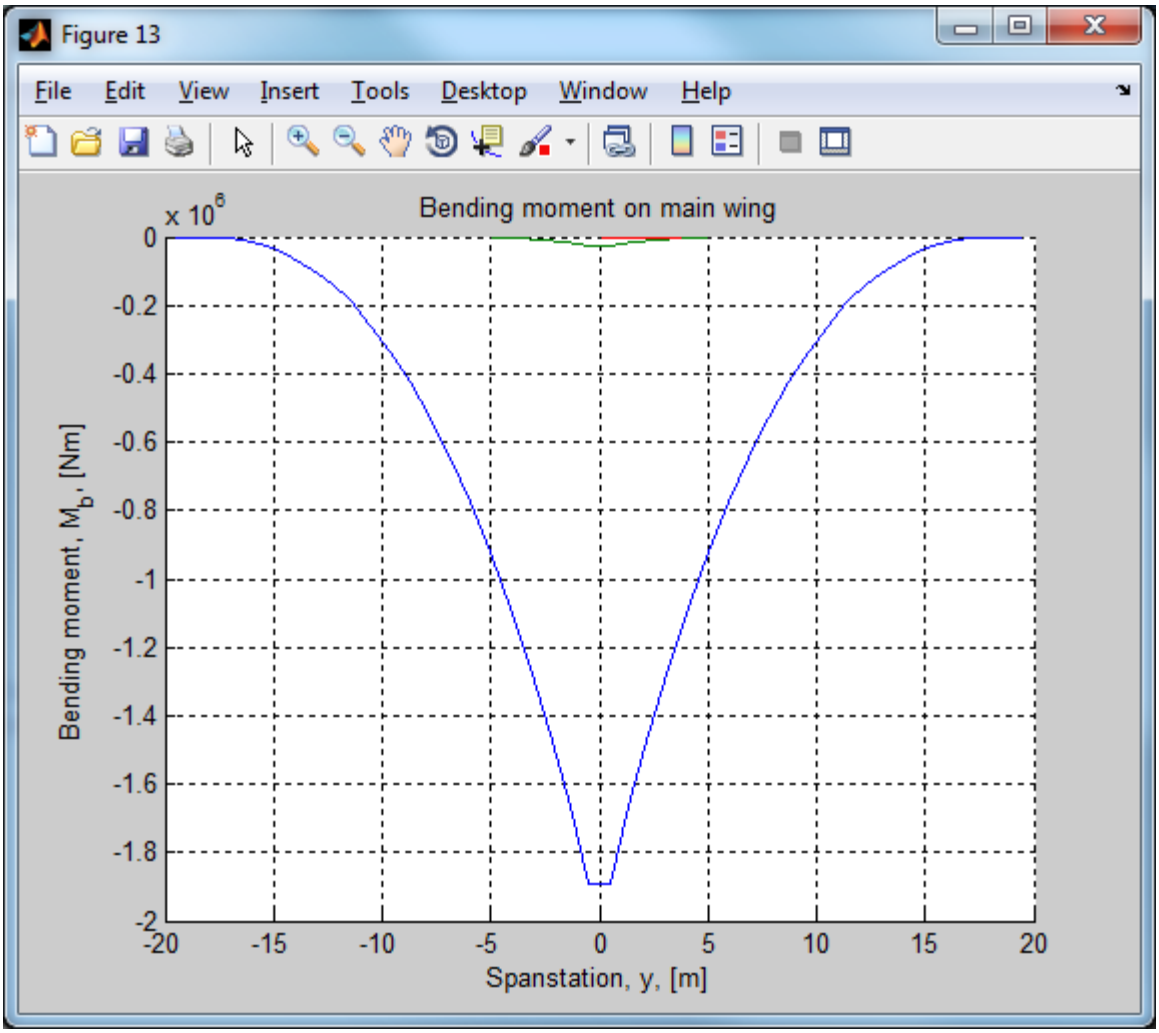
Figure 13
File Edit View Insert Tools Desktop Window Help
Bending moment on main wing
x 10^6
0
-0.2
-0.4
-0.6
-0.8
-1
-1.2
-1.4
-1.6
-1.8
-2
Bending moment, M_b, [Nm]
-20 -15 -10 -5 0 5 10 15 20
Spanstation, y, [m]

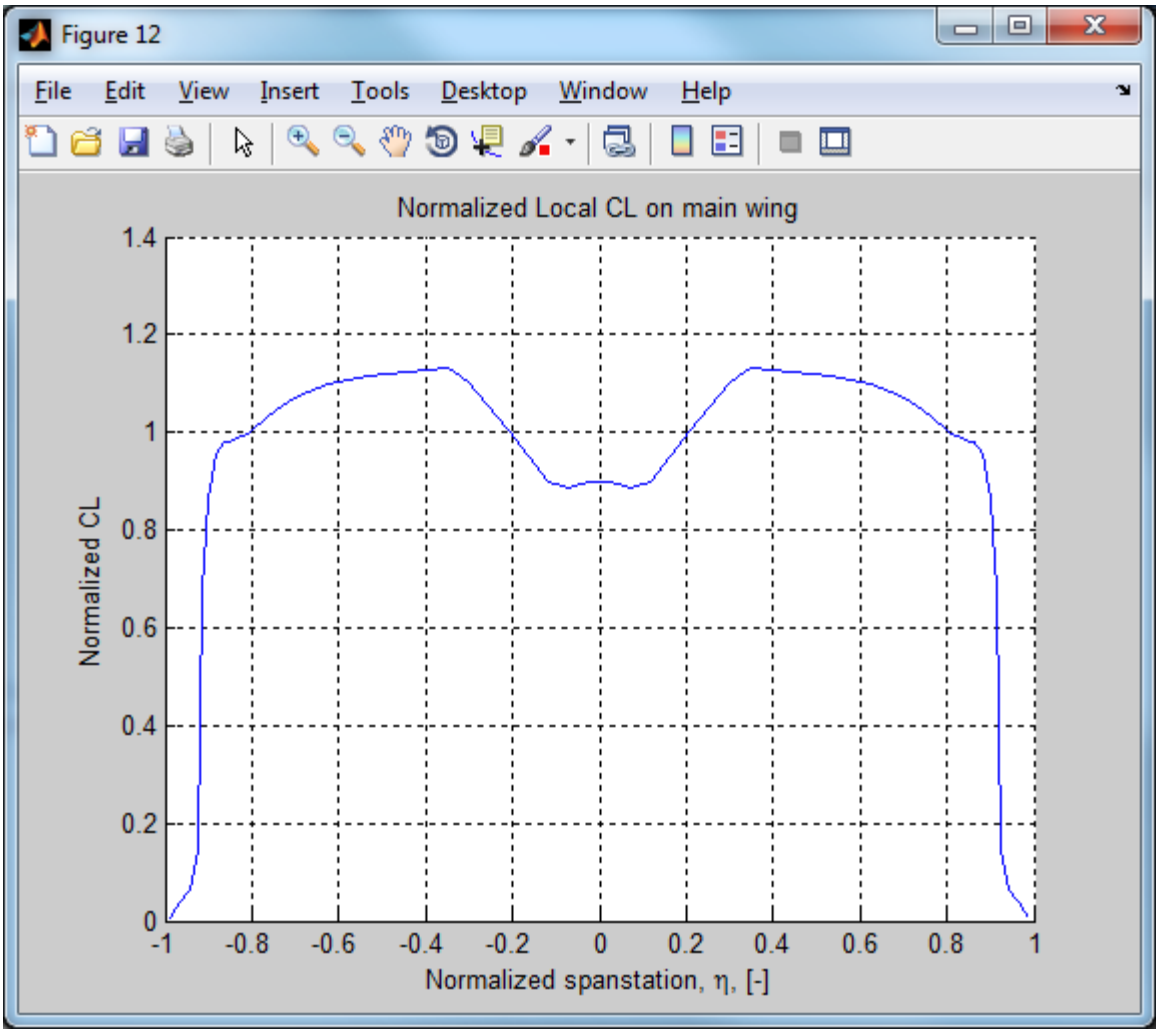
Figure 12
File Edit View Insert Tools Desktop Window Help
Normalized Local CL on main wing
Normalized CL
1.4
1.2
1
0.8
0.6
0.4
0.2
0
-1 -0.8 -0.6 -0.4 -0.2 0 0.2 0.4 0.6 0.8 1
Normalized spanstation, η, [-]

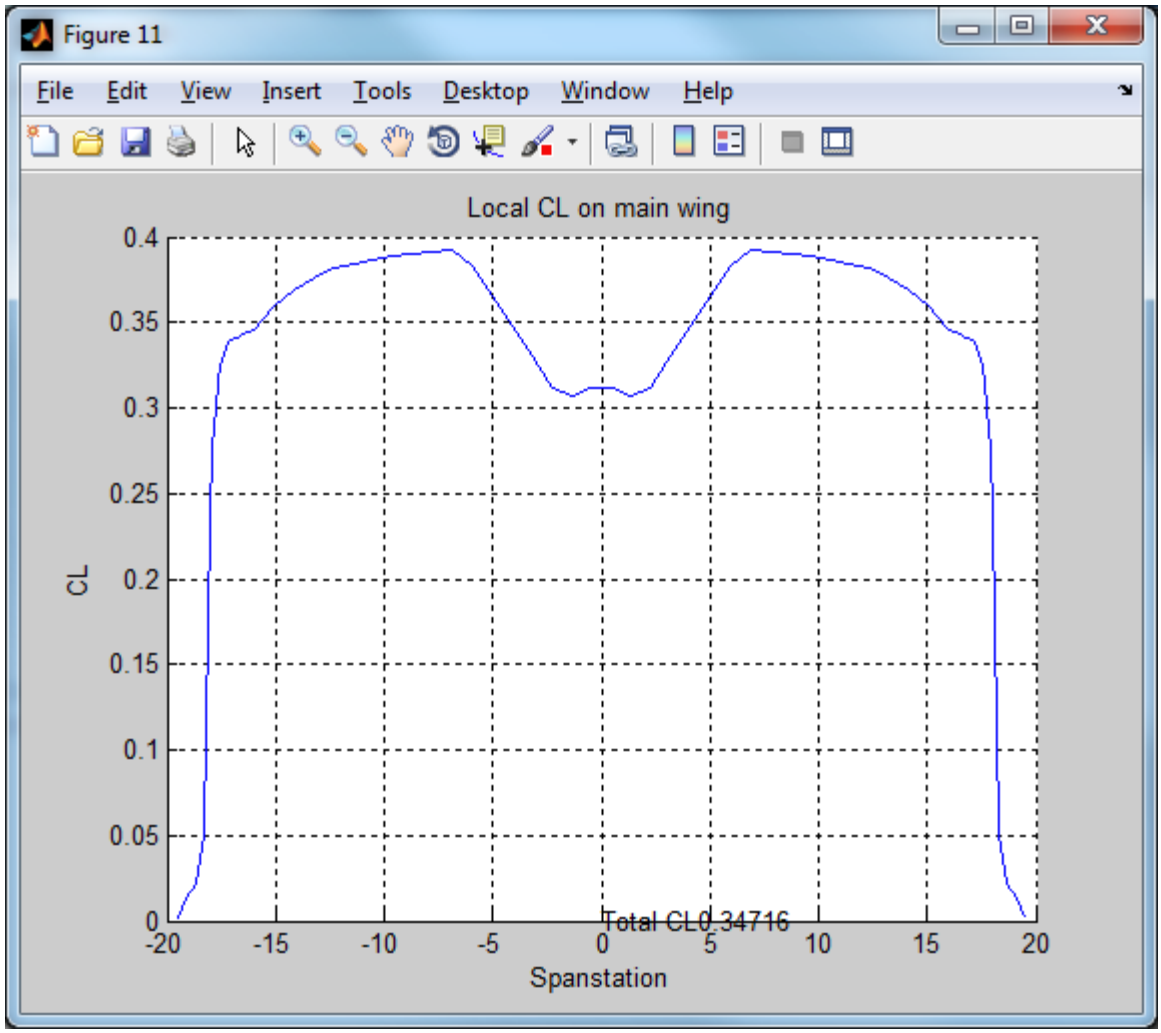
Figure 11
File Edit View Insert Tools Desktop Window Help
Local CL on main wing
CL
Spanstation
Total CL0.34716
0.4
0.35
0.3
0.25
0.2
0.15
0.1
0.05
0
-20
-15
-10
-5
0
5
10
15
20

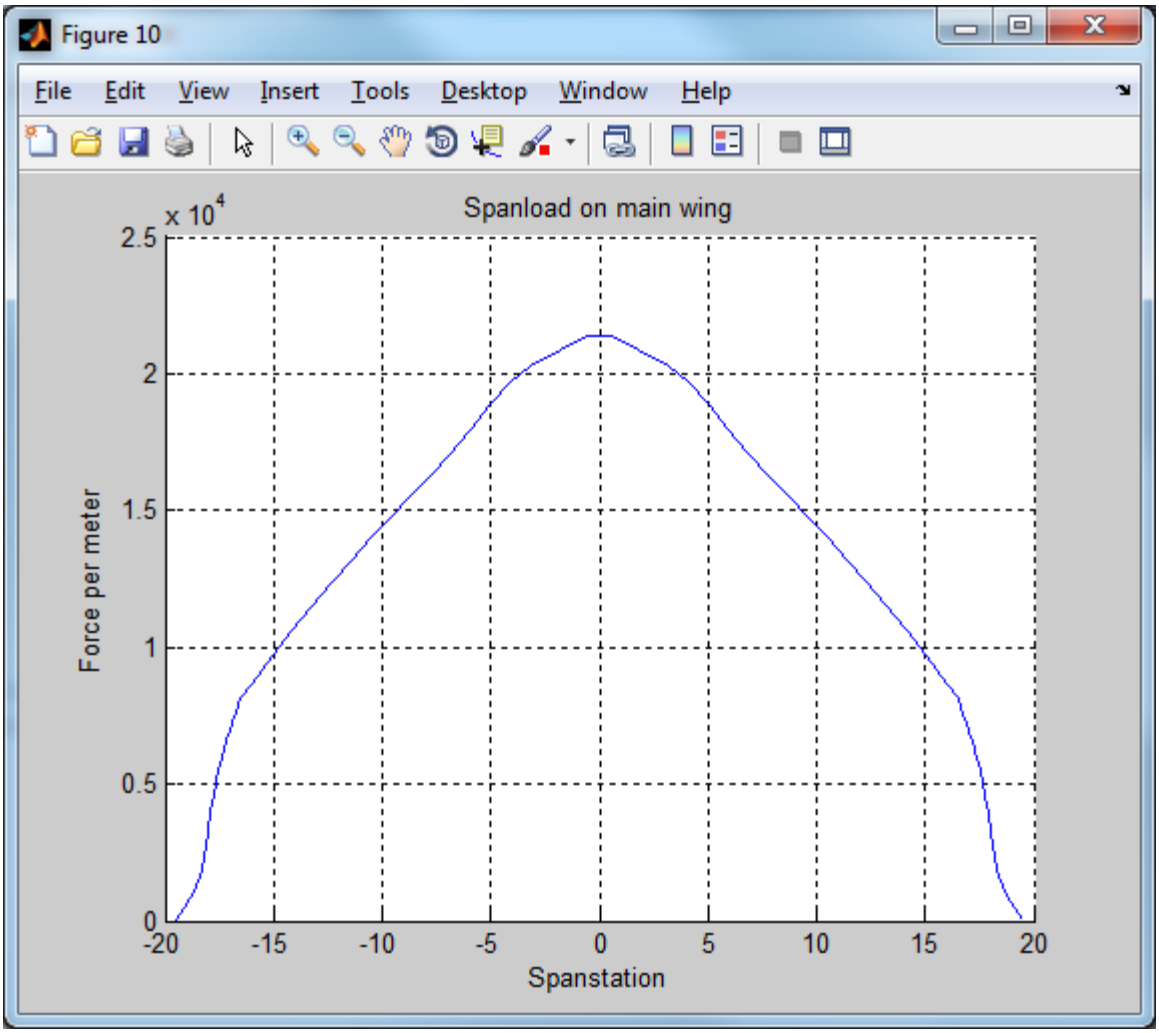
Figure 10
File Edit View Insert Tools Desktop Window Help
Spanload on main wing
x 10^4
2.5
2
1.5
1
0.5
0
Force per meter
-20 -15 -10 -5 0 5 10 15 20
Spanstation

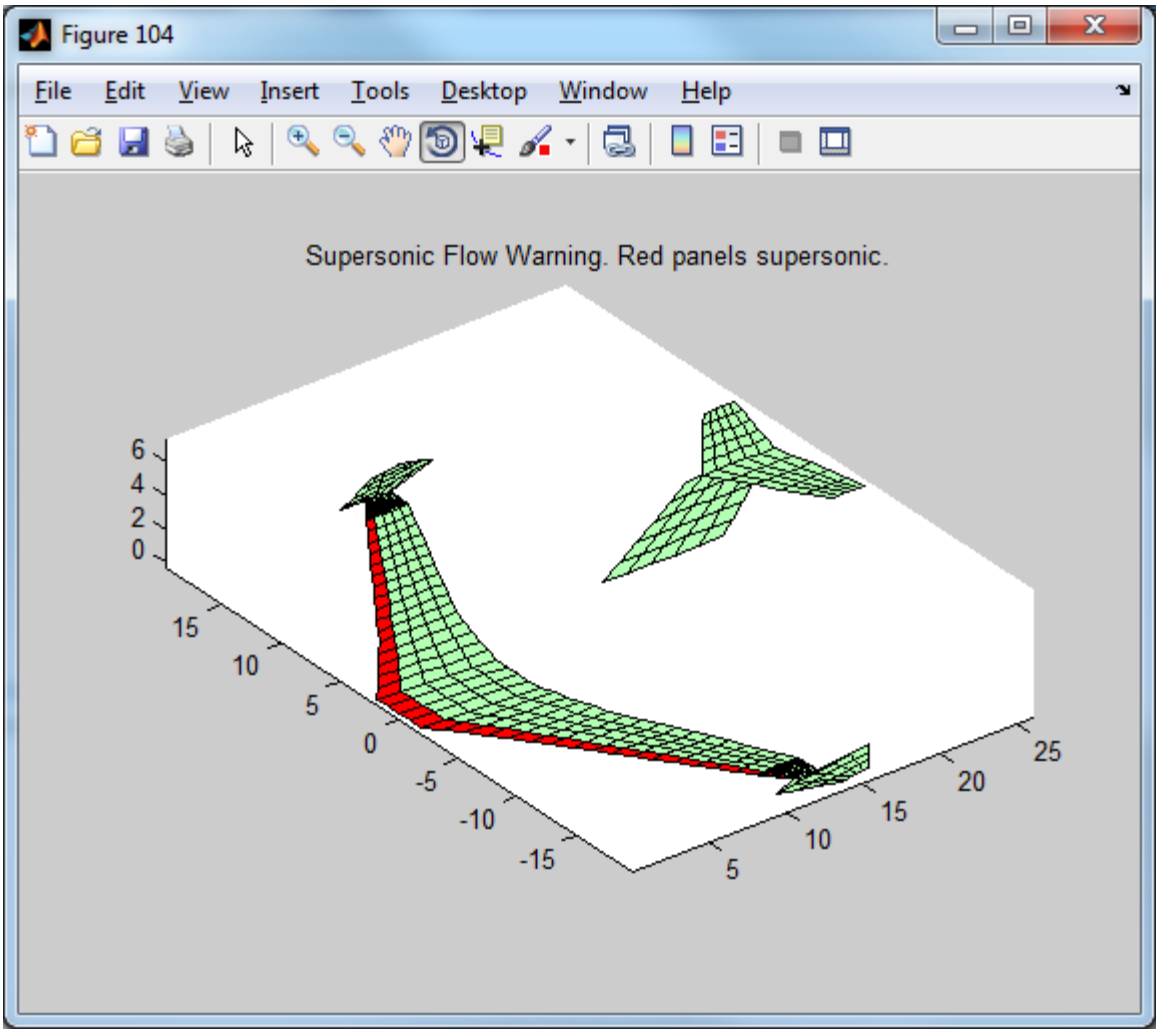
Figure 104
File Edit View Insert Tools Desktop Window Help
Supersonic Flow Warning. Red panels supersonic.
6
4
2
0
15
10
5
0
-5
-10
-15
5
10
15
20
25

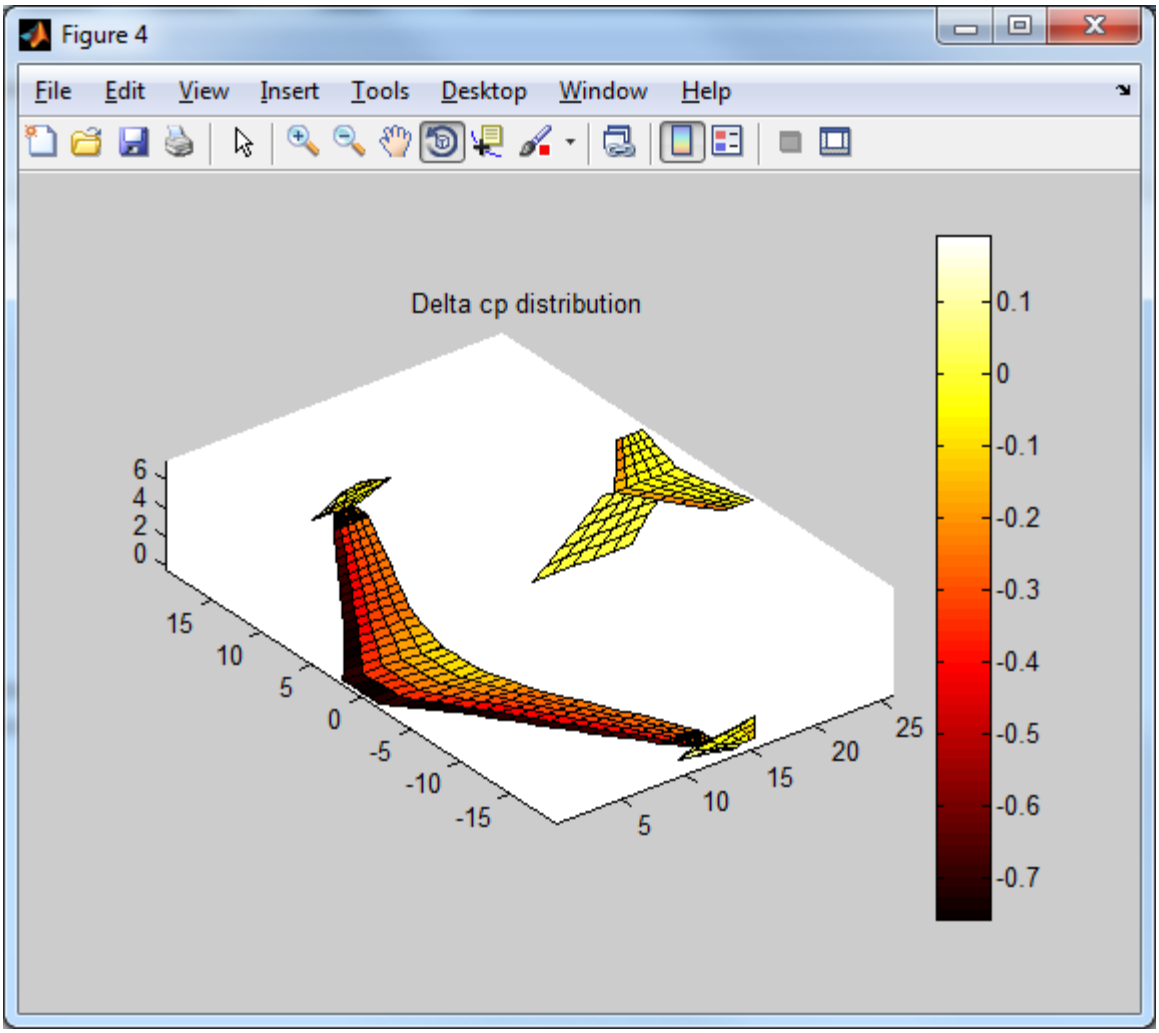

A parameter sweep case was also run for each wingtip extension design. This was done as follows:

[1]. Aircraft geometry setup
[2]. Flight condition setup
[3]. Change rudder setting
[4]. Move reference point

Lattice operations.
[5]. Generate lattice.

Computation operations.
[6]. Processor access

Post processing and interactive operations.
[7]. Post processing, Result/Plot functions
[8]. Keyboard access

Auxiliary operations.
[10]. About / Release Info
[100]. Help files
[0]. Exit Tornado

Please enter choice from above: 6

Low order solutions:
[1]. Static computation at selected state.
[2]. Sequential state parameter sweep menu:

High order methods:
[3]. Trimmed aircraft polar point.
[4]. Trimmed pitch sweep, polar.
[5]. Unsteady, acceleration free, time coefficients only.
[6]. Unsteady, acceleration free, all inviscous coefficients.

Auxillary operations:
[7]. Viscous Drag Estimation Methods Menu:
[8]. Grid convergence study.
[9]. Find stall angle of attack.
[10]. Find alpha at prescribed CL.
[11]. Compute static margin.

[0]. Cancel / up menu.

Enter choice from above please: 2
Enter Job IDentity tag (JID): wingtip1alphasweep

Available sequences:
[1]. Alpha sweep
[2]. Beta sweep
[3]. Delta sweep (control surface deflection.)
[4]. Roll rate sweep
[5]. Pitch rate sweep
[6]. Yaw rate sweep

[0]. Cancel / up menu.

Sweep parameter: 1

From alpha [deg]: 0
Increment [deg]: 2
To alpha [deg]: 12

Solution available in output/wingtip1alphasweep-Cx_alpha

---

[1]. Aircraft geometry setup
[2]. Flight condition setup
[3]. Change rudder setting
[4]. Move reference point

Lattice operations.
[5]. Generate lattice.

Computation operations.
[6]. Processor access

Post processing and interactive operations.
[7]. Post processing, Result/Plot functions
[8]. Keyboard access

Auxiliary operations.
[10]. About / Release Info
[100]. Help files
[0]. Exit Tornado

Please enter choice from above: 7

---

[1]. Clear plots
[2]. Geometry plot

Solution plots
[3]. Static state
[4]. Parameter sweep sub menu
[5]. Unsteady state, time coefficients only
[6]. Unsteady state, all coefficients

Viscous drag estimation plots
[7]. Plot wing system zero lift drag estimation
[8]. Plot body friction drag estimation

Post processing computations
[9]. Perform a trefftz plane analysis, (experimental)
[10]. Export simple state results to textfile

[0]. Back / up menu

Please enter choice from above: 4

Solution plots, parameter sweep.

[1]. Alpha
[2]. Beta
[3]. Roll rate, P
[4]. Pitch rate, Q
[5]. Yaw rate, R

[6]. Delta, control surface deflection

Please enter choice from above: 1

Enter JID to plot: wingtip1alphasweep

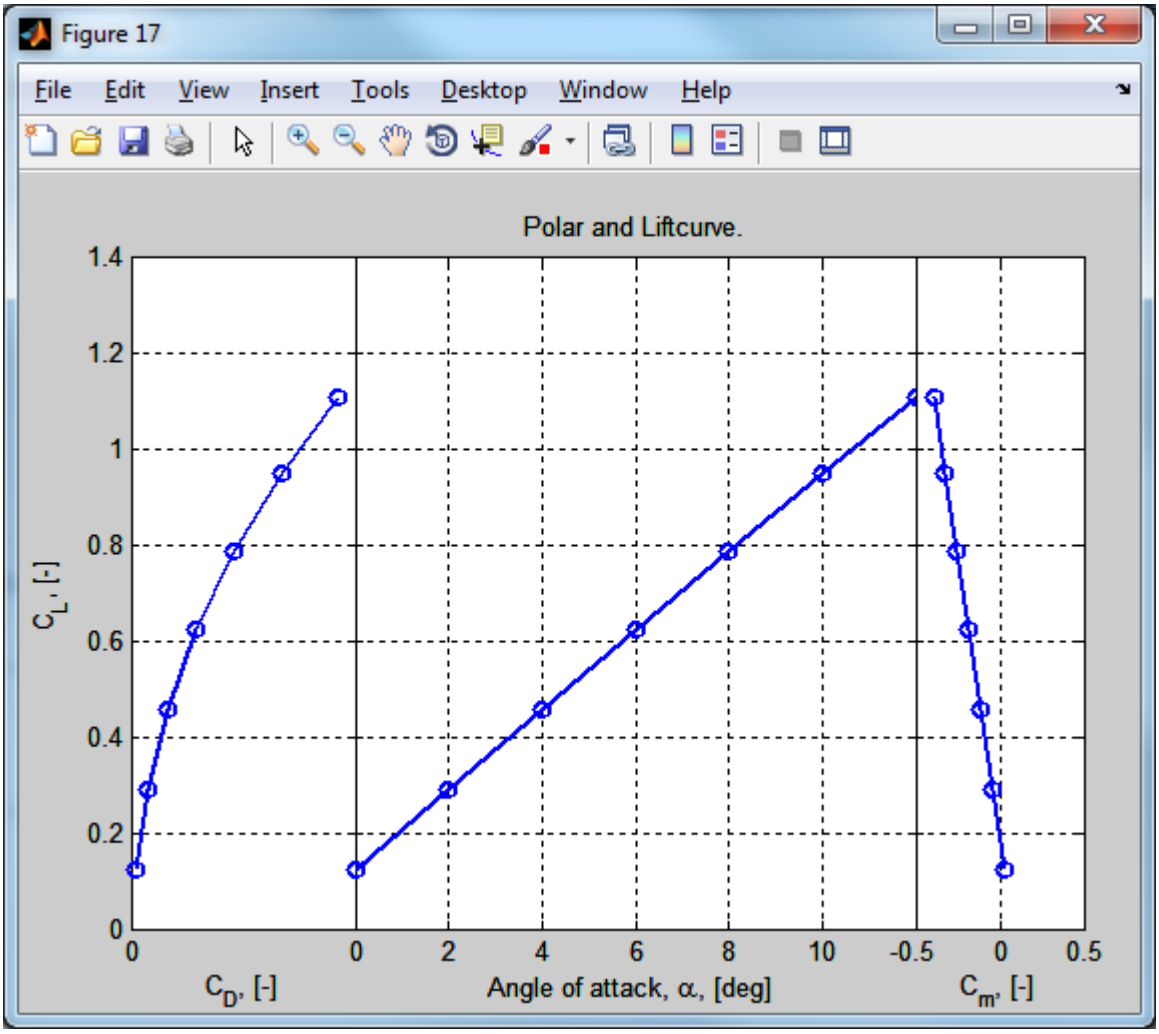

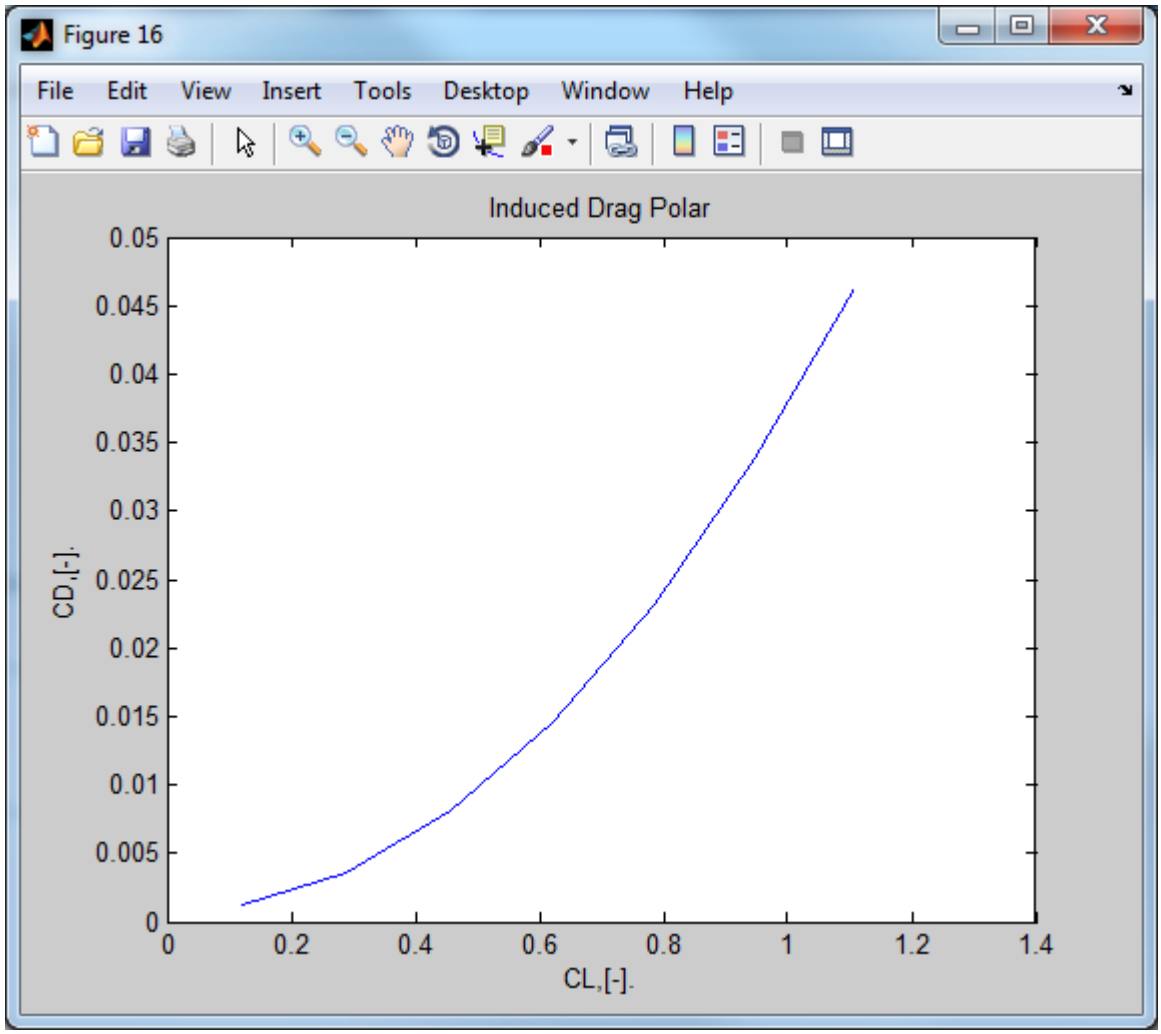
Figure 16
File Edit View Insert Tools Desktop Window Help
Induced Drag Polar
0.05
0.045
0.04
0.035
0.03
0.025
0.02
0.015
0.01
0.005
0
CD,[-].
0
0.2
0.4
0.6
0.8
1
1.2
1.4
CL,[-].

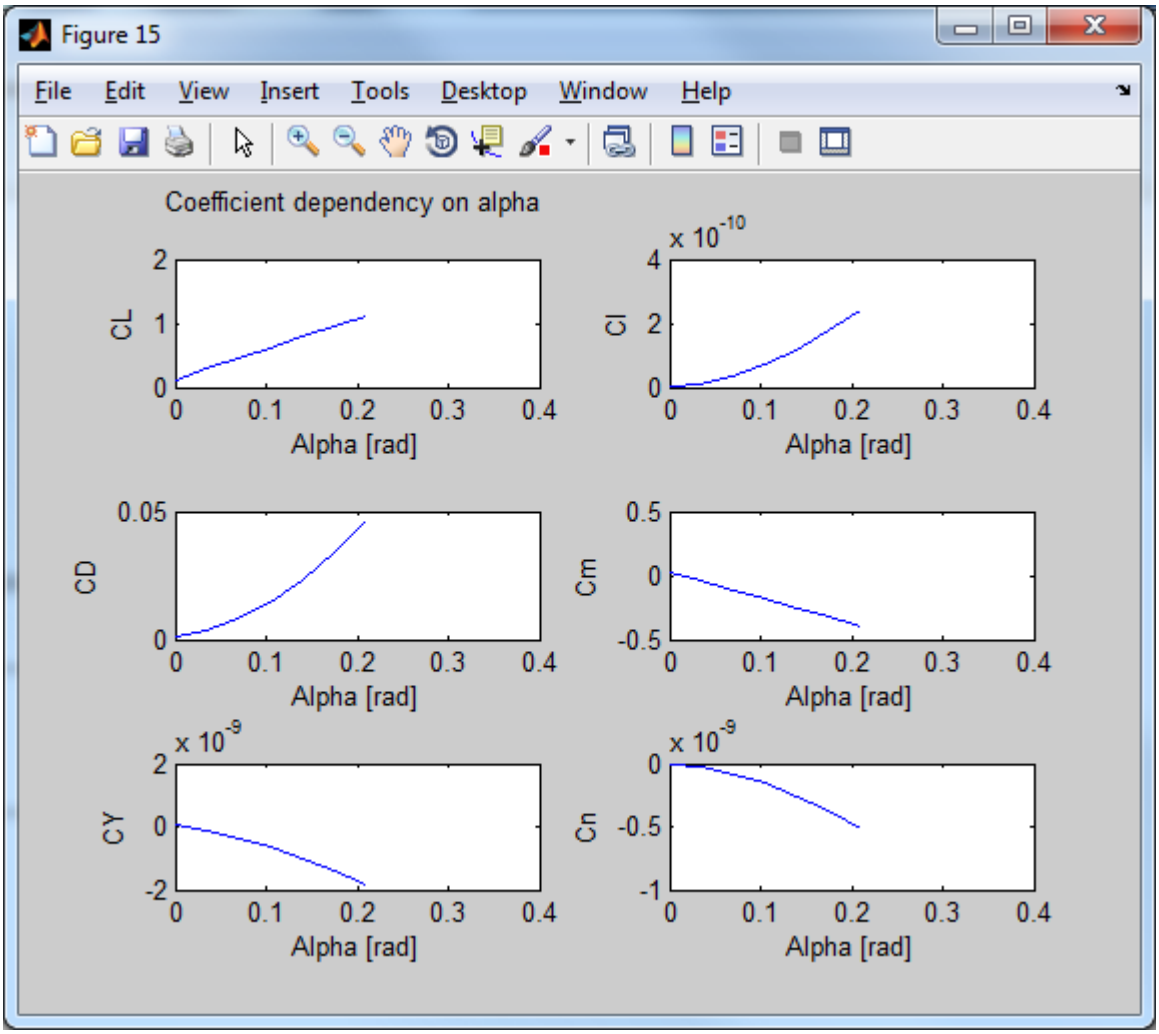
Figure 15
File Edit View Insert Tools Desktop Window Help
Coefficient dependency on alpha
CL
Alpha [rad]
x 10^-10
Cl
Alpha [rad]
CD
Alpha [rad]
Cm
Alpha [rad]
x 10^-9
CY
Alpha [rad]
x 10^-9
Cn
Alpha [rad]